NATIONAL ADVISORY COMMITTEE FOR AERONAUTICS

TECHNICAL NOTE 2994

COLUMN STRENGTH OF H-SECTIONS AND SQUARE TUBES IN POSTBUCKLING RANGE OF COMPONENT PLATES

By P. P. Bijlaard and G. P. Fisher

Cornell University

Washington
August 1953

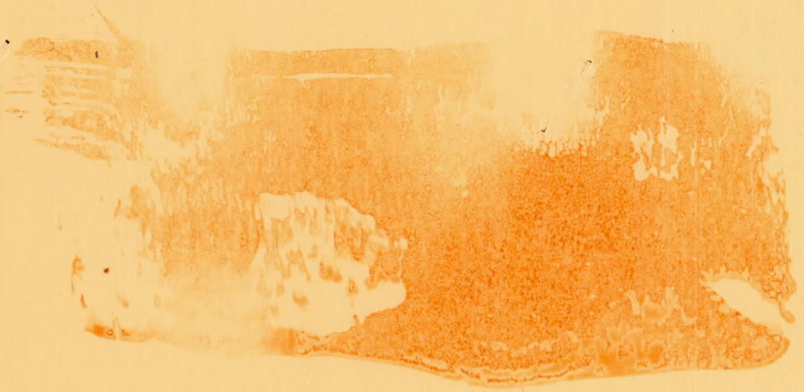

NATIONAL ADVISORY COMMITTEE FOR AERONAUTICS

TECHNICAL NOTE 2994

COLUMN STRENGTH OF H-SECTIONS AND SQUARE TUBES IN POSTBUCKLING RANGE OF COMPONENT PLATES

By P. P. Bijlaard and G. P. Fisher

SUMMARY

The column buckling stress in the range where the component plates have buckled is calculated by the method of split rigidities. For the elastic range simple formulas are derived which explicitly express the column buckling stress in terms of the Euler buckling stress of the column, the plate or local buckling stress, and the local buckling stress for a higher mode of buckling. For the plastic range a Johnson parabola is proposed which in the buckling-stress - slenderness diagram is tangent to the curve for the elastic column buckling stress in the postbuckling range. Also the case of initially crooked columns is considered.

Tests were carried out for a considerable range of slenderness ratios on three H-sections and two square tube sections. The experimental ultimate buckling stresses are in excellent agreement with those predicted by the theory.

INTRODUCTION

The theoretical investigation is primarily concerned with buckling phenomena in the elastic range. The influence of plasticity is taken care of by using an appropriate Johnson parabola.

In the elastic range columns with given cross section and with slenderness ratios for which the column buckling stress (the Euler stress σ_E) is lower than the plate or local buckling stress σ_{crl} fail by column buckling at the stress σ_E (fig. 1). If the slenderness ratio is smaller than that value $(L/r)_{in}$ in figure 1 at which $\sigma_E = \sigma_{crl}$, local buckling occurs at a stress σ_{crl} independent of the slenderness ratio. It was shown in reference 1 that for the sections considered in this paper, that is, H-sections and square tubes, the interaction between column and local buckling is negligible.

In short columns after local buckling, the average compressive stress may still increase considerably above the critical plate buckling stress σ_{cr1} before the ultimate stress σ_u is reached. For very short columns where, also after the decrease of the rigidity of the column by plate buckling, no column buckling can occur, the ultimate stress σ_u will be equal to the crushing strength σ_{cc} in figure 1. For longer columns, but with a slenderness ratio smaller than $(L/r)_{in}$ in figure 1, the ultimate stress is smaller than σ_{cc} because the local buckling of the component plate decreases the effective flexural rigidity of the column as a whole, so that the columns fail by column buckling at an average stress σ_u smaller than σ_{cc}.

As an example, a tube with square cross section is considered. At the critical stress σ_{cr1}, the walls will buckle as plates which are simply supported at the unloaded edges (solid lines in fig. 2(a)). In the postbuckling range, the rigidity of the column against further compression will decrease. This is shown in figure 3, where the average stress σ_{av} is plotted against the unit shortening ϵ_{av} of the column. The diagram OAB shows that for average stresses higher than σ_{cr1} the modulus $d\sigma_{av}/d\epsilon_{av} = \tan \varphi_1$ against further compression is smaller than the elastic modulus $E = \tan \varphi_0$. For the present case, where the unloaded edges of the plates are free to translate in the lateral direction and are not held straight, it follows from reference 2 that $\tan \varphi_1 = 0.41E$ (fig. 3). Assume that at an average stress $\sigma_{av} = \sigma_u$ (fig. 3) the effective flexural rigidity of the column has become so small that it begins to buckle in the direction a (fig. 2(a)) as a column. This will generate bending stresses σ_2 in the column (fig. 2(b)), that is, extra compressive stresses σ_2 to the right and extra tensile stresses σ_2 to the left of the axis. The extra compressive stresses to the right will cause deflecting forces $-t\sigma_2\left(\partial^2 w/\partial x^2\right)$ per unit surface (measuring the coordinate x in the direction of the column axis), as indicated by arrows in figure 2(a), which tend to increase the plate deflections w_1 by amounts w_2. The extra tensile stresses σ_2 to the left cause deflecting forces that diminish the plate deflections w_1, as also indicated in figure 2(a). Hence the cross section will tend to assume the dashed form, superimposing deflections w_2, as sketched in figure 2(c), upon the deflections w_1.

In the plates BC and AD the extra stresses σ_2 are higher than in the plates AB and DC. Moreover, with respect to the extra deflections w_2,

BC and AD act as plates with widths b, while AB and DC act as plates with widths AG = GB = DH = HC = b/2 (fig. 2(c)). Hence BC and AD tend to bend out much more than AB and DC, so that the former will be elastically restrained by the latter. If no initial deflections are present, an elastically restrained plate behaves as shown by the diagram ODE in figure 4. The critical stress σ_{cr2} is higher than σ_{cr1} from the diagram OAB in figure 3, while the initial slope angle φ_2 of the curve DE is larger than φ_1 in figure 3. However, in the present case there are initial deflections w_1. In case of initial deflections, instead of ODE, the diagram of σ_{av} against ϵ_{av} of the elastically restrained plate has a shape as shown by the curve OF in figure 4, which is generally similar to the pertinent curve for a simply supported plate (refs. 3 and 4). The curve OF approximates the curve DE asymptotically. Hence, returning to figure 3, with column buckling at an average stress σ_u the average stress σ_{av} in plate BC tends to follow a curve CF, which is similar to part of the curve OF of figure 4 (for the appropriate initial deflection) that passes through C. Also diagram ODE from figure 4 is shown in figure 3.

In plate AD, where during column buckling in the direction a (fig. 2(a)) the average stress decreases, σ_{av} will tend to follow the dashed part CO of curve OF downward. Similar considerations as for the plates BC and AD apply for the parts of the plates AB and DC to the right and to the left of the line GH, respectively.

At point C (fig. 3) the curvature of a typical curve OF will tend to increase with increasing average stress σ_{av} (refs. 3 and 4). Hence the over-all rigidity of the plates, which governs column buckling and which is determined by the slope of curve OF, will be highest at incipient column buckling, where it is determined by the slope angle φ_3 at point C. For with further buckling the effective modulus for the plates to the right of line GH in figure 2(c), as determined by curve CF, will decrease more than the effective modulus for the plate to the left, as determined by curve CO, increases. Consequently in the postbuckling range the ultimate stress which the column can sustain is the average stress at incipient column buckling.

Similar considerations apply for H-sections buckling in the direction perpendicular to the web. The correctness of these considerations was confirmed by the experiments, described later in this paper, which showed that after incipient buckling the average stress decreases monotonically. To emphasize this point the influence of initial crookedness of the column is considered in a separate section of this paper.

In the theoretical part of the paper the ultimate stress at incipient column buckling is calculated, taking account of the actual shapes of the deflection surfaces w_1 and w_2. Since with incipient buckling the stresses σ_2 and the deflections w_2 are infinitely small they are called σ_2' and w_2'. Simple formulas are found by the method of split rigidities. Plastic deformation is taken into account by using a Johnson parabola, which in the buckling stress-slenderness diagram is tangent to the curve for the ultimate stress in the elastic region. The experimental results are in excellent agreement with the theory.

The present investigation was carried out at Cornell University under the sponsorship and with the financial assistance of the National Advisory Committee for Aeronautics. The theoretical part was carried out by Professor P. P. Bijlaard and the experimental part was carried out by Professor G. P. Fisher. The project was directed by Professor George Winter.

SYMBOLS

A	area of cross section and constant in equation (103)
A,B	constants in equations (127); A = 1.183, B = 1.844
$B = b'/b$	
C, C_1, C_2, C_3, C_4	constants
D	deflecting force in method of split rigidities
E	modulus of elasticity
$E_{1,eq}$	postbuckling modulus
I	moment of inertia
L	column or plate length
M	bending moment
N	flexural plate rigidity, in particular for walls of tubes
N_f	flexural rigidity of flange of H-section

P,Q constants given by equations (56) and (57) for H-sections and by equations (138) for square tubes

V energy or work

X,Y,Z coordinate axes

a half wave length of plate buckling

b plate width, in particular of flanges of H-sections and of walls of square tubes, and length of web

b' width of web of H-section

c constant in equation (104)

j constant in equation (104)

$$k = \frac{84\left(40 + \delta_t B^3\right)}{504 + \gamma\delta_t B^5}$$

$$k_f = b^2 t_f \sigma_{cr_1} \Big/ \pi^2 N_f$$

k_1,k_2,k_3,k_4,k_5,k_6 constants given by equations (129)

p,q,q_1 parameters in equation (63)

r radius of gyration

$$s = \left(\sigma_{cc} - \sigma_{ul}\right) \Big/ (L/r)_1^2$$

t plate thickness in general and wall thickness of tubes in particular

w plate deflection

w_1 plate deflection by local buckling

w_2' infinitely small plate deflection from second mode of plate buckling superimposed at incipient column buckling

x,y coordinates

$$\alpha = \sigma_{cr2} \Big/ \sigma_{cr1}$$

$\alpha_1,\alpha_2,\alpha_1',\alpha_2'$	coefficients defined by equations (86) and (88)
β	ratio between half wave length a and plate width b, a/b
β'	given by equation (43) for H-section and by equation (131) for square tubes, w_{2m}'/w_{1m}
γ	constant given by equation (30)
δ	stretching of plate in postbuckling range
$\delta_t = t_w/t_f$	
ϵ	plate shortening per unit length
θ	coefficient of restraint given by equation (85)
$\lambda = \pi/a = \pi/b$	
μ	constant given by equation (110)
ρ	radius of curvature of column axis at incipient column buckling
σ	normal stress
σ_{cc}	crushing strength
σ_{cy}	yield stress in compression (0.2-percent offset)
$\varphi_0,\varphi_1,\varphi_2,\varphi_3$	slope angles
$\psi = A_f/A$	
$'$	infinitely small when applied to w and σ
$\bar{(\ )}$	uniformly distributed

Subscripts:

a	asymmetric
av	average

b	bending or flexural
c	column
cc	crushing
clear	clear inside dimension
cr	critical
d	exerted by deflecting forces
E	Euler
e	external, elastic
eq	equivalent
f	flange
h	exerted on length equal to half wave length of buckles
i	internal, initial
in	interaction
k	at point K (fig. 13(a))
l	left
m	maximum
o	at crest of waves
out	outside dimension
r	right
s	symmetric
u	ultimate, particularly in elastic range
ul	ultimate at tangent point between curves for σ_u and σ_{up}
ult	ultimate, in general
up	ultimate in plastic range
w	web

x	in X-direction
y	in Y-direction
1	at local buckling, or in postbuckling range
2	at second mode of plate buckling superimposed at incipient column buckling

THEORETICAL INVESTIGATION

Ultimate Strength of Columns with H-Shaped Cross Sections

Survey of distortions and stress distribution.- First the modes of distortion of a cross section are considered in the postbuckling range, before as well as after column buckling. This distortion, which may be assumed to vary sinusoidally in the X-direction (fig. 5(a)), will involve deflecting forces $-t\sigma_x \partial^2 w/\partial x^2$ per unit surface acting transversely on flanges and web, where σ_x includes the membrane stresses caused by finite deflections in the postbuckling range. The deflecting forces are held in equilibrium by restraining forces caused by transverse shearing stresses in the component plates. Since these restraining forces do not include the influence of the membrane stresses, they are proportional to the deflections. They may be expressed in terms of the local buckling stress σ_{cr1} of the cross section and of the local buckling stress σ_{cr2} for the mode of buckling of the cross section which is superimposed with incipient column buckling. In order to be able to take account more accurately of the form of the deflection surfaces of the plates, the deflecting and restraining forces are not compared directly, but the work done by these forces is compared.

This leads to two equations referring to the postbuckling range before and after incipient column buckling, respectively. These two equations have general validity and hence they apply for square tubes as well. After the variables in these equations have been expressed in terms of the maximum deflections and of the abscissas of the pertinent points of the cross section, the equations lead to an explicit formula for the ultimate stress in the elastic range.

An H-section of effective length L is considered (fig. 5(a)). Its cross section is given in figure 5(b). With equal effective length for buckling in the Y- and Z-directions, for the H-sections considered and used in the tests column buckling will occur in a direction perpendicular to the plane of the web.

At the local buckling stress σ_{crl} the cross section at the crest of the local buckling waves in the X-direction will distort as shown in figure 5(b). The stress σ_{crl} and the half wave length a of local buckling follow from the theory of buckling of plate assemblies (refs. 5 and 6) and the pertinent tables (ref. 7) and graphs (ref. 8). The local buckling stress may be expressed as

$$\sigma_{crl} = k_f \frac{\pi^2 N_f}{b^2 t_f} \tag{1}$$

where N_f is the flexural rigidity of the flanges and b and t_f are indicated in figure 5(b).

With further increase of the compressive force the deflections w_{lf} and w_{lw} of the cross section will increase until at a certain load the flexural rigidity of the column as a whole has become so small that it will fail by column buckling. At this load the stress distribution in the flanges, just before column buckling, is given in figure 5(c). The maximum stress σ_m occurs at the line of intersection of flanges and web, which remains straight. (From ref. 1, interaction between column and local buckling can be neglected.) In other points of the flanges (and in the web) the compressive stress σ_1 is less than σ_m because of the superimposed membrane tensile stresses owing to the deflections w_{lf} (and w_{lw}). All these stresses refer to the stresses σ_x in the middle plane of the plates, so that they do not contain the plate bending stresses caused by the deflections w_{lf} and w_{lw}.

With incipient column buckling infinitely small stresses σ_2' are superimposed upon the stresses σ_1 in the flanges. If no additional deflections of the flanges would accompany the column buckling, these extra stresses σ_2' would show a linear distribution (fig. 5(e)). Assuming column buckling in the direction of the arrow a in figure 5(d), with a radius of curvature ρ of the column, the extra stresses at the free edges of the flanges would be Eb/ρ (fig. 5(e)).

However, the extra compressive stresses σ_2' in the right flange will cause extra deflecting forces. These will increase the flange deflection by an infinitely small amount w_2' (fig. 5(d)), with the same wave length in the X-direction as that of w_{lf}. At the same time

the extra tensile stresses σ_2' in the left flange decrease its deflection by an infinitely small amount w_2'. Since w_2' is infinitely small with respect to w_{1f}, it is evident that with equal bending stresses σ_2' in the right and left flange, the extra deflections w_2' of both flanges are equal. Moreover, the extra deflections w_2' cause a change in the deflecting forces due to the original compressive stresses σ_1. This will again increase w_2' for the right and left flange by equal amounts. Hence the deflections w_2' caused by column buckling are symmetrical with respect to the intersection 0 of flange and web (figs. 5(d) and 5(f)). Thus also the membrane tensile stresses caused by the extra deflections w_2' of the right flange are equal to the membrane compressive stresses caused by the extra deflections w_2' of the left flange. These membrane stresses diminish the column bending stresses Ey/ρ in the right and left flange by equal amounts, so that the remaining extra compressive stresses σ_2' in the right flange are equal to the remaining extra tensile stresses σ_2' in the left flange, as was assumed above.

The extra deflection w_2' of the flange, being symmetrical with respect to point 0 (fig. 5(f)), is practically similar to the deflection of a flange clamped at one unloaded side and free at the other which buckles in pure compression. The buckling stress of such a flange is, from reference 9,

$$\sigma_{cr2} = \left[\left(\frac{1}{\beta^2}\right) + 0.57 + 0.125\beta^2\right]\frac{\pi^2 N_f}{b^2 t_f} \qquad (2)$$

where $\beta = a/b$ and a is the half wave length of buckles. In the present case this half wave length is the same as that of the original local buckles which occurred at the local buckling stress σ_{cr1} from equation (1). This similarity will be used in calculating the restraining forces caused by the extra deflections w_2'.

The extra deflections w_2' of the flanges do not involve any rotation in the line of intersection 0 of web and flanges. Moreover, since with incipient column buckling the extra stresses σ_2' are symmetrical with respect to 0, there will not occur any extra stresses σ_2' in the

web, so that they do not cause extra deflecting forces there. However, extra deflecting forces will work on elements of the web owing to the curvature $1/\rho$ of the column, with a half wave length equal to the column length L. But since the web has buckled in many small half waves, the deflecting forces by this curvature $1/\rho$ will tend to increase the deflection of one half wave and to decrease that of the adjacent ones, so that they will not affect the average deflections of the web buckling mode w_{lw} (figs. 5(b) and 5(d)).

Derivation of energy equations by method of split rigidities.- To determine the average buckling stress σ_{av} of the column the method of split rigidities will be used. The principles of this method were explained in earlier papers, of which some of the earliest and latest are given as references 1, 4, 10, 11, and 12.

With this method equations are established that express the equilibrium between the deflecting and resisting actions during buckling, as explained in a generalized form in reference 1, pages 19 and 20. If the deflecting forces $-t\sigma_x\left(\partial^2 w/\partial x^2\right) dx\, dy$ caused by the compressive forces $t\sigma_x\, dx\, dy$ acting on elements $t\, dx\, dy$ have to be compared for two different modes of deflection for which their distributions in the Y-direction are different (in the X-direction, as sketched in fig. 5(a), all modes and deflecting forces have the same sine distribution), not the deflecting forces themselves, but their influences on the considered deflection have to be compared.

In reference 1 these influences, expressed by the coefficients ϕ and γ, affected only the decrease of the column or plate buckling stress by the interaction with plate or column buckling, respectively, which itself was a small fraction of the actual buckling stress (compare eqs. (74) and (75) of ref. 1). Therefore these influences could sufficiently accurately be estimated by simple means.

In the present case more intricate modes of deflection occur, especially in the case of square tubes. Moreover the influence of the actual form of the different modes is here somewhat larger than in the case of reference 1. Therefore a more rigorous method will be used in determining the relative influences of differently distributed deflecting forces; they will be determined by comparing the work done by them during the pertinent deflections, as was proposed in reference 4.

First, the postbuckling stage of the plate-buckling process is considered (fig. 5(b)). At the critical stress σ_{crl} known from equation (1) flanges and web begin to buckle. With increased load further

buckling occurs. This induces membrane stresses, so that the compressive stress σ_{1f} in the flanges will vary in the Y-direction (fig. 5(c)). The flange deflection $w_{1f} \sin(\pi x/a)$ causes deflecting forces

$$D_1 = -t_f \sigma_{1f} \frac{\partial^2}{\partial x^2} w_{1f} \sin\left(\frac{\pi}{a} x\right) dx\, dy$$

$$= \frac{\pi^2}{a^2} t_f \sigma_{1f} w_{1f} \sin\left(\frac{\pi}{a} x\right) dx\, dy \qquad (3)$$

A difficulty in determining the work done by these deflecting forces during buckling seems to be that during this process σ_{1f} changes, so that the deflecting forces at a certain point do not increase linearly with the deflection. This difficulty may be solved, however, by observing that the resulting deformation of the flange will be the same as if the deflecting forces had increased linearly with the deflections $w_{1f} \sin(\pi x/a)$ and hence, at any point, σ_{1f} had been equal to its final value after the deflection $w_{1f} \sin(\pi x/a)$ (figs. 6(a) and 6(b)). This is evident because in that case the resulting deflection and the internal work would be the same as in the actual case. Hence the total work during the deflection $w_{1f} \sin(\pi x/a)$ exerted by the deflecting forces, for example, on a length of the right flange equal to the half wave length a of buckles, is

$$\left(V_{1df}\right)_h = \frac{1}{2} \int_0^a \int_0^b D_1 w_{1f} \sin\left(\frac{\pi}{a} x\right)$$

$$= \frac{1}{2} \frac{\pi^2}{a^2} t_f \int_0^a \int_0^b \sigma_{1f} w_{1f}^2 \sin^2\left(\frac{\pi}{a} x\right) dx\, dy$$

$$= \frac{1}{2} \frac{\pi^2}{2a} t_f \int_0^b \sigma_{1f} w_{1f}^2\, dy$$

$$= \frac{1}{2} C_1 t_f \int_0^b \sigma_{1f} w_{1f}^2\, dy \qquad (4)$$

where the subscript h indicates half wave length and where C_1 is a constant.

In all cases that have to be considered the deflecting forces and deflections vary sinusoidally in the X-direction with the same half wave length a. Hence it is sufficient to consider the work done on an element of unit length in the X-direction at the crest of the waves only. From equation (3) the deflecting force exerted on an element dy of such a strip may be denoted as $Ct_f\sigma_{1f}w_{1f}\,dy$, where $C = \pi^2/a^2$ is a constant. The total work during the deflection w_{1f} is then

$$V_{1df} = \frac{1}{2} Ct_f \int_0^b \sigma_{1f} w_{1f}^2 \, dy \tag{5}$$

analogous to equation (4).

The same explanation applies to the web, if also the work by membrane stresses σ_y in the Y_w-direction (fig. 5(b)) is considered. This work can be calculated by assuming a total equivalent stress $(\sigma_{1w})_{eq}$ in the X-direction, which includes the influence of these membrane stresses σ_y. In the flange these stresses σ_y are practically zero. Hence for the entire cross section the work of the deflecting forces is

$$V_{1d} = \frac{1}{2} C \oint t(\sigma_1)_{eq} \, w_1^2 \, dy_1 \tag{6}$$

where the sign $\oint$ means that the integral has to be extended along the entire cross section of the column (so that, in considering the web, t is the thickness t_w of the web, and y_1 is the coordinate y_w). In calculating the work V_{1d}, the influence of the membrane stresses was taken into account in determining the deflecting forces. Hence the work V_{1d} is transformed exclusively into bending energy of the plate, that is, without any stretching energy. In the considered initial stage of postbuckling the shape of the deflection surface may be assumed to remain similar to that at incipient buckling. It was shown in reference 4 that, in the case of a compressed plate that is simply supported at the unloaded edges, such an assumption leads to practically exact results. Hence the required bending energy for the finite deflections involved is determined by the same equations that apply for the infinitely small deflections occurring at incipient buckling. Analogous to equation (6), at incipient buckling the work done by the deflecting

forces, and hence the bending energy required for the deflections w_1, may be expressed as

$$V_{1b} = \frac{1}{2} C\sigma_{cr1} \oint t w_1^2 \, dy_1 \tag{7}$$

where σ_{cr1} is the local buckling stress from equation (1). As explained above, this same equation obtains for the finite deflections considered here. Hence V_{1d} from equation 6 should be equal to V_{1b} from equation (7), so that

$$\oint t(\sigma_1)_{eq} \, w_1^2 \, dy_1 = \sigma_{cr1} \oint t w_1^2 \, dy_1 \tag{8}$$

The subsequent column buckling will be considered next. As explained above, it induces extra flange deflections w_2' and no extra web deflections. The deflections w_2' are symmetrical with respect to the plane of the web and are similar to those of a compressed flange with one unloaded side clamped and the other free, as illustrated in figure 5(f), for which the critical stress σ_{cr2} is given by equation (2). Analogous to equation (7) the flexural energy required for the deflections w_2' may be expressed as

$$V_{2b} = \frac{1}{2} C\sigma_{cr2} \oint t(w_2')^2 \, dy_1 \tag{9}$$

This integral extends over the flanges only, since for the web $w_2' = 0$.

The best way to explain how the work done by the deflecting forces during the actual deflection w_2' of the flanges is calculated seems to be to show first how the total deflecting forces acting on the flanges develop - or may be assumed to develop - with increasing crest deflections w_{1f} and w_2'. Figure 6(a) shows how the compressive stress (averaged over the flange thickness) at a certain point of the right flange develops. As stated above, during the deflection w_{1f} it may be assumed to remain constant. Hence at the crest of the waves it develops a deflecting force which increases linearly with w_{1f} with

a final value $Ct_f\sigma_{1f}w_{1f}$, as indicated in figures 5(d) and 6(b). The column buckling stresses σ_2' as well as the extra deflections w_2' are proportional to the infinitely small column deflections, so that σ_2' increases linearly with w_2' (fig. 6(a)). The deflections w_2' with the same half wave length a as w_{1f} cause an increase of the deflecting forces by the stresses σ_{1f} of a final amount $Ct_f\sigma_{1f}w_2'$ (fig. 5(d)), increasing linearly with w_2' (fig. 6(b)). The extra stresses σ_2' increase the deflecting forces by an amount $Ct_f\sigma_2'\left(w_{1f} + w_2'\right)$ (figs. 5(d) and 6(b)). The part $Ct_f\sigma_2'w_{1f}$ increases linearly with w_2', while the part $Ct_f\sigma_2'w_2'$ increases proportionally to $\left(w_2'\right)^2$ (fig. 6(b)). Since both σ_2' and w_2' are infinitely small, this last term may be neglected with respect to the first one.

With deflecting forces D and deflections w the total work done by the deflecting forces is $\int_0^w D\,dw$. Hence it is given by the hatched area of the diagram for the deflecting forces in figure 6(b), so that for an element of the right flange at the crest of the wave and of unit length in the X-direction this work is

$$V_{dr} = \frac{1}{2} Ct_f \int_0^b \sigma_{1f}\left(w_{1f} + w_2'\right)^2 dy + \frac{1}{2} Ct_f \int_0^b \sigma_2' w_{1f} w_2'\, dy \qquad (10)$$

In the left flange, the extra stresses σ_2' (fig. 5(e)) are opposite to the stresses σ_{1f} (fig. 5(c)) and w_2' is opposite to w_{1f} (fig. 5(d)), so that the stresses vary with the deflection as indicated in figure 6(c). After reaching a value $Ct_f\sigma_{1f}w_{1f}$ just before column buckling, with a deflection w_{1f}, the deflecting force caused by the stresses σ_{1f} will decrease by an amount $Ct_f\sigma_{1f}w_2'$ (figs. 5(d) and 6(d)). The extra tensile stresses σ_2' decrease the deflecting force by an amount $Ct_f\sigma_2'\left(w_{1f} - w_2'\right)$. For similar reasons as given for the right flange, $Ct_f\sigma_{1f}w_2'$ and $Ct_f\sigma_2'w_1$ decrease here linearly with the deflection, while the term $Ct_f\sigma_2'w_2'$ may be neglected. Hence from figure 6(d) the

total work done by the deflecting forces, as given by the hatched area, is (fig. 5(d))

$$V_{dl} = \frac{1}{2} Ct_f \int_0^b \sigma_{lf}\left(w_{lf} - w_2'\right)^2 dy' + \frac{1}{2} Ct_f \int_0^b \sigma_2' w_{lf} w_2' \, dy' \quad (11)$$

During incipient buckling the web does not undergo extra deflections w_2', so that the total work for the web is (fig. 5(d))

$$V_{dw} = \frac{2}{2} Ct_w \int_0^{b'/2} \left(\sigma_{lw}\right)_{eq} w_{lw}^2 \, dy_w \quad (12)$$

Here $\left(\sigma_{lw}\right)_{eq}$ is inserted instead of σ_{lw} to take account of membrane stresses σ_y in the web. Hence, for the entire section, the total work by the deflecting forces is

$$V_d = 2V_{dr} + 2V_{dl} + V_{dw}$$

$$= \frac{1}{2} C \oint t\left[\left(\sigma_1\right)_e w_1^2 \, dy_1 + \sigma_1\left(w_2'\right)^2 dy_1 + \sigma_2' w_1 w_2' \, dy_1\right] \quad (13)$$

where $\oint$, t, and y_1 have the same meaning as in equation (6).

As stated above, the bending energy required for the deflections w_1 and w_2' is given by V_{1b} and V_{2b} from equations (7) and (9). It could be argued that in the present case the extra energy required for the extra deflections w_2' may differ from V_{2b} in equation (9) because the stresses which were caused by the deflections w_1 may do some work during the extra deflections w_2'. Indeed, in the right flange, where w_2' is of the same sign as w_1, some stress components may do work during the extra deflections w_2'. But in the left flange w_2' has a direction opposite to w_1, so that the same stress components will do

there an equal and opposite amount of work. Hence the total work done by these stresses is zero, so that indeed V_d from equation (13) must be equal to the sum of V_{1b} and V_{2b} from equations (7) and (9). This yields

$$\oint t(\sigma_1)_{eq} w_1^2 \, dy_1 + \oint t\sigma_1 (w_2')^2 \, dy_1 + \oint t\sigma_2' w_1 w_2' \, dy_1 =$$

$$\sigma_{cr1} \oint t w_1^2 \, dy_1 + \sigma_{cr2} \oint t (w_2')^2 \, dy_1 \tag{14}$$

Subtracting equation (8) from equation (14) leads to the following basic condition:

$$\oint t\sigma_1 (w_2')^2 \, dy_1 + \oint t\sigma_2' w_1 w_2' \, dy_1 = \sigma_{cr2} \oint t (w_2')^2 \, dy_1 \tag{15}$$

Derivations of formulas for stresses σ_1 and σ_2'.- The variables in equations (8) and (15) may be expressed in terms of the maximum deflections w_{1m} and w_{2m}' (fig. 5(d)) and the abscissas of the pertinent points to which they refer. The stress σ_{1f} in the flanges differs from σ_m at $y = 0$ because of the stretching of the flange in the X-direction by its deflection w_{1f}. Although the flanges are rotationally restrained by the web, during local buckling they practically do not bend in the Y-direction, as is substantiated by tests, so that the deflection w_{1f} (fig. 5(b)) may be expressed as

$$w_1 = w_{1f} \sin\left(\frac{\pi}{a} x\right) \tag{16}$$

where

$$w_{1f} = w_{1m} \frac{y}{b} \tag{17}$$

Hence for a half wave length the dilatation is

$$\delta = \frac{1}{2}\int_0^a \left(\frac{\partial w}{\partial x}\right)^2 dx$$

$$= \frac{1}{2}\int_0^a \frac{\pi^2}{a^2} w_{1f}^2 \cos^2 \frac{\pi}{a} x$$

$$= \frac{\pi^2}{4a} w_{1f}^2 \tag{18}$$

so that the stress σ_{1f} at any point of the flanges (fig. 5(c)) is

$$\sigma_{1f} = \sigma_m - \frac{E\delta}{a}$$

$$= \sigma_m - \frac{\pi^2 E}{4a^2} w_{1f}^2 \tag{19}$$

In the same way the compressive stress in the web is

$$\sigma_{1w} = \sigma_m - \frac{\pi^2 E}{4a^2} w_{1w}^2 \tag{20}$$

Both equations (19) and (20) neglect the influence of membrane stresses σ_y and assume that σ_1 does not vary in the X-direction. For the flanges the membrane stresses σ_y are indeed negligible. Moreover it was shown in reference 4 that for a web plate which is simply supported and held straight at the unloaded edges the above assumption leads to exact results. Hence it may be assumed that for the present case also equation (20) is sufficiently accurate.

However, to calculate the total work, the membrane stresses σ_y in the web should be taken into account. At the unloaded edges $y_w = \pm b'/2$

of the web the membrane stresses σ_y vanish. According to reference 2 for such a case, if the plate is simply supported at the unloaded edges, in the postbuckling range the stiffness against further compression is 0.41 times that before buckling, which may be expressed by the formula

$$\sigma_{av} = \sigma_{cr} + 0.41E(\epsilon_x - \epsilon_{cr}) \tag{21}$$

where σ_{av} is the average compressive stress σ_x, σ_{cr} is the critical stress, ϵ_x is the shortening of the plate per unit length, and $\epsilon_{cr} = \sigma_{cr}/E$. Since at the unloaded edges the plate does not bend, $\epsilon_x = \sigma_m/E$, where σ_m is the maximum edge compressive stress (fig. 7). Insertion in equation (21) gives

$$\sigma_{av} = \sigma_{cr} + 0.41(\sigma_m - \sigma_{cr}) \tag{22}$$

It was shown in reference 4 that for membrane stresses σ_x with a distribution (fig. 7)

$$\sigma_{xm} = \sigma_{om} \cos^2 \frac{\pi}{b} y_w \tag{23}$$

their effect upon the buckling deflections of the plate is equivalent to that of uniformly distributed stresses

$$\bar{\sigma}_{x,eq} = 0.75\sigma_{om} \tag{24}$$

It may be assumed that equation (23) gives the distribution of the membrane stresses σ_{xm} also in the present case. Moreover, let the influence of all membrane stresses σ_{xm} and σ_{ym} be equivalent to that of equally distributed stresses

$$\sigma_{x,eq} = \alpha\sigma_{om} \tag{25}$$

Hence, according to the reasoning advanced in reference 4, the total equivalent compressive stress $\sigma_x = \sigma_m - \alpha\sigma_{om}$ must be equal to the critical stress, or

$$\sigma_m - \alpha\sigma_{om} = \sigma_{cr} \tag{26}$$

so that

$$\alpha = \frac{\sigma_m - \sigma_{cr}}{\sigma_{om}} \tag{27}$$

Observing that with the stress distribution from equation (23) $\sigma_{om} = 2(\sigma_m - \sigma_{av})$ in figure 7 and using equation (22), it follows from equations (25) and (27) that

$$\sigma_{x,eq} = 0.848\sigma_{om} \tag{28}$$

From equation (24) the equivalent stress $\bar{\sigma}_{x,eq}$ for membrane stresses σ_{xm} only is $0.75\sigma_{om}$, so that the membrane stresses σ_{ym} may be taken into account, in calculating the total work, by assuming equivalent membrane stresses

$$\left(\sigma_{xm}\right)_{eq} = \frac{0.848}{0.750}\sigma_{xm} = \gamma\sigma_{xm} \tag{29}$$

where

$$\gamma = 1.13 \tag{30}$$

Hence in calculating the total work the stresses in the web should be assumed as

$$\left(\sigma_{lw}\right)_{eq} = \sigma_m - \gamma\frac{\pi^2 E}{4a^2}w_{lw}^2 \tag{31}$$

instead of σ_{lw} from equation (20).

For a column deflection in the direction a (fig. 5(d)), with a radius of curvature ρ the bending stresses in a nondistorted section would be Ey/ρ. However, the excess flange deflections w_2' (fig. 5(d)) generate excess membrane stresses σ_{xm}'. Analogous to equation (19) and considering that w_2' is infinitely small, this leads to actual stresses (fig. 5(e)):

$$\sigma_2' = \frac{E}{\rho} y - \frac{\pi^2 E}{4a^2}\left[\left(w_{1f} + w_2'\right)^2 - w_{1f}^2\right] = \frac{E}{\rho} y - \frac{\pi^2 E}{2a^2} w_{1f} w_2' \qquad (32)$$

As shown in the section entitled "Survey of distortions and stress distribution," the column deflection does not introduce any excess stresses in the web, so that for the web $\sigma_2' = 0$.

Derivation of formulas for deflections.- After formulas for the stresses σ_1 and σ_2' have been derived, the deflections w_1 and w_2' have yet to be expressed in terms of the maximum deflections w_{1m} and w_{2m}' (fig. 5(d)) and of the abscissas of the pertinent points considered. The flange deflection w_{1f} is given by equation (17). The web is bent by moments M_y exerted by the flanges and may sufficiently accurately be assumed to bend parabolically in the Y_w-direction. Hence from figure 5(d) at the crest of the waves the maximum web deflection is

$$w_o = \frac{b' w_{1m}}{4b} \qquad (33)$$

so that the web deflection

$$w_{1w} = w_o\left[1 - \frac{4y_w^2}{(b')^2}\right] = \frac{b' w_{1m}}{4b}\left[1 - \frac{4y_w^2}{(b')^2}\right] \qquad (34)$$

The flange deflection w_2' is similar to that of a fully clamped flange. Analogous to equation (15b) of reference 1 it will be assumed as

$$w_2' = w_{2m}' \frac{y^4 - 4by^3 + 6b^2y^2}{3b^4} \qquad (35)$$

As explained above, for the web $w_2' = 0$.

Energy equations.- Equations (17), (19), (31), (32), (34), and (35) express all variables of the basic equations (8) and (15) in terms of the maximum deflections w_{1m} and w_{2m}', the maximum stress σ_m, the half wave length a of local buckling, the plate and web widths b and b', and the coordinates y and y_w (figs. 5(c), 5(d), and 5(e)). Using equations (17), (19), (31), and (34), equation (8) yields

$$4\frac{w_{1m}^2}{b^2}t_f\left(\sigma_m\int_0^b y^2\,dy - \frac{\pi^2E}{4a^2}\frac{w_{1m}^2}{b^2}\int_0^b y^4\,dy\right) +$$

$$2\left(\frac{b'}{4b}\right)^2 w_{1m}^2 t_w\left\{\sigma_m\int_0^{b'/2}\left[1-\frac{4}{(b')^2}y_w^2\right]^2 dy_w -\right.$$

$$\left.\gamma\frac{\pi^2E}{4a^2}\left(\frac{b'}{4b}\right)^2 w_{1m}^2\int_0^{b'/2}\left[1-\frac{4}{(b')^2}y_w^2\right]^4 dy_w\right\} = 4\frac{w_{1m}^2}{b^2}t_f\sigma_{cr1}\int_0^b y^2\,dy +$$

$$2\left(\frac{b'}{4b}\right)^2 w_{1m}^2 t_w\sigma_{cr1}\int_0^{b'/2}\left[1-\frac{4}{(b')^2}y_w^2\right]^2 dy_w \qquad (36)$$

The terms referring to the four flanges and those referring to the web may be recognized by the factors t_f and t_w, respectively. After integration the above equation leads to the result

$$\frac{\pi^2E}{a^2}w_{1m}^2 = k\left(\sigma_m - \sigma_{cr1}\right) \qquad (37)$$

or

$$w_{1m} = \frac{a}{\pi}\left[\frac{k}{E}\left(\sigma_m - \sigma_{cr1}\right)\right]^{1/2} \qquad (38)$$

where

$$k = \frac{84\left(40 + \delta_t B^3\right)}{504 + \gamma\delta_t B^5} \tag{39}$$

and

$$B = b'/b \tag{40}$$

$$\delta_t = t_w/t_f \tag{41}$$

All terms of equation (15) vanish as far as they refer to the web, so that it is sufficient to consider this equation for one flange only. Using equations (17), (19), (32), and (35), equation (15) transforms into

$$\frac{\left(w_{2m}'\right)^2}{9b^8}\left[\sigma_m \int_0^b \left(y^4 - 4by^3 + 6b^2y^2\right)^2 dy - \right.$$

$$\left. \frac{\pi^2 E}{4a^2} \frac{w_{1m}^2}{b^2} \int_0^b y^2\left(y^4 - 4by^3 + 6b^2y^2\right)^2 dy\right] +$$

$$\frac{w_{1m}}{b} \frac{w_{2m}'}{3b^4}\left[\frac{E}{\rho} \int_0^b y^2\left(y^4 - 4by^3 + 6b^2y^2\right) dy - \right.$$

$$\left. \frac{\pi^2 E}{2a^2} \frac{w_{1m}}{b} \frac{w_{2m}'}{3b^4} \int_0^b y^2\left(y^4 - 4by^3 + 6b^2y^2\right)^2 dy\right] =$$

$$\frac{\left(w_{2m}'\right)^2}{9b^8} \sigma_{cr2} \int_0^b \left(y^4 - 4by^3 + 6b^2y^2\right)^2 dy \tag{42}$$

After integration and with the aid of equation (37) this equation results in

$$\beta' = \frac{w_{2m}'}{w_{1m}} = \frac{0.2254Eb/\rho}{0.12874k\left(\sigma_m - \sigma_{cr1}\right) + 0.2568\left(\sigma_{cr2} - \sigma_m\right)} \tag{43}$$

Calculation of postbuckling column modulus and of ultimate strength.- The internal bending moment M_c in the column is practically given by the total bending moment in the flanges so that

$$M_c = 4t_f \int_0^b \sigma_2' y \, dy \tag{44}$$

Inserting equation (32), in which w_{1f} and w_2' are given by equations (17) and (35), and using equations (37) and (43), equation (44) yields

$$M_c = 4b^2 t_f \left[\frac{Eb}{3\rho} - \frac{71}{630} k(\sigma_m - \sigma_{cr1}) \beta' \right] \tag{45}$$

If the column had a constant equivalent postbuckling modulus $E_{1,eq}$ the internal moment would be

$$M_c = \frac{E_{1,eq} I}{\rho} = \frac{4}{3} b^3 t_f \frac{E_{1,eq}}{\rho} \tag{46}$$

By equating the right-hand members in equations (45) and (46) and using equation (43) the equivalent postbuckling modulus is obtained

$$E_{1,eq} = \frac{0.20456k(\sigma_m - \sigma_{cr1}) + (\sigma_{cr2} - \sigma_m)}{0.50132k(\sigma_m - \sigma_{cr1}) + (\sigma_{cr2} - \sigma_m)} E \tag{47}$$

In order to express $E_{1,eq}$ in terms of the ultimate stress σ_u, that is, the average stress σ_x at incipient column buckling, it is observed that the total compressive force in a flange may be written as

$$t_f b \sigma_{uf} = t_f \int_0^b \sigma_{1f} \, dy \tag{48}$$

where σ_{uf} is the average stress in the flanges at incipient column buckling. Substituting σ_{lf} from equation (19) and w_{lf} from equation (17) and using equation (37), equation (48) transforms into

$$\sigma_{uf} = \frac{1}{12}\left[(12 - k)\sigma_m + k\sigma_{crl}\right] \tag{49}$$

The compressive force in the web is

$$t_w b' \sigma_{uw} = 2t_w \int_0^{b'/2} \sigma_{lw}\, dy_w \tag{50}$$

Using equations (20), (34), (37), and (40), this gives the average stress in the web,

$$\sigma_{uw} = \left(1 - \frac{kB^2}{120}\right)\sigma_m + \frac{kB^2}{120}\sigma_{crl} \tag{51}$$

The ultimate stress σ_u for the entire section follows from the condition

$$A\sigma_u = 4A_f\sigma_{uf} + A_w\sigma_{uw} \tag{52}$$

where A is the total cross section, A_f is the cross section of one flange, and A_w is the cross section of the web. With equations (49) and (51) and with the notation

$$\psi = A_f/A \tag{53}$$

this leads to the relation

$$\sigma_m = \frac{\sigma_u - \left[\frac{kB^2}{120} + \frac{k}{3}\left(1 - \frac{B^2}{10}\right)\psi\right]\sigma_{crl}}{\left(1 - \frac{kB^2}{120}\right) - \frac{k}{3}\left(1 - \frac{B^2}{10}\right)\psi} \tag{54}$$

Inserting this in equation (47) one obtains

$$\frac{E_{1,eq}}{E} = \frac{P\left(\sigma_u - \sigma_{cr1}\right) + \left(\sigma_{cr2} - \sigma_{cr1}\right)}{Q\left(\sigma_u - \sigma_{cr1}\right) + \left(\sigma_{cr2} - \sigma_{cr1}\right)} \tag{55}$$

where

$$P = \frac{0.20456k - 1}{\left(1 - \frac{kB^2}{120}\right) - \frac{k}{3}\left(1 - \frac{B^2}{10}\right)\psi} \tag{56}$$

$$Q = \frac{0.50132k - 1}{\left(1 - \frac{kB^2}{120}\right) - \frac{k}{3}\left(1 - \frac{B^2}{10}\right)\psi} \tag{57}$$

From the definition of $E_{1,eq}$ it follows that the ultimate stress

$$\sigma_u = \frac{\pi^2 E_{1,eq}}{(L/r)^2} \tag{58}$$

Substituting this in equation (55) and observing that the Euler stress

$$\sigma_E = \frac{\pi^2 E}{(L/r)^2} \tag{59}$$

from equation (55)

$$\sigma_u = \left(\frac{Q + 1 - \alpha}{2Q}\,\sigma_{cr1} + \frac{P}{2Q}\,\sigma_E\right)\left(1 + \left\{1 - \frac{4Q(P + 1 - \alpha)}{\left[(Q + 1 - \alpha)\sigma_{cr1} + P\sigma_E\right]^2}\,\sigma_E\sigma_{cr1}\right\}^{1/2}\right) \tag{60}$$

where

$$\alpha = \sigma_{cr2}/\sigma_{cr1} \tag{61}$$

Column buckling in plastic range.- Equation (60) is valid only if plastic deformations do not occur anywhere in the postbuckling range before column buckling. In figure 8 the elastic ultimate stress σ_u is sketched in the buckling-stress - slenderness diagram. It is proposed to define the column buckling stress σ_{up} in the plastic range (that is, in the case when in the postbuckling stage the local stress at some points of the column is in the plastic range) by a Johnson parabola, as given by the curve σ_{up} in figure 8. Hence it is given by the formula

$$\sigma_{up} = \sigma_{cc} - s(L/r)^2 \tag{62}$$

where σ_{cc} is the crushing strength for short columns, where only plate buckling and no column buckling can occur, and where s is determined as follows:

It appeared that, for all sections considered and tested, the expression in the second parentheses in equation (60) is practically independent of σ_E and thus of L/r. Hence equation (60) and the corresponding curve for σ_u become a hyperbola

$$\sigma_u = p + q_1\sigma_E = p + \frac{q}{(L/r)^2} \tag{63}$$

where p, q, and q_1 are parameters determined by approximating equation (60) by a hyperbola. From equation (59),

$$q = q_1\sigma_E(L/r)^2 = q_1\pi^2E \tag{64}$$

At the tangent point between the curves for σ_u and σ_{up}, with coordinates $L/r = (L/r)_1$ and $\sigma = \sigma_{ul}$ (fig. 8),

$$\left.\begin{aligned} \sigma_{up} &= \sigma_u \\ \frac{d\sigma_{up}}{d(L/r)} &= \frac{d\sigma_u}{d(L/r)} \end{aligned}\right\} \tag{65}$$

Using equations (62), (63), and (64), one finds from equations (65)

$$\sigma_{ul} = \frac{1}{2}(\sigma_{cc} + p) \tag{66}$$

$$\left(\frac{L}{r}\right)_1 = \pi\sqrt{\frac{2q_1 E}{\sigma_{cc} - p}} \tag{67}$$

$$\sigma_{up} = \sigma_{cc} - \frac{(\sigma_{cc} - p)^2}{4q}\left(\frac{L}{r}\right)^2 = \sigma_{cc} - \frac{(\sigma_{cc} - p)^2}{4q_1\sigma_E} \tag{68}$$

Since the actual curve for σ_u according to equation (60) is not exactly a hyperbola, the best way to draw a continuous curve for σ_u and σ_{up} is first to calculate σ_{ul} from equation (66). Then from the curve for σ_u the value of $(L/r)_1$ for $\sigma_u = \sigma_{ul}$ can be read. This gives the curve for the Johnson parabola as

$$\sigma_{up} = \sigma_{cc} - (\sigma_{cc} - \sigma_{ul})\left[\frac{L/r}{(L/r)_1}\right]^2 \tag{68a}$$

It may happen that the slenderness $(L/r)_1$ is larger than the interaction slenderness $(L/r)_{in}$ in figure 8. This is illustrated in figure 9. In such a case the ultimate load is determined by σ_{cr1} and by σ_{up} from equation (68) only, and not by the curve for σ_u.

Application to test columns with H-section.- The formulas for σ_u and σ_{up} were used to calculate the ultimate stress of the 75S-T6 aluminum-alloy H-sections used in the tests, of which the pertinent data are given in table 1. The dimensions b and b' in the table refer to distances center to center of the plates, as indicated in figure 10. Factors k_f in equation (1) for σ_{cr1} were found from figure 2 of reference 8. The critical stress σ_{cr2} for the mode of plate buckling which is superimposed during column buckling is given by equation (2) in which $\beta = a/b$ refers to the half wave length of local buckling before column buckling. This half wave length was determined for the "L"-series columns on page 44 of reference 1 and was found to be equal to twice the web width, which in the present paper is denoted as b', so that $a/b' = 2$. The same ratio a/b' is found for the "J"- and "K"-series columns. Since for all series $b'/b = 1.24$, the ratio $\beta = a/b$ in equation (2) is $(a/b')(b'/b) = 2.48$. Hence from equation (2)

$$\sigma_{cr2} = 1.50 \frac{\pi^2 N_f}{b^2 t_f} \tag{69}$$

so that the ratio $\alpha = \sigma_{cr2}/\sigma_{cr1}$, or, from equations (1) and (69), $\alpha = 1.50/k_f$, may be calculated. The crushing strength σ_{cc} in table 1 was found from figure 18(b) of reference 13, using the average yield stress $\sigma_{cy} = 83{,}000$ psi of the column material. Constants P and Q in equation (60) are functions of the cross-sectional dimensions only and may be calculated from equations (56) and (57).

Using the values of table 1 in equation (60) one finds the following expressions for σ_u: For "J"-series columns

$$\sigma_u = (22{,}650 + 0.0846\sigma_E)\left[1 + \sqrt{1 + \frac{248{,}000\sigma_E}{(212{,}000 + 0.792\sigma_E)^2}}\right] \text{ psi} \tag{70}$$

for "K"-series columns

$$\sigma_u = (12{,}150 + 0.0846\sigma_E)\left[1 + \sqrt{1 + \frac{165{,}000\sigma_E}{(113{,}500 + 0.792\sigma_E)^2}}\right] \text{ psi} \tag{71}$$

and for "L"-series columns

$$\sigma_u = \left(8{,}080 + 0.0845\sigma_E\right)\left[1 + \sqrt{1 + \frac{77{,}000\sigma_E}{\left(74{,}300 + 0.776\sigma_E\right)^2}}\right] \text{ psi} \qquad (72)$$

Curves for σ_u are given in figure 11 by the unbroken lines.

Equations (70), (71), and (72), in which the terms in the square brackets are practically constant, may be written sufficiently accurately as follows:

For the "J" series

$$\sigma_u = \left(47{,}100 + 0.176\sigma_E\right) \text{ psi} \qquad (73)$$

for the "K" series

$$\sigma_u = \left(26{,}200 + 0.183\sigma_E\right) \text{ psi} \qquad (74)$$

and for the "L" series

$$\sigma_u = \left(17{,}100 + 0.179\sigma_E\right) \text{ psi} \qquad (75)$$

so that, in equations (66), (67), (68), and (68a), for the "J" series

$$p = 47{,}100 \text{ psi}$$

$$q_1 = 0.176$$

for the "K" series

$$p = 26{,}200 \text{ psi}$$

$$q_1 = 0.183$$

and for the "L" series

$$p = 17{,}100 \text{ psi}$$

$$q_1 = 0.179$$

Hence from equations (66), (68), and (68a) and table 1, for the "J" series

$$\sigma_{up} = \left[60{,}500 - \left(254 \times 10^6/\sigma_E\right)\right] \text{ psi}$$

$$= \left[60{,}500 - 2.46(L/r)^2\right] \text{ psi} \tag{76}$$

for the "K" series

$$\sigma_{ul} = 39{,}350 \text{ psi} \tag{77}$$

$$\sigma_{up} = \left[52{,}500 - 8.73(L/r)^2\right] \text{ psi} \tag{78}$$

and for the "L" series

$$\sigma_{ul} = 31{,}800 \text{ psi} \tag{79}$$

$$\sigma_{up} = \left[46{,}600 - 11.75(L/r)^2\right] \text{ psi} \tag{80}$$

This is shown graphically by the unbroken curves in figure 11. The graph for the "J" series has the shape sketched in figure 9, so that only σ_{crl} and σ_{up} are governing here. This may be understood in such a way that, although the local buckling stress σ_{crl} is still in the elastic range, in the postbuckling region plastic deformation occurs before column buckling.

Similar curves have been calculated by using the clear distances b_{clear} and b_{clear}' of the cross sections, as indicated in figure 10. They are given by the dotted curves in figure 11.

Ultimate Strength of Tubes with Square Cross Section

Energy equations by method of split rigidities.- The cross section of a square tube will deform by plate buckling, as shown in figure 12(a) for the crest of the waves. The plate deflections w_1 will cause a distribution of the compressive stresses σ_1 as indicated in figure 12(b). When the compressive force and the deflections w_1 increase, a situation will be reached where the tube will buckle as a column. If no extra plate deflections would occur, incipient column buckling would cause bending stresses Ey'/ρ, where ρ is the radius of curvature of the column deflection. However, the bending stresses σ_2' (figs. 12(d) and 12(e)) will cause extra plate deflections as indicated in figure 12(c) by w_{2a}' (a for asymmetrical) for plate AB and by w_{2s}' (s for symmetrical) for plate BC. The deflections w_{2a}' and w_{2s}' cause decreases of bending stress, as indicated in figures 12(d) and 12(e). At the corners, where $w_{2a}' = w_{2s}' = 0$, the bending stresses remain $Eb/(2\rho)$. The infinitely small extra plate deflections w_2' occurring with incipient column buckling are sketched separately in figure 12(f).

Using exactly the same reasoning as given for H-sections, one arrives again at the result that the average column buckling stress σ_u is determined by the two equations (8) and (15). Since here in all plates membrane stresses σ_{ym} also arise, equivalent stresses $(\sigma_1)_{eq}$ and $(\sigma_2')_{eq}$ have to be used throughout instead of the actual stresses σ_1 and σ_2'. In the present case all wall thicknesses are equal, so that equations (8) and (15) become

$$\oint (\sigma_1)_{eq} w_1^2 \, dy_1 = \sigma_{cr1} \oint w_1^2 \, dy_1 \tag{81}$$

$$\oint (\sigma_1)_{eq} (w_2')^2 \, dy_1 + \oint (\sigma_2')_{eq} w_1 w_2' \, dy_1 = \sigma_{cr2} \oint (w_2')^2 \, dy_1 \tag{82}$$

The stresses σ_1 and σ_2' and the deflections w_1 and w_2' are indicated in figure 12.

Derivation of formulas for stresses.- Obviously, σ_{cr1} in equation (81) is the plate-buckling stress for the tube. Since the webs do not restrain each other, this is from reference 14

$$\sigma_{cr1} = 4 \frac{\pi^2 N}{b^2 t} \tag{83}$$

where N is the flexural rigidity of the plates.

Similarly as for H-sections, σ_{cr2} is the compressive stress required for buckling in the mode determined by the extra deflections w_2', as sketched for the tube in figure 12(f). Furthermore σ_{cr2} has to be calculated for the same half wave length a as that of the original plate buckling as sketched in figure 12(a), that is, for $a = b$.

The mode of buckling in figure 12(f) is similar to that of a column with a cross section as given in figure 12(g), of which the narrower plates are simply supported at G and H. Formulas for the buckling stress of such columns were derived in reference 5. Calculating the buckling stress from these formulas it was found in equation (106) of reference 1 that

$$\sigma_2 = 4.84E(t/b)^2 = 5.34 \frac{\pi^2 N}{b^2 t}$$

if a Poisson's ratio of 0.3 is assumed. However, this is the critical stress for the optimum half wave length of buckling, while σ_{cr2} has to be calculated for a half wave length $a = b$. The buckling condition for this case is given by equation (49) of reference 5

$$\alpha_1 \tanh\left(\alpha_1 \frac{b}{2}\right) + \alpha_2 \tan\left(\alpha_2 \frac{b}{2}\right) + \left(\alpha_1^2 + \alpha_2^2\right)\theta = 0 \tag{84}$$

where θ is given by equation (48) of reference 5. In the present case the thicknesses of the buckling plate BC and the restraining plates GB and HC are equal, so that, in equation (48) of reference 5, $h = h'$. Hence

$$\theta = \frac{\alpha_1' \coth \alpha_1' b' - \alpha_2' \cot \alpha_2' b'}{\left(\alpha_1'\right)^2 + \left(\alpha_2'\right)^2} \tag{85}$$

The width b' of the restraining plates GB and HC is equal to b/2. Furthermore, from the equations below equation (61) in reference 5, in the elastic range and with the present notations

$$\alpha_{1,2} = \sqrt{\pm\lambda^2 + \lambda\sqrt{t\sigma_{cr2}/N}} \tag{86}$$

where

$$\lambda = \frac{\pi}{a} = \frac{\pi}{b} \tag{87}$$

and[1]

$$\alpha_{1,2}' = \sqrt{\pm\lambda^2 + \lambda\sqrt{t'\sigma_{cr2}/N'}} \tag{88}$$

Since here $t' = t$,

$$\alpha_{1,2}' = \alpha_{1,2} \tag{89}$$

Hence, using equation (85), equation (84) becomes

$$\alpha_1 \tanh\left(\alpha_1 \frac{b}{2}\right) + \alpha_2 \tan\left(\alpha_2 \frac{b}{2}\right) = \alpha_2 \cot\left(\alpha_2 \frac{b}{2}\right) - \alpha_1 \coth\left(\alpha_1 \frac{b}{2}\right) \tag{90}$$

By trial and error it follows from this equation that

$$\sigma_{cr2} = 5.75 \frac{\pi^2 N}{b^2 t} \tag{91}$$

The same result is obtained by using the tables of reference 7, which are based on the same equations, but the above equations will also be used to find the equations for w_{2s}' and w_{2a}'.

---

[1]Because of a printing error in reference 5 two of the primes in the present equation (88) were omitted.

The variables σ_1, σ_2', w_1, and w_2' in equations (81) and (82) may be expressed in terms of the maximum deflections w_{1m} and w_{2m}' and the abscissas of the pertinent points to which they refer (fig. 12(c)). In the same way as was found in equations (19) and (20) for H-sections, the stresses σ_1 (fig. 12(b)) are

$$\sigma_1 = \sigma_m - \frac{\pi^2 E}{4b^2} w_1^2 \tag{92}$$

since here the half wave length $a = b$. As far as the influence of the membrane stresses σ_y is concerned, the plates are here in the same condition as the web of an H-section, so that, analogous to equation (31) and with $a = b$, the equivalent stress $(\sigma_1)_{eq}$ to be used in equations (81) and (82) is

$$(\sigma_1)_{eq} = \sigma_m - \gamma \frac{\pi^2 E}{4b^2} w_1^2 \tag{93}$$

where $\gamma = 1.13$ from equation (30). Analogous to equation (32), for the plates AB and CD (fig. 12(c)), with $a = b$ (fig. 12(d))

$$\sigma_{2a}' = \frac{E}{\rho} y' - \frac{\pi^2 E}{2b^2} w_1 w_{2a}' \tag{94}$$

For the plates BC and DA, $y' = b/2$, so that (figs. 12(c) and 12(e))

$$\sigma_{2s}' = \frac{Eb}{2\rho} - \frac{\pi^2 E}{2b^2} w_1 w_{2s}' \tag{95}$$

As far as the membrane stresses σ_y are concerned, the plates BC and DA are in about the same condition as in case of the initial deflections w_1, so that, in determining the total work done, they can be taken into account by using in equation (82) equivalent stresses

$$(\sigma_{2s}')_{eq} = \frac{Eb}{2\rho} - \gamma \frac{\pi^2 E}{2b^2} w_1 w_{2s}' \tag{96}$$

The plates AB and CD are in a different position. From equation (94) in the X-direction the deflection w_{2a}' causes extra membrane tensile stresses

$$\sigma_{xm}' = \frac{\pi^2 E}{2b^2} w_1 w_{2a}' \tag{97}$$

where w_1 and w_{2a}' are the deflections at the crest of the waves (at $x = 0$ in fig. 13(a)). These stresses σ_{xm}' are zero for $y' = 0$ and $y' = \pm b/2$, where w_{2a}' and w_1 are zero, respectively. From reference 4 the deflection w_1 may be assumed to have the same shape as with incipient buckling, so that

$$w_1 = w_{1m} \cos \frac{\pi}{b} x \cos \frac{\pi}{b} y' \tag{98}$$

and at $x = 0$

$$w_1 = w_{1m} \cos \frac{\pi}{b} y' \tag{98a}$$

At point K (fig. 13(a)) for $x = 0$ and $y' = b/4$, from equation (98a) $w_1 = 0.71 w_{1m}$. Denoting w_{2a}' at this point as w_{2ak}', from equation (97)

$$\left(\sigma_{xm}'\right)_{y'=b/4} = 0.355 \frac{\pi^2}{b^2} E w_{1m} w_{2ak}' \tag{99}$$

The extra membrane stresses σ_{ym}' caused by the extra deflections w_{2a}' have relatively little influence. The equivalent membrane stresses σ_{xm}' may be approximated as follows. If at $y' = 0$ and $y' = \pm b/2$ no displacement in the Y'-direction were possible, the increase w_{2ak}' of the deflection $0.21 w_{1m}$ of a strip at $x = 0$ with

respect to the straight line G_1B would cause a dilation of that strip, which, from equation (18), is

$$\delta = \frac{\pi^2}{4\frac{b}{2}}\left[\left(0.21w_{1m} + w_{2ak}'\right)^2 - \left(0.21w_{1m}\right)^2\right]$$

With the same assumptions that were used in deriving equations (19) and (20) and considering that w_{2ak}' is infinitely small, this leads to membrane tensile stresses at $x = 0$ and $y' > 0$ of

$$\left(\sigma_{ym}'''\right)_{x'=0} = E\frac{\delta}{b/2} = 0.42\frac{\pi^2}{b^2}Ew_{1m}w_{2ak}' \tag{100}$$

Since w_{1m} and w_{2a}' vary sinusoidally in the X-direction, in general for $y' > 0$ (fig. 13(c))

$$\sigma_{ym}''' = 0.42\frac{\pi^2}{b^2}Ew_{1m}w_{2ak}'\cos^2\frac{\pi}{b}x$$

$$= 0.21\frac{\pi^2}{b^2}Ew_{1m}w_{2ak}'\left(1 + \cos\frac{2\pi}{b}x\right) \tag{101}$$

Equal and opposite stresses σ_{ym}''' would occur for $y' < 0$.

In reality at $y' = 0$ and $y' = \pm b/2$ the plate is free to move in the Y'-direction. If at the same time the lines $y' = 0$ and $y' = \pm b/2$ were held straight $\int\sigma_{ym}''\,dx$ would become zero, so that from equation (101) for $y' > 0$

$$\sigma_{ym}'' = 0.21\frac{\pi^2}{b^2}Ew_{1m}w_{2ak}'\cos\frac{2\pi}{b}x \tag{102}$$

as shown in figures 13(d) and 13(f).

Actually the lines $y' = 0$ and $y' = \pm b/2$ are not held straight, so that at $y' = \pm b/2$ and, from symmetry, at $y' = 0$, $\sigma_{ym}' = 0$. This case may be obtained from the former one by superimposing, for example for $y' > 0$, stresses $\sigma_y = -\sigma_{ym}''$ at $y' = 0$ and $y' = b/2$, which may be denoted as compressive stresses (fig. 13(h))

$$\left(\sigma_{y1}''\right)_{y'=0} = \left(\sigma_{y1}''\right)_{y'=b/2} = A \cos \frac{2\pi}{b} x \tag{103}$$

This superimposed case is identical to that in reference 15, page 47, from which it follows that at $y' = b/4$

$$\sigma_{y1}'' = 2A \frac{jc \cosh jc + \sinh jc}{\sinh 2jc + 2jc} \cos \frac{2\pi}{b} x \tag{104}$$

where $j = 2\pi/b$ and $c = b/4$, so that at $y' = b/4$ (fig. 13(h))

$$\sigma_{y1}'' = 0.85A \cos \frac{2\pi}{b} x \tag{105}$$

By superimposing these stresses upon the tensile stresses σ_{ym}'' the actual membrane stresses σ_{ym}' are obtained, as shown in figures 13(e) and 13(g). Hence at point K, for $x = 0$ and $y' = b/4$,

$$\left(\sigma_{ym}'\right)_k = 0.15\sigma_{ym}'' = 0.0315 \frac{\pi^2}{b^2} w_{1m} w_{2ak}' \cos \frac{2\pi}{b} x \tag{106}$$

so that from equation (99)

$$\left(\sigma_{ym}'\right)_k = 0.089\left(\sigma_{xm}'\right)_{y'=b/4} \tag{107}$$

Since w_2' is infinitely small with respect to w_1, from equation (98) the deflecting forces $-t\sigma_{xm}' \partial^2 w_1/\partial x^2$ and $-t\sigma_{ym}' \partial^2 w_1/(\partial y')^2$, caused by membrane stresses σ_{xm}' and σ_{ym}', respectively, are equal to $t\sigma_{xm}'\left(\frac{\pi^2}{b^2}\right)w_1$ and $t\sigma_{ym}'\left(\frac{\pi^2}{b^2}\right)w_1$, respectively. Hence membrane stresses σ_{ym}' are equivalent to membrane stresses σ_{xm}' of the same magnitude, since they cause equal deflecting forces.

From equation (97), σ_{xm}' does not vary in the X'-direction. In the Y'-direction it varies proportionally to $w_1 w_{2a}'$. The membrane stresses σ_{ym}' vary as shown in figures 13(e) and 13(g). About similar distributions of σ_{xm}' and σ_{ym}' as occur here in the area $b/2 > x > -b/2$, $b/2 > y' > 0$, prevail in the area of a square buckle of a compressed plate that is simply supported and free to move laterally at the unloaded edges, such as the web of H-sections and the plates of square tubes. For that case it was found in equation (29) that the influence of the membrane stresses σ_{ym} could be taken into account by multiplying the membrane stresses σ_{xm} by 1.13, so that the influence of the stresses σ_{ym} was 0.13 times that of the stresses σ_{xm}. Also in this case from equation (98) the deflecting forces $-t\sigma_{xm} \partial^2 w_1/\partial x^2$ and $-t\sigma_{ym} \partial^2 w_1/\partial y^2$ caused by equal stresses σ_{xm} and σ_{ym} are equal. In case the unloaded edges are held straight the stresses σ_{ym} follow, for example, from reference 4. The stresses σ_{ym} in case the edges are not held straight are found by superposition of loads σ_{yl}'' as was done in equation (103) in the present case. The superimposed stresses are calculated from equation (104) where now $j = 2\pi/b$ and $c = b/2$. This leads for the middle of the square buckle to a membrane stress

$$\sigma_{ym} = 0.325\sigma_{xm} \tag{108}$$

Since in this case the influence of the membrane stresses σ_{ym} is 0.13 times that of the membrane stresses σ_{xm}, in the present case, from equation (107), the influence of the stresses σ_{ym}' will be $(0.089/0.325)0.13 = 0.035$ times that of the membrane stresses σ_{xm}'.

Hence they may be taken into account by using in equations (81) and (82) equivalent stresses

$$\left(\sigma_{2a}'\right)_{eq} = \frac{E}{\rho} y' - \mu \frac{\pi^2 E}{2b^2} w_1 w_{2a}' \tag{109}$$

instead of σ_{2a}' from equation (94). Consequently

$$\mu = 1.035 \tag{110}$$

Derivation of formulas for deflections.- Finally the superimposed deflections w_{2s}' and w_{2a}' have to be expressed in terms of the maximum deflection w_{2m}' (fig. 12(c)). The form of the deflection w_2' may sufficiently accurately be assumed to be similar to that in which a column with cross section GBCH, as given in figure 12(g), buckles. In reference 5 the deflections w_{2s}' and w_{2a}' are given by equations (40) and (44), respectively, while, as pointed out on page 58 of reference 5, for the present case in equation (40) $C_2 = C_4 = 0$ and in equation (44) $C_1' = C_3' = 0$, so that

$$w_{2s}' = \left(C_1 \cosh \alpha_1 y + C_3 \cos \alpha_2 y\right) \cos \frac{\pi}{a} x \tag{111}$$

$$w_{2a}' = \left(C_2' \sinh \alpha_1' y' + C_4' \sin \alpha_2' y'\right) \cos \frac{\pi}{a} x \tag{112}$$

Considering w_{2s}' first, from equation (111) the condition that $w = 0$ at $y = b/2$ yields

$$C_1 = - \frac{\cos\left(\alpha_2 \frac{b}{2}\right)}{\cosh\left(\alpha_1 \frac{b}{2}\right)} C_3$$

so that, since here $a = b$,

$$w_{2s}' = C_3\left[\cos \alpha_2 y - \frac{\cos\left(\alpha_2 \frac{b}{2}\right)}{\cosh\left(\alpha_1 \frac{b}{2}\right)} \cosh \alpha_1 y\right] \cos \frac{\pi}{b} x \tag{113}$$

From equations (86), (87), and (91) of the present paper

$$\left.\begin{aligned} \alpha_1 &= 1.844 \frac{\pi}{b} \\ \alpha_2 &= 1.183 \frac{\pi}{b} \end{aligned}\right\} \tag{114}$$

Inserting these in equation (113) results in

$$w_{2s}' = C_3\left(\cos 1.183 \frac{\pi}{b} y + 0.03116 \cosh 1.844 \frac{\pi}{b} y\right) \cos \frac{\pi}{b} x \tag{115}$$

At $y = 0$, from equation (115), $w_{2s}' = 1.03116C_3 = w_{2m}'$ (fig. 12(c)), so that $C_3 = 0.96978w_{2m}'$, and from equation (115)

$$w_{2s}' = 0.96978w_{2m}'\left(\cos 1.183 \frac{\pi}{b} y + 0.03116 \cosh 1.844 \frac{\pi}{b} y\right) \cos \frac{\pi}{b} x \tag{116}$$

From equation (112) the condition that $w = 0$ at $y' = b/2$ leads to the relation

$$C_2' = -\frac{\sin\left(\alpha_2' \frac{b}{2}\right)}{\sinh\left(\alpha_1' \frac{b}{2}\right)} C_4'$$

From equation (89) $\alpha_{1,2}' = \alpha_{1,2}$, so that, from equation (112), with $a = b$,

$$w_{2a}' = C_4' \left[\sin \alpha_2 y' - \frac{\sin\left(\alpha_2 \frac{b}{2}\right)}{\sinh\left(\alpha_1 \frac{b}{2}\right)} \sinh \alpha_1 y' \right] \cos \frac{\pi}{b} x \qquad (117)$$

or, from equations (114),

$$w_{2a}' = C_4' \left(\sin 1.183 \frac{\pi}{b} y' - 0.10583 \sinh 1.844 \frac{\pi}{b} y' \right) \cos \frac{\pi}{b} x \qquad (118)$$

At B (fig. 12(c)) continuity requires that

$$-\left(\partial w_{2a}'/\partial y'\right)_{y'=b/2} = -\left(\partial w_{2s}'/\partial y\right)_{y=b/2} \qquad (119)$$

Using equations (116) and (118) this gives

$$C_4' = 0.28145 w_{2m}' \qquad (120)$$

so that from equation (118)

$$w_{2a}' = 0.28145 w_{2m}' \left(\sin 1.183 \frac{\pi}{b} y' - 0.10583 \sinh 1.844 \frac{\pi}{b} y' \right) \cos \frac{\pi}{b} x \qquad (121)$$

Solving of energy equations.- All variables in equations (81) and (82) have now been expressed in terms of the maximum deflections w_{1m} and w_{2m}' (fig. 12(c)) and of the abscissas of the pertinent points. For reasons of symmetry (fig. 12(a)) in equation (81) it is sufficient to integrate over one-half wall only, so that for square tubes equation (81) becomes

$$\int_0^{b/2} (\sigma_1)_{eq} w_1^2 \, dy = \sigma_{crl} \int_0^{b/2} w_1^2 \, dy \tag{122}$$

The deflections w_2' are symmetrical with respect to the Z-axis (fig. 12(c)). Furthermore, for negative values of y' the values of σ_2' and w_2' are both equal and opposite to those for positive values of y', so that all terms in equation (82) are symmetrical with respect to the Z'-axis (fig. 12(c)). Hence in equation (82) it is sufficient to integrate over one-half wall AB and one-half wall BC only, by which equation (82) becomes

$$\int_0^{b/2} (\sigma_1)_{eq} (w_{2s}')^2 \, dy + \int_0^{b/2} (\sigma_{2s}')_{eq} w_1 w_{2s}' \, dy +$$

$$\int_0^{b/2} (\sigma_1)_{eq} (w_{2a}')^2 \, dy' + \int_0^{b/2} (\sigma_{2a}')_{eq} w_1 w_{2a}' \, dy' =$$

$$\sigma_{cr2} \left[\int_0^{b/2} (w_{2s}')^2 \, dy + \int_0^{b/2} (w_{2a}')^2 \, dy' \right] \tag{123}$$

From equation (122), using equations (93) and (98a),

$$w_{1m}^2 \left(\sigma_m \int_0^{b/2} \cos^2 \frac{\pi}{b} y \, dy - \frac{\pi^2 E}{4b^2} \gamma w_{1m}^2 \int_0^{b/2} \cos^4 \frac{\pi}{b} y \, dy \right) =$$

$$w_{1m}^2 \sigma_{crl} \int_0^{b/2} \cos^2 \frac{\pi}{b} y \, dy \tag{124}$$

from which

$$\frac{\pi^2 E}{b^2} w_{1m}^2 = \frac{16}{3\gamma}\left(\sigma_m - \sigma_{cr1}\right) \tag{125}$$

or

$$w_{1m} = \frac{b}{\pi}\left[\frac{16}{3\gamma E}\left(\sigma_m - \sigma_{cr1}\right)\right]^{1/2} \tag{126}$$

From equation (123), using equations (93), (96), (98a), (109), (113), and (121),

$$\sigma_m \int_0^{b/2} \left(w_{2s}'\right)^2 dy + \frac{Eb}{2\rho} \int_0^{b/2} w_1 w_{2s}' \, dy -$$

$$\frac{3\pi^2 E}{4b^2} \gamma \int_0^{b/2} w_1^2 \left(w_{2s}'\right)^2 dy + \sigma_m \int_0^{b/2} \left(w_{2a}'\right)^2 dy' +$$

$$\frac{E}{\rho} \int_0^{b/2} w_1 w_{2a}' y' \, dy' - \frac{\pi^2 E}{4b^2} (\gamma + 2\mu) \int_0^{b/2} w_1^2 \left(w_{2a}'\right)^2 dy' =$$

$$\sigma_{cr2}\left[\int_0^{b/2} \left(w_{2s}'\right)^2 dy + \int_0^{b/2} \left(w_{2a}'\right)^2 dy'\right] \tag{127}$$

where

$$\int_0^{b/2} \left(w_{2s}'\right)^2 dy = 0.94047\left(w_{2m}'\right)^2\left(\int_0^{b/2} \cos^2 A \frac{\pi}{b} y \, dy + \right.$$

$$0.0009709 \int_0^{b/2} \cosh^2 B \frac{\pi}{b} y \, dy +$$

$$\left. 0.06232 \int_0^{b/2} \cos A \frac{\pi}{b} y \cosh \frac{\pi}{b} y \, dy\right) \tag{127a}$$

$$\int_0^{b/2} w_1 w_{2s}' \, dy = 0.96978 w_{1m} w_{2m}' \left(\int_0^{b/2} \cos \frac{\pi}{b} y \cos A \frac{\pi}{b} y \, dy + 0.03116 \int_0^{b/2} \cos \frac{\pi}{b} y \cosh B \frac{\pi}{b} y \, dy \right) \quad (127b)$$

$$\int_0^{b/2} w_1^2 (w_{2s}')^2 \, dy = 0.94047 w_{1m}^2 (w_{2m}')^2 \left(\int_0^{b/2} \cos^2 \frac{\pi}{b} y \cos^2 A \frac{\pi}{b} y \, dy + 0.0009709 \int_0^{b/2} \cos^2 \frac{\pi}{b} y \cosh^2 B \frac{\pi}{b} y \, dy + 0.06232 \int_0^{b/2} \cos^2 \frac{\pi}{b} y \cos A \frac{\pi}{b} y \cosh B \frac{\pi}{b} y \, dy \right) \quad (127c)$$

$$\int_0^{b/2} (w_{2a}')^2 \, dy' = 0.079214 (w_{2m}')^2 \left(\int_0^{b/2} \sin^2 A \frac{\pi}{b} y' \, dy' + 0.0112 \int_0^{b/2} \sinh^2 B \frac{\pi}{b} y' \, dy' - 0.21166 \int_0^{b/2} \sin A \frac{\pi}{b} y' \sinh B \frac{\pi}{b} y' \, dy' \right) \quad (127d)$$

$$\int_0^{b/2} w_1 w_{2a}' y' \, dy' = 0.28145 w_{1m} (w_{2m}')^2 \left(\int_0^{b/2} y' \cos \frac{\pi}{b} y' \sin A \frac{\pi}{b} y' \, dy' - 0.10583 \int_0^{b/2} y' \cos \frac{\pi}{b} y' \sinh B \frac{\pi}{b} y' \, dy' \right) \quad (127e)$$

$$\int_0^{b/2} w_1^2 \left(w_{2a}'\right)^2 dy' = 0.079214 w_{1m}^2 \left(w_{2m}'\right)^2 \left(\int_0^{b/2} \cos^2 \frac{\pi}{b} y' \sin^2 A \frac{\pi}{b} y' \, dy' + \right.$$

$$0.0112 \int_0^{b/2} \cos^2 \frac{\pi}{b} y' \sinh^2 B \frac{\pi}{b} y' \, dy' -$$

$$\left. 0.21166 \int_0^{b/2} \cos^2 \frac{\pi}{b} y' \sin A \frac{\pi}{b} y' \sinh B \frac{\pi}{b} y' \, dy' \right) \tag{127f}$$

where $A = 1.183$ and $B = 1.844$. After evaluating the integrals

$$\left.
\begin{aligned}
&\int_0^{b/2} \left(w_{2s}'\right)^2 dy = k_1 \left(w_{2m}'\right)^2 b \\
&\int_0^{b/2} w_1 w_{2s}' \, dy = 2k_2 w_{1m} w_{2m}' b \\
&\int_0^{b/2} w_1^2 \left(w_{2s}'\right)^2 dy = k_3 w_{1m}^2 \left(w_{2m}'\right)^2 b \\
&\int_0^{b/2} \left(w_{2a}'\right)^2 dy' = k_4 \left(w_{2m}'\right)^2 b \\
&\int_0^{b/2} w_1 w_{2a}' y' \, dy' = k_5 w_{1m} w_{2m}' b^2 \\
&\int_0^{b/2} w_1^2 \left(w_{2a}'\right)^2 dy' = k_6 w_{1m}^2 \left(w_{2m}'\right)^2 b
\end{aligned}
\right\} \tag{128}$$

in which

$$\left.\begin{aligned} k_1 &= 0.22910 \\ k_2 &= 0.11938 \\ k_3 &= 0.17794 \\ k_4 &= 0.00753 \\ k_5 &= 0.00786 \\ k_6 &= 0.00323 \end{aligned}\right\} \tag{129}$$

Insertion of equations (128) in equation (127) yields

$$\left(k_2 + k_5\right)\frac{E}{\rho} w_{1m} w_{2m}' b^2 - \left[3k_3\gamma + k_6(\gamma + 2\mu)\right]\frac{\pi^2 E}{4b^2} w_{1m}^2 \left(w_{2m}'\right)^2 b - \left(k_1 + k_4\right)\left(\sigma_{cr2} - \sigma_m\right) b \left(w_{2m}'\right)^2 = 0 \tag{130}$$

Using equation (125) this results in

$$\beta' = \frac{w_{2m}'}{w_{1m}} = \frac{\left(k_2 + k_5\right) E \frac{b}{\rho}}{(4/3\gamma)\left[3k_3\gamma + k_6(\gamma + 2\mu)\right]\left(\sigma_m - \sigma_{cr1}\right) + \left(k_1 + k_4\right)\left(\sigma_{cr2} - \sigma_m\right)} \tag{131}$$

Calculation of postbuckling column modulus and of ultimate strength.- The total internal moment at incipient column buckling is

$$M_c = 4(b/2)\int_0^{b/2} t\sigma_{2s}' \, dy + 4\int_0^{b/2} t\sigma_{2a}' y' \, dy' \tag{132}$$

Using equations (94) and (95) this becomes

$$M_c = \frac{2}{3}\frac{E}{\rho} b^3 t - \frac{\pi^2 E t}{b^2}\left(b\int_0^{b/2} w_1 w_{2s}'\, dy + 2\int_0^{b/2} w_1 w_{2a}'y'\, dy'\right) \quad (133)$$

and using equations (125), (128), and (131)

$$M_c = 2b^2 t\left[\frac{1}{3}\frac{Eb}{\rho} - \frac{16}{3\gamma}\left(k_2 + k_5\right)\left(\sigma_m - \sigma_{cr1}\right)\beta'\right] \quad (134)$$

If the column had a constant equivalent postbuckling modulus $E_{1,eq}$ the internal moment would be

$$M_c = \frac{E_{1,eq} I}{\rho} = \frac{2}{3} b^3 t \frac{E_{1,eq}}{\rho} \quad (135)$$

From equations (134) and (135) and using equations (30), (110), (129), and (131)

$$E_{1,eq} = \frac{2.09\left(\sigma_m - \sigma_{cr1}\right) + \left(\sigma_{cr2} - \sigma_m\right)}{3.055\left(\sigma_m - \sigma_{cr1}\right) + \left(\sigma_{cr2} - \sigma_m\right)} E \quad (136)$$

The relation between the edge stress σ_m and the average stress σ_{av} is given by equation (22), which applies for the webs of the tubes as well and where now $\sigma_{cr} = \sigma_{cr1}$. Since now σ_{av} is the ultimate stress σ_u, it may be written as

$$\sigma_m - \sigma_{cr1} = 2.44\left(\sigma_u - \sigma_{cr1}\right) \quad (137)$$

Inserting this in equation (136) gives

$$\frac{E_{1,eq}}{E} = \frac{P(\sigma_u - \sigma_{cr1}) + (\sigma_{cr2} - \sigma_{cr1})}{Q(\sigma_u - \sigma_{cr1}) + (\sigma_{cr2} - \sigma_{cr1})} \tag{55}$$

analogous to the previous equation (55), where now

$$\left.\begin{aligned} P &= 2.66 \\ Q &= 5.01 \end{aligned}\right\} \tag{138}$$

Hence, similarly to the case of H-sections, the ultimate stress is given by equation (60):

$$\sigma_u = \left(\frac{Q+1-\alpha}{2Q}\sigma_{cr1} + \frac{P}{2Q}\sigma_E\right)\left(1 + \left\{1 - \frac{4Q(P+1-\alpha)}{\left[(Q+1-\alpha)\sigma_{cr1} + P\sigma_E\right]^2}\sigma_E\sigma_{cr1}\right\}^{1/2}\right) \tag{60}$$

where P and Q are given by equations (138) and

$$\alpha = \sigma_{cr2}/\sigma_{cr1} \tag{61}$$

The critical stresses σ_{cr1} and σ_{cr2} are given by equations (83) and (91), so that

$$\alpha = 1.4375 \tag{139}$$

Hence

$$\sigma_u = \left(0.456\sigma_{crl} + 0.265\sigma_E\right)\left[1 + \sqrt{1 - \frac{44.60\sigma_E\sigma_{crl}}{\left(4.57\sigma_{crl} + 2.66\sigma_E\right)^2}}\right] \quad (140)$$

Column buckling in plastic range.- For tubes as for H-sections equation (140) may be written approximately in the form of equation (63), so that for column buckling in the plastic range equations (66), (67), (68), and (68a) apply.

Application to test columns with square-tube section.- The dimensions of the 61S-T6 aluminum columns (fig. 14) used in the experiments were for the "D" series $b_{out} = 2.5$ inches and $t = 0.046$ inch and for the "E" series $b_{out} = 3$ inches and $t = 0.044$ inch. Hence the center-to-center distances b of the webs are 2.454 inches and 2.956 inches, respectively. Thus from equation (83) for "D" and "E" series $\sigma_{crl} = 13{,}600$ and $8{,}560$ psi, respectively, so that from equation (140) for the "D" series columns

$$\sigma_u = \left(6{,}200 + 0.265\sigma_E\right)\left[1 + \sqrt{1 - \frac{608{,}000\sigma_E}{\left(62{,}200 + 2.66\sigma_E\right)^2}}\right] \text{ psi} \quad (141)$$

and for the "E" series columns

$$\sigma_u = \left(3{,}900 + 0.265\sigma_E\right)\left[1 + \sqrt{1 - \frac{382{,}000\sigma_E}{\left(39{,}200 + 2.66\sigma_E\right)^2}}\right] \text{ psi} \quad (142)$$

or, approximately, for the "D" series

$$\sigma_u = \left(8{,}050 + 0.345\sigma_E\right) \text{ psi} \quad (143)$$

and for the "E" series

$$\sigma_u = \left(5{,}070 + 0.345\sigma_E\right) \text{ psi} \quad (144)$$

Hence in equations (66), (67), and (68), for the "D" series $p = 8{,}050$ psi and $q_1 = 0.345$ and for the "E" series $p = 5{,}070$ psi and $q_1 = 0.345$:

The crushing strength σ_{cc} was found from figure 18(d) of reference 13, using for the "D" and "E" series the averaged yield stresses of 43,500 and 39,500 psi, respectively, from which σ_{cc} is 22,600 and 18,600 psi, respectively. Hence from equations (66) and (68), for the "D" series

$$\sigma_{ul} = 15{,}320 \text{ psi} \tag{145}$$

$$\sigma_{up} = \left[22{,}600 - 1.45(L/r)^2\right] \text{ psi} \tag{146}$$

and for the "E" series

$$\sigma_{ul} = 11{,}830 \text{ psi} \tag{147}$$

$$\sigma_{up} = \left[18{,}600 - 1.24(L/r)^2\right] \text{ psi} \tag{148}$$

Curves for σ_u and σ_{up} for the "D" and "E" series are given in figure 15 as functions of L/r.

If instead of center distances the clear distances between the plates are considered as the width b of the plates, that is for the "D" and "E" series $b = b_{clear} = 2.408$ inches and 2.912 inches, respectively, the dotted curves in figure 15 apply.

Effect of Crookedness of Column on Load-Deflection Curve

In the postbuckling range a simply supported and initially straight column will buckle in a half sine wave under a load $A\sigma_u$, where from equation (58)

$$\sigma_u = \frac{\pi^2 E_{1,eq}}{(L/r)^2} \tag{58}$$

Here the postbuckling modulus $E_{1,eq}$ is given by equation (55). Since at incipient buckling the external moment $M_e = A\sigma_u w$ (fig. 16(a)) for any cross section is equal to the internal moment M_i, the internal moment is likewise

$$M_i = A\sigma_u w \tag{149}$$

A column with initial deflections w_i is considered next (fig. 16(b)). Under a load $A\sigma_a$ an excess elastic deflection w_e will occur. From equation (149) under a load $A\sigma_u$ an elastic deflection according to a sine wave causes internal moments $A\sigma_u w$, where σ_u is given by equation (58). Assuming that w_i and w_e in figure 16(b) also vary sinusoidally, the deflection w_e would cause internal moments $M_i = A\sigma_u w_e$ if the postbuckling modulus would be the same for the initially straight column. However, since the average stress σ_{av} is here smaller than σ_u, the postbuckling modulus $E_{1,eq}$ is now found by replacing σ_u by σ_{av} in equation (55). Thus, from equation (55)

$$E_{1,eq} = \frac{P(\sigma_{av} - \sigma_{cr1}) + (\sigma_{cr2} - \sigma_{cr1})}{Q(\sigma_{av} - \sigma_{cr1}) + (\sigma_{cr2} - \sigma_{cr1})} \tag{150}$$

Hence the internal moment is (fig. 16(b))

$$M_i = A\sigma_u w_e = A\sigma_u(w - w_i) \tag{151}$$

where σ_u is given by equation (58) in which $E_{1,eq}$ is determined by equation (150). The external moment is

$$M_e = A\sigma_{av} w \tag{152}$$

Since $M_e = M_i$, from equations (151) and (152)

$$\sigma_{av}w = \sigma_u(w - w_i)$$

or

$$w = \frac{\sigma_u/\sigma_{av}}{(\sigma_u/\sigma_{av}) - 1} w_i \tag{153}$$

where σ_{av} is the average stress in the column and σ_u is given by equations (58) and (150).

For example, consider a column with a square tube section of the "E" series, where, from equations (138) and (139), $P = 2.66$, $Q = 5.01$, and $\alpha = \sigma_{cr2}/\sigma_{cr1} = 1.4375$, while from equation (83) $\sigma_{cr1} = 8{,}560$ psi, so that from equation (150)

$$E_{1,eq} = \frac{(2.66\sigma_{av} - 19{,}000)\ \text{psi}}{(5.01\sigma_{av} - 39{,}100)\ \text{psi}} E \tag{154}$$

This equation applies if the average stresss σ_{av} is above the critical plate buckling stress σ_{cr1}. Below σ_{cr1} the buckling modulus to be inserted in equation (58) is simply $E_{1,eq} = E$. This assumes that the eccentricity is so small that it does not influence the average stress at which the plates begin to buckle. For a column with a slenderness ratio $L/r = 75$, equations (58), (150), and (153) lead to the results given in table 2 and figure 17.

It is seen from table 2 that above the critical plate buckling stress σ_{cr1} the deflection increases rapidly, owing to the sudden decrease of σ_u and σ_u/σ_{av}.

Load-deflection diagrams like that of figure 17 appeared also in the tests. At first sight such a diagram could be mistaken for that of an initially straight column, of which the resistance increases with increasing deflection. This would be in contradiction with the contention that the ultimate resistance of an initially straight column is

attained at incipient column buckling, as was explained in the introduction. It is clear from the above that actually such a diagram is due to an initial column deflection which, however, below the critical plate buckling stress σ_{crl} can hardly be detected.

Theoretical Results

For slenderness ratios larger than $(L/r)_{in}$ (fig. 8), where the column buckling strength, according to Euler or Shanley, is lower than the critical plate buckling stress σ_{crl}, the ultimate strength is determined by this unreduced column buckling strength.

For slenderness ratios between $(L/r)_1$ and $(L/r)_{in}$ (fig. 8), where plate buckling is governing, and where at all points the stresses remain in the elastic domain, the ultimate strength is given by σ_u from equation (60). In particular for H-sections, in equation (60) σ_{crl}, σ_E, P, Q, and α are given by equations (1), (59), (56), (57), and (61). For square tubes equation (60) reduces to equation (140), where σ_{crl} and σ_E are given by equations (83) and (59).

For slenderness ratios smaller than $(L/r)_1$, where plastic deformations occur, the ultimate strength is given by σ_{up}, determined by equation (68a). This is a Johnson parabola, with its apex at the crushing strength σ_{cc} of the section and tangent to the curve for σ_u at the slenderness $(L/r)_1$.

If the critical plate buckling stress is near the proportional limit, $(L/r)_1$ may be larger than $(L/r)_{in}$, in which case the ultimate strength is determined by σ_E, σ_{crl}, and σ_{up}, as is sketched in figure 9 and as is the case for series "J" of the H-sections, as shown by the unbroken lines in figure 11. If the crushing strength σ_{cc} is equal to the critical plate buckling stress σ_{crl} the ultimate strength is determined by σ_E and $\sigma_{crl} = \sigma_{cc}$ alone, as is the case for series "J" of the H-sections (fig. 11) if the plate widths are assumed to be equal to the clear distances.

The method for determining the ultimate strength as used till now in aircraft design (ref. 16) and in light-gage steel structures (refs. 17 and 18) is to draw a Johnson parabola tangent to the curve for the Euler column buckling stress σ_E with its apex at the crushing strength σ_{cc}.

As follows from the present theory, which is in excellent agreement with the test results given in the experimental part of this paper, this method can be considerably improved by interposing the curve for σ_u, as given by equation (60).

Curves for ultimate strength against slenderness ratio of the particular H-sections and square tubes used in the tests are given in figures 11 and 15, respectively. These curves are confirmed closely by experimental investigation.

EXPERIMENTAL INVESTIGATION

Description of Specimens

The specimens used for the experimental program were as follows:

(a) H-sections, extruded, of 75S-T6 aluminum alloy with the nominal dimensions shown in the order: Depth, flange width, plate thickness.

$1\frac{7}{8}$ by $2\frac{13}{16}$ inches by $\frac{1}{8}$ inch, designated "J"

$2\frac{1}{2}$ by $3\frac{13}{16}$ inches by $\frac{1}{8}$ inch, designated "K"

3 by $4\frac{5}{8}$ inches by $\frac{1}{8}$ inch, designated "L"

All H-sections had the same and constant nominal thickness for web and flange plates.

(b) Square tubes, drawn, of 61S-T6 aluminum alloy with the nominal dimensions shown.

2 by 2 inches by 0.063 inch, designated "B"

$2\frac{1}{2}$ by $2\frac{1}{2}$ inches by 0.047 inch, designated "D"

3 by 3 inches by 0.047 inch, designated "E"

All tubes were special drawings of the Aluminum Company of America with square corners and slight thickening of the walls on the inside near the corners.

Deviations from flatness, straightness, and squareness were well within tolerable limits with one exception. The series "E" square tubes

had component plates bowed outward an amount approximately equal to one-half the plate thickness. The consequences of this initial curvature are explained in a following section.

Compressive stress-strain tests for the H-sections were performed on coupon specimens by, and data therefrom supplied through the courtesy of, the Aluminum Company of America. Each of the stress-strain curves given in figure 18 is a weighted average of stress-strain curves for coupons taken from edge-of-flange, center-of-flange, and web locations and as such represents the composite stress-strain curve for the whole H-section.

Compressive stress-strain characteristics for the square tubes, as shown in figure 19, are from tests performed on complete sections with the walls supported to prevent premature local buckling. The detailed procedure for these tests was reported in reference 1.

Lengths of column specimens were selected to cover sufficiently the range for which postbuckling strength is important. The lower limit of L/r ratio was determined by the shortest length possible to test without end effects and the upper limit, by the interaction length, except for a few specimens in the Euler range for the purpose of checking test technique. The geometric properties of all specimens tested are given in tables 3 and 4.

Instrumentation and Test Procedure

The instrumentation for measurement of local and column buckling and the knife-edge end supports have been described in detail in reference 1 and were used for this series of tests with only minor revisions required for the H-sections.

The test procedure was likewise identical to that described in reference 1. The general test setup is shown in figures 20 and 21.

Evaluation and Comparison of Experimental Results

The results of the experimental investigation are exhibited in three forms: (1) Ultimate and critical plate stresses compared with theoretical values, (2) column-deflection curves, and (3) buckle-depth variation. Each of these will be discussed in some detail.

The comparisons of the experimental values with the theoretical values are presented in tables 5 and 6 and in figures 22 to 27. Particular note should be given to the last three columns of these tables,

two of which indicate deviation of experimental from theoretical values, and the third of which gives some indication of the postbuckling strength.

The postbuckling strength is markedly illustrated in the figures. The double-branched curve for theoretical ultimate stress is the same as that described generally in figure 8. The parabolic branch for the plastic region partly depends for its location upon empirical values of the crushing strength σ_{cc} of short columns tested with flat ends to avoid buckling. Such tests were not performed for this program, but the values were taken in this instance from curves recently recommended in reference 13.

Experimental critical plate buckling stress was evaluated by means of the top-of-knee method as given in reference 3. Theoretical critical plate stresses were computed for a plate width measured from the centers of adjoining plates. As the width-to-thickness ratio of the plate decreases, the boundary effect of the plate junction apparently becomes more pronounced, such that theoretical values of critical plate stress based on the clear plate width more nearly check the experimental values. As a practical design matter, this is not important, since the midwall values should always be conservative and appear to be so from the test results.

Figure 22 for the series "J" H-sections shows experimental values of ultimate stress which lie between the theoretical values based on midwall plate width and clear plate width, respectively. On the latter basis, the crushing strength σ_{cc} is identical to the critical plate stress. Stresses based on the clear plate width are presented since this series had the smallest b/t ratio of the H-sections tested and therefore the largest percentage difference between clear and midwall dimensions. The parabolic branch of the ultimate-stress curve based on midwall plate width is defined by equation (76); no elastic branch occurs for this case. (See also figs. 9 and 11.)

Figure 23 for the series "K" H-sections shows an ultimate-stress curve as defined by equations (71) and (78).

Figure 24 for the series "L" H-sections has an ultimate-stress curve as defined by equations (72) and (80).

Figure 25 for series "B" square tubes shows no postbuckling strength. When the critical plate stress occurs in the plastic range, plate buckling is immediately followed by complete collapse of the column. As a direct consequence, it was not possible to measure experimental values of critical plate stress by the top-of-knee method.

Figure 26 for series "D" square tubes shows a theoretical ultimate-stress curve as given by equation (141) for the elastic branch and equation (146) for the plastic branch. (See also fig. 15.)

Figure 27 for series "E" square tubes has a theoretical ultimate-stress curve as given by equations (142) and (148). It will be noted that the experimental values of critical plate stress are considerably higher than the theoretical values. As indicated before, the specimens in series "E" were the only ones which showed significant deviation from flatness of plates. Measurements showed the initial plate deflection to be 0.018 inch on the average. That the elevated values of the critical plate stress are likely the result of this initial plate curvature may be demonstrated as follows: From reference 19, where R is the radius of curvature

$$\left(\frac{\sigma_{cr}}{E}\right)_{cylinder} = 0.3\,\frac{t}{R}$$

and for a stiffened curved plate (ref. 16)

$$\left(\frac{\sigma_{cr}}{E}\right)_{combined} = \sqrt{\left(\frac{\sigma_{cr}}{E}\right)_{cylinder}^{2} + \left(\frac{\sigma_{cr}}{E}\right)_{flat}^{2}} + \frac{1}{2}\left(\frac{\sigma_{cr}}{E}\right)_{flat}$$

where $\left(\frac{\sigma_{cr}}{E}\right)_{flat} = \frac{\pi^2}{3(1-\nu)^2}\left(\frac{t}{b}\right)^2 = 3.62\left(\frac{t}{b}\right)^2$ for the corresponding flat plate. For a curved element of the square tube under consideration with $E = 10.67 \times 10^6$ psi, $t = 0.044$ inch, $b = 2.956$ inches, and a center-line deviation from flatness of 0.018 inch from which may be derived a radius of curvature $R = 63.4$ inches, one finds that the critical stress for the curved element is $\sigma_{cr} = 9{,}100$ psi, whereas for the flat plate $\sigma_{cr} = 8{,}560$ psi. The order of increase in this stress due to the effect of curvature will be seen, by reference to figure 27, to be the same as that measured experimentally.

Column-deflection curves, presented in figures 28 to 32, show variation of column-center deflection with load, and have been taken well beyond the ultimate load and to the point of complete collapse or nearly

so. The general character of these curves has been developed theoretically. It is represented by equation (153) and shown in figure 17, clearly indicating the effect of initial imperfections.

Buckle-depth variation has been plotted in figures 33 and 34 for the two larger H-sections and in figure 35 as typical of the square tubes. It is clearly evident from the former that the local deflection curve is roughly parabolic in shape and therefore in qualitative agreement with theory.

CONCLUDING REMARKS

It is well-known that very short columns for which column buckling does not occur can show definite postbuckling strength, that is, excess strength beyond that indicated by the critical plate buckling stress. The ultimate stress can exceed appreciably the plate critical stress, especially if the latter is well within the elastic range.

This postbuckling strength decreases with increasing slenderness ratio L/r because column buckling becomes the governing influence except for extremely small slenderness ratios. It becomes zero at that L/r at which the plate buckling stress is equal to the column buckling stress. Approximate methods of accounting for this effect have mostly consisted in using a Johnson parabola tangent to the Euler column curve with apex at the local crushing strength and $L/r = 0$.

In the present investigation, general energy equations are derived from which the ultimate strength in the postbuckling range can be calculated for columns of any shape and slenderness. Specific expressions are derived for columns with H- and square-box sections and numerous tests have been made on columns of these two shapes. The results, reported herein, show consistent agreement with the developed theory. The reported results of measurements of plate and of column deflections indicate the magnitude of the deformations which occur before as well as after the ultimate load.

Cornell University,
Ithaca, N. Y., May 1, 1952.

REFERENCES

1. Bijlaard, P. P., and Fisher, G. P.: Interaction of Column and Local Buckling in Compression Members. NACA TN 2640, 1952.

2. Hemp, W. S.: The Theory of Flat Panels Buckled in Compression. R. & M. No. 2178, British A.R.C., 1945.

3. Hu, Pai C., Lundquist, Eugene E., and Batdorf, S. B.: Effect of Small Deviations From Flatness on Effective Width and Buckling of Plates in Compression. NACA TN 1124, 1946.

4. Bijlaard, P. P.: Determination of the Effective Width of Plates With Small Deviations From Flatness by the Method of Split Rigidities. Proc. First U. S. Nat. Cong. Appl. Mech. (June 1951, Chicago, Ill.), A.S.M.E., 1952, pp. 357-362.

5. Bijlaard, P. P.: Theory of the Plastic Stability of Thin Plates. Pub. Int. Assoc. Bridge and Structural Eng., vol. 6, 1940-41, pp. 45-69.

6. Lundquist, Eugene E., Stowell, Elbridge Z., and Schuette, Evan H.: Principles of Moment Distribution Applied to Stability of Structures Composed of Bars or Plates. NACA Rep. 809, 1945.

7. Kroll, W. D.: Tables of Stiffness and Carry-Over Factor for Flat Rectangular Plates Under Compression. NACA ARR 3K27, 1943.

8. Kroll, W. D., Fisher, Gordon P., and Heimerl, George J.: Charts for Calculation of the Critical Stress for Local Instability of Columns With I-, Z-, Channel, and Rectangular-Tube Section. NACA ARR 3K04, 1943.

9. Bleich, Friedrich: Theorie und Berechnung der eisernen Brücken. Julius Springer (Berlin), 1924.

10. Bijlaard, P. P.: Nauwkeurige Berekening van de Plooispanning van Hoekstalen, zoowel voor het Elastische als voor het Plastische Gebied. De Ingenieur Ned.-Indië, vol. 6, no. 3, Mar. 1939, pp. I.35-I.45.

11. Bijlaard, P. P.: Berekening van de Knikspanning van Gekoppelde Profielen volgens een Nieuwe Methode. De Ingenieur Ned.-Indië, vol. 6, no. 3, Mar. 1939, pp. I.45-I.46.

12. Bijlaard, P. P.: Analysis of the Elastic and Plastic Stability of Sandwich Plates by the Method of Split Rigidities-I. Jour. Aero. Sci., vol. 18, no. 5, May 1951, pp. 339-349.

13. Stowell, Elbridge Z., Heimerl, George J., Libove, Charles, and Lundquist, Eugene E.: Buckling Stresses for Flat Plates and Integral Flat-Plate Sections. Trans. Am. Soc. Civ. Eng., vol. 117, 1952, pp. 545-575.

14. Timoshenko, S.: Theory of Elastic Stability. First ed., McGraw-Hill Book Co., Inc., 1936.

15. Timoshenko, S.: Theory of Elasticity. First ed., McGraw-Hill Book Co., Inc., 1934.

16. Sechler, Ernest E., and Dunn, Louis G.: Airplane Structural Analysis and Design. First ed., John Wiley & Sons, Inc., 1942.

17. Winter, G.: Performance of Compression Plates as Parts of Structural Members. Res. Eng. Structures Supp., Academic Press, 1949, pp. 179-185.

18. Winter, George, Lansing, Warner, and McCalley, R. P.: Four Papers on the Performance of Thin Walled Steel Structures. Reprint No. 33, Eng. Exp. Station, Cornell Univ., 1950, pp. 51-57.

19. Niles, Alfred S., and Newell, Joseph S.: Airplane Structures. Vol. I. Third ed., John Wiley & Sons, Inc., 1943.

TABLE 1.- DATA FOR 75S-T6 ALUMINUM-ALLOY H-SECTIONS

Series	b, in.	b', in.	t_f, in.	t_w, in.	$E/10^6$, psi	k_f	σ_{crl}, psi	α	σ_{cc}, psi	P	Q
"J"	$\frac{45}{32}$	$\frac{7}{4}$	0.128	0.125	10.45	0.741	58,000	2.02	60,500	0.792	4.68
"K"	$\frac{61}{32}$	$\frac{19}{8}$	.129	.122	10.43	.727	31,500	2.07	52,500	.792	4.68
"L"	$\frac{37}{16}$	$\frac{23}{8}$	.124	.126	10.41	.760	20,500	1.98	46,600	.776	4.60

NACA

TABLE 2.- STRESSES FOR SQUARE COLUMNS

σ_{av}, psi	$E_{l,eq}/E$	σ_u, psi	σ_u/σ_{av}	w/w_i
4,280	1	18,800	4.4	1.29
[a]8,560	1	18,800	2.2	1.83
9,000	.882	15,440	1.72	2.39
10,000	.69	12,970	1.30	4.36
11,000	.64	12,000	1.09	12.1
11,300	.629	11,800	1.043	24.3

[a] σ_{crl}.

NACA

TABLE 3.- GEOMETRIC PROPERTIES OF H-SECTIONS

Series	Depth, in.	Average r, in.	Piece	Column	Cut length, in.	Weight, grams	Area, sq in.	Corrected free length, L, in.	L/r
"J"	$1\frac{7}{8}$	0.704	"J"-1	SS-1	13.03	557.4	0.960	17.62	25
			"J"-1	ES-1	16.50	705.3	.959	21.16	30
			"J"-1	S-1	19.94	852.5	.960	24.65	35
			"J"-2	I-1	23.98	1,025	.960	28.84	40.8
			"J"-1	L-1	24.98	1,064	.958	29.84	42.5
			"J"-1	L-2	24.98	1,069	.960	29.84	42.5
			"J"-1	E-1	30.34	1,297	.960	35.20	50
"K"	$2\frac{1}{2}$	0.967	"K"-1	SS-1	19.50	1,142	1.317	24.15	25
			"K"-3	ES-1	24.28	1,413	1.309	29.03	30
			"K"-1	S-1	29.06	1,700	1,314	33.84	35
			"K"-3	MS-1	33.91	1,976	1.310	38.70	40
			"K"-1	M-1	38.72	2,264	1.314	43.53	45
			"K"-3	ML-1	43.42	2,522	1.309	48.37	50
			"K"-2	I-1	49.25	2,887	1.317	54.11	55.9
"L"	3	1.172	"L"-2	SS-1	24.47	1,660	1.525	29.23	25
			"L"-1	ES-1	36.30	2,495	1.542	41.10	35
			"L"-2	R-1	42.03	2,844	1.521	46.86	40
			"L"-2	M-1	47.72	3,245	1.528	52.27	44.9
			"L"-1	S-1	59.63	4,085	1.540	64.48	55
			"L"-2	ML-1	67.81	4,610	1.527	72.66	62
			"L"-3	ML-2	67.81	4,650	1.542	72.66	62
			"L"-1	I-1	76.11	5,205	1.538	80.97	69.1
			"L"-3	E-1	88.94	6,097	1.540	93.80	80

TABLE 4.- GEOMETRIC PROPERTIES OF SQUARE TUBES

Series	Dimensions, in.	Average r, in.	Piece	Column	Cut length, in.	Weights, grams	Area, sq in.	Corrected free length, L, in.	L/r
"B"	2 by 2 by 0.062	0.792	"B"-1	SS-1	8.05	171.7	0.481	11.82	14.95
			"B"-2	SS-2	8.11	169.1	.470	11.88	15.00
			"B"-1	ES-1	11.38	238.9	.474	15.23	19.25
			"B"-2	ES-2	11.39	238.6	.473	15.24	19.25
			"B"-1	S-1	17.48	368.7	.476	21.45	27.15
			"B"-2	S-2	17.49	366.6	.474	21.46	27.15
			"B"-1	M-1	26.00	551.8	.478	30.02	37.95
			"B"-1	M-2	26.00	549.2	.476	30.02	37.95
			"B"-2	I-1	32.34	677.3	.473	36.37	45.95
			"B"-2	I-2	32.36	677.2	.473	36.39	45.95
			"B"-2	I-3	32.36	676.2	.472	36.39	45.95
			"B"-3	ML-1	36.35	771.4	.479	40.38	51.00
			"B"-3	L-1	40.23	853.0	.479	44.26	56.00
			"B"-3	L-2	40.23	850.2	.477	44.26	56.00
"D"	$2\frac{1}{2}$ by $2\frac{1}{2}$ by 0.047	1.001	"D"-4	SS-1	17.31	346.2	0.452	21.25	21.23
			"D"-1	S-1	38.88	780.0	.452	43.03	43.00
			"D"-2	DS-1	53.94	1,092.0	.455	58.06	58.00
			"D"-2	RM-1	67.00	1,349.7	.455	71.09	71.02
			"D"-4	MS-1	72.16	1,446.0	.452	76.25	76.17
			"D"-3	I-2	81.78	1,635.2	.452	85.87	85.78
			"D"-1	I-1	81.81	1,641.0	.453	85.90	85.81
			"D"-5	L-1	123.49	2,545.0	.465	127.58	127.45
"E"	3 by 3 by 0.047	1.206	"E"-3	SS-1	20.40	475.4	0.523	24.41	20.2
			"E"-2	ES-1	44.14	1,028	.522	48.23	40.0
			"E"-5	DS-1	56.21	1,309	.523	60.30	50.0
			"E"-1	S-1	68.14	1,565	.517	72.23	59.9
			"E"-9	MS-1	86.36	1,995	.520	90.45	75.0
			"E"-1	M-1	92.30	2,125	.518	96.39	79.9
			"E"-11	MA-1	95.91	2,200	.516	100.00	83.0
			"E"-4	MA-2	95.91	2,210	.518	100.00	83.0
			"E"-5	RM-1	106.16	2,450	.519	110.25	91.5
			"E"-2	ML-1	116.54	2,685	.517	120.63	100.0
			"E"-3	I-1	129.82	3,000	.519	133.91	111.0
			"E"-10	LL-1	140.63	3,255	.520	144.72	120.0

TABLE 5.- TEST RECORD, H-SECTIONS

Designation			Theoretical		Experimental		Ratio, experimental to theoretical		
Piece	Column	$\frac{L}{r}$	σ_{ult}, psi	σ_{cr}, psi	σ_{ult}, psi	σ_{cr}, psi (a)	$\frac{\sigma_{ult}}{\sigma_{ult}}$	$\frac{\sigma_{cr}}{\sigma_{cr}}$	$\frac{\sigma_{ult}}{\sigma_{cr}}$
"J"-1	SS-1	25	58,910	58,000	62,500	56,800	1.060	0.979	1.079
"J"-1	ES-1	30	58,300	58,000	61,000	57,000	1.045	.983	1.052
"J"-1	S-1	35	58,000	58,000	59,200	56,300	1.020	.971	1.021
"J"-2	I-1	40.8	58,000	58,000	56,300	------	.970	-----	.972
"J"-1	L-1	42.5	[b]57,600	58,000	54,850	------	.952	-----	-----
"J"-1	L-2	42.5	[b]57,600	58,000	55,200	------	.968	-----	-----
"J"-1	E-1	50	[b]41,700	58,000	41,750	------	1.001	-----	-----
"K"-1	SS-1	25	47,000	31,500	49,900	33,050	1.061	1.050	1.585
"K"-3	ES-1	30	44,650	31,500	47,600	32,100	1.065	1.019	1.510
"K"-1	S-1	35	41,800	31,500	42,600	31,950	1.018	1.013	1.352
"K"-3	MS-1	40	38,500	31,500	39,200	32,100	1.018	1.019	1.243
"K"-1	M-1	45	35,750	31,500	36,150	31,750	1.011	1.007	1.147
"K"-3	ML-1	50	33,750	31,500	33,800	32,100	1.001	1.019	1.072
"K"-2	I-1	55.9	31,950	31,500	31,800	------	.997	-----	1.009
"L"-2	SS-1	25	39,250	20,500	41,300	20,750	1.052	1.011	2.018
"L"-1	ES-1	35	32,200	20,500	32,400	21,550	1.005	1.050	1.580
"L"-2	R-1	40	29,050	20,500	28,800	20,700	.981	1.010	1.405
"L"-2	M-1	44.9	26,500	20,500	26,200	19,650	.988	.959	1.278
"L"-1	S-1	55	23,400	20,500	23,800	20,950	1.018	1.021	1.160
"L"-2	ML-1	62	21,950	20,500	20,650	19,650	.942	.959	1.008
"L"-3	ML-2	62	21,950	20,500	21,600	20,150	.985	.983	1.053
"L"-1	I-1	69.1	20,750	20,500	20,350	------	.982	-----	.993
"L"-3	E-1	80	[b]16,080	20,500	15,600	------	.972	-----	-----

[a]Plate critical stress as determined by NACA top-of-knee method.

[b]Euler stress.

TABLE 6.- TEST RECORD, SQUARE TUBES

Designation			Theoretical		Experimental		Ratio, experimental to theoretical		
Piece	Column	$\frac{L}{r}$	σ_{ult}, psi	σ_{cr}, psi	σ_{ult}, psi	σ_{cr}, psi (a)	$\frac{\sigma_{ult}}{\sigma_{ult}}$	$\frac{\sigma_{cr}}{\sigma_{cr}}$	$\frac{\sigma_{ult}}{\sigma_{c}}$
"B"-1	SS-1	15.0	37,250	37,250	37,150	------	0.997	-----	0.997
"B"-2	SS-2	15.0	37,250	37,250	37,650	------	1.012	-----	1.012
"B"-1	ES-1	19.3	37,250	37,250	37,800	------	1.016	-----	1.016
"B"-2	ES-2	19.3	37,250	37,250	36,800	------	.988	-----	.988
"B"-1	S-1	27.2	37,250	37,250	37,270	------	1.002	-----	1.002
"B"-2	S-2	27.2	37,250	37,250	36,800	------	.988	-----	.988
"B"-1	M-1	38.0	37,250	37,250	36,600	------	.983	-----	.983
"B"-1	M-2	38.0	37,250	37,250	36,200	-----	.972	-----	.972
"B"-2	I-1	46.0	37,250	37,250	35,750	------	.960	-----	.960
"B"-2	I-2	46.0	37,250	37,250	36,800	------	.988	-----	.988
"B"-2	I-3	46.0	37,250	37,250	36,350	------	.976	-----	.976
"B"-3	ML-1	51.0	[b]36,500	37,250	35,800	------	.982	-----	-----
"B"-3	L-1	56.0	[b]33,600	37,250	32,200	------	.958	-----	-----
"B"-3	L-2	56.0	[b]33,600	37,250	32,350	------	.963	-----	-----
"D"-4	SS-1	21.2	21,950	13,600	21,390	14,290	0.975	1.050	1.570
"D"-1	S-1	43.0	19,920	13,600	20,350	14,200	1.020	1.044	1.497
"D"-2	DS-1	58.0	17,700	13,600	17,750	13,960	1.002	1.027	1.305
"D"-2	RM-1	71.0	15,320	13,600	14,920	13,875	.975	1.020	1.097
"D"-4	MS-1	76.2	14,500	13,600	14,420	14,270	.995	1.049	1.061
"D"-3	I-2	85.8	13,740	13,600	13,790	------	1.010	-----	1.013
"D"-1	I-1	85.8	13,740	13,600	13,330	------	.970	-----	.982
"D"-5	L-1	127.5	[b]6,480	13,600	6,240	------	.963	-----	-----
"E"-3	SS-1	20.2	18,090	8,560	16,820	9,560	0.930	1.118	1.967
"E"-2	ES-1	40	16,620	8,560	16,300	10,070	.982	1.177	1.906
"E"-5	DS-1	50	15,500	8,560	15,930	10,030	1.028	1.172	1.863
"E"-1	S-1	59.9	14,140	8,560	13,900	10,450	.983	1.222	1.625
"E"-9	MS-1	75	11,600	8,560	11,640	9,530	1.003	1.113	1.361
"E"-1	M-1	79.9	10,700	8,560	10,710	9,880	1.000	1.154	1.252
"E"-11	MA-1	83	10,200	8,560	10,420	9,500	1.021	1.110	1.219
"E"-4	MA-2	83	10,200	8,560	10,420	9,950	1.021	1.163	1.219
"E"-5	RM-1	91.5	9,380	8,560	10,220	9,930	1.088	1.160	1.193
"E"-2	ML-1	100	8,860	8,560	9,440	9,440	1.064	1.103	1.103
"E"-3	I-1	111	8,560	8,560	8,300	------	.970	-----	.970
"E"-10	LL-1	120	[b]7,300	8,560	7,120	------	.975	-----	-----

[a]Plate critical stress as determined by NACA top-of-knee method.

[b]Euler stress.

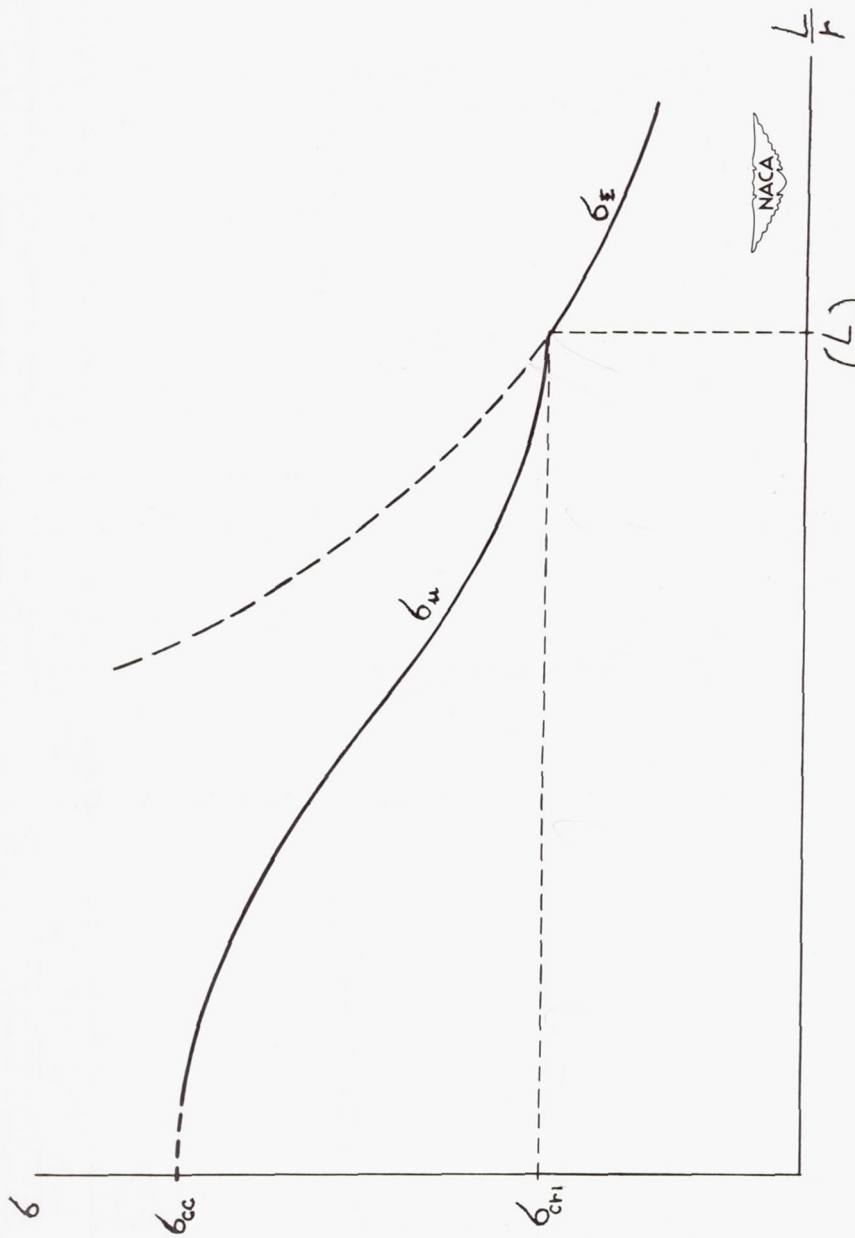

Figure 1.- Variation of ultimate stress σ_u with slenderness L/r.

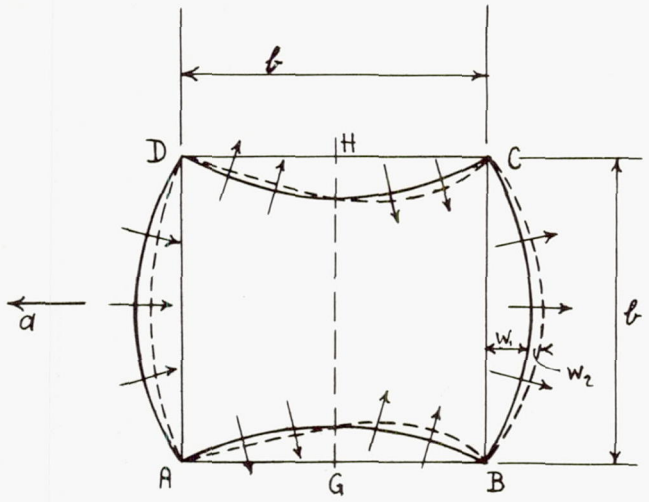

(a) Local deflections w_1 in postbuckling range of straight column and local deflections w_2 imposed during column buckling.

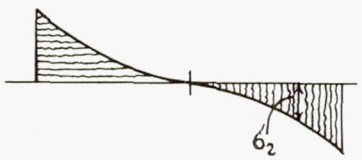

(b) Column bending stresses σ_2 caused by column buckling.

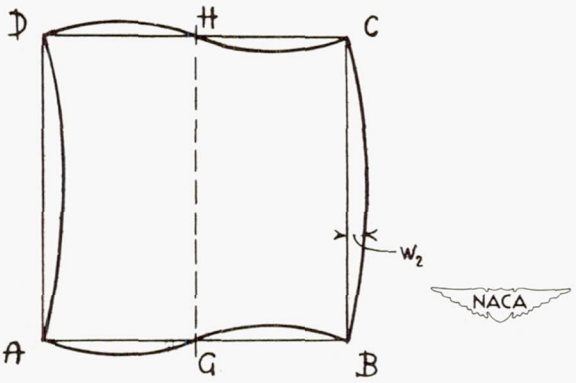

(c) Superimposed local deflections w_2 caused by column buckling.

Figure 2.- Distortions of and column bending stresses in the cross section of square tubes after column buckling in the postbuckling range of the plates.

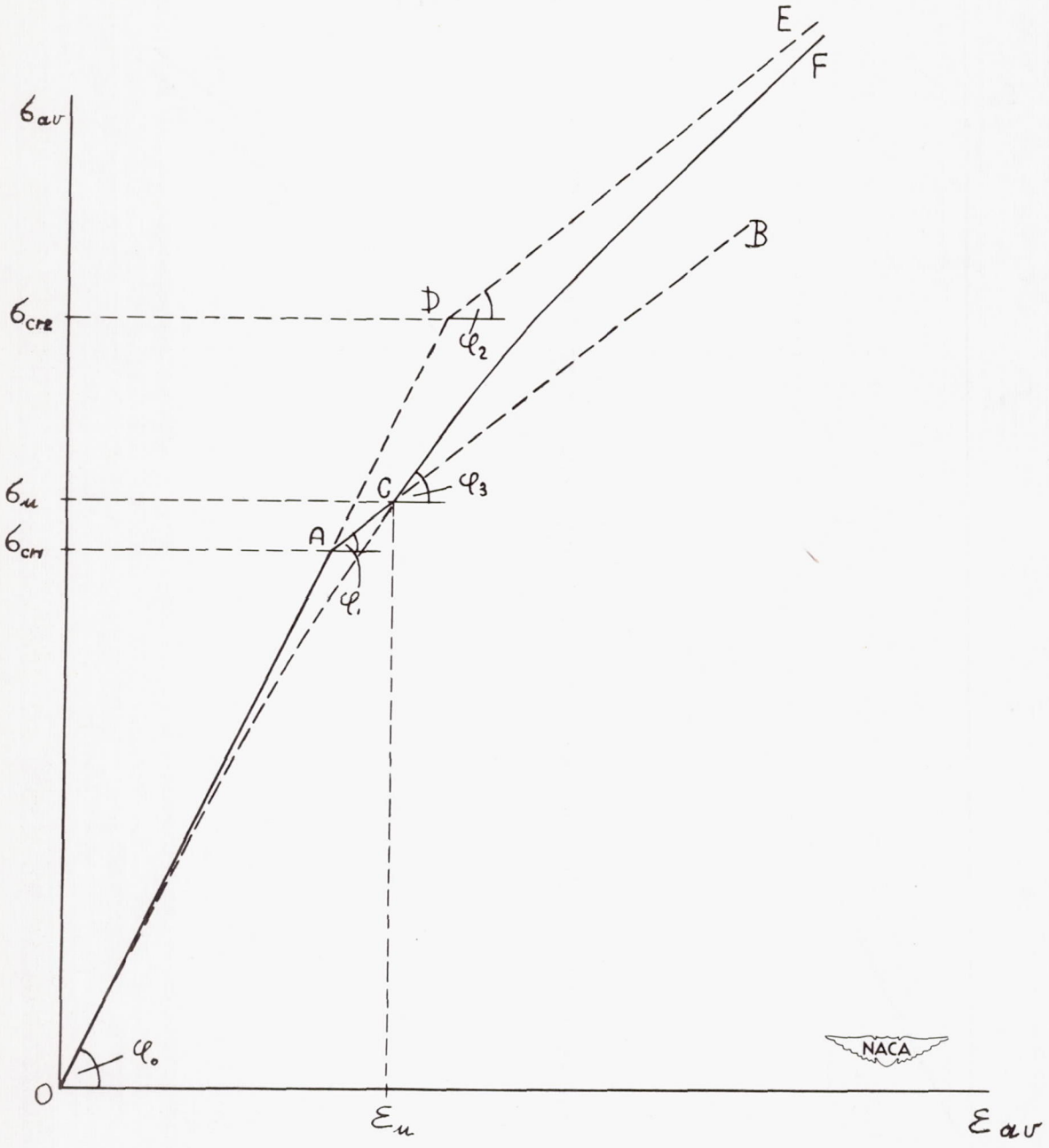

Figure 3.- Diagram of average stress σ_{av} plotted against unit shortening ϵ_{av} for tube with square cross section. Broken line OAB applies if column remains straight. After column buckling at average stress σ_u average stress in plates BC and AD (fig. 2) follows the curves CF and CO, respectively.

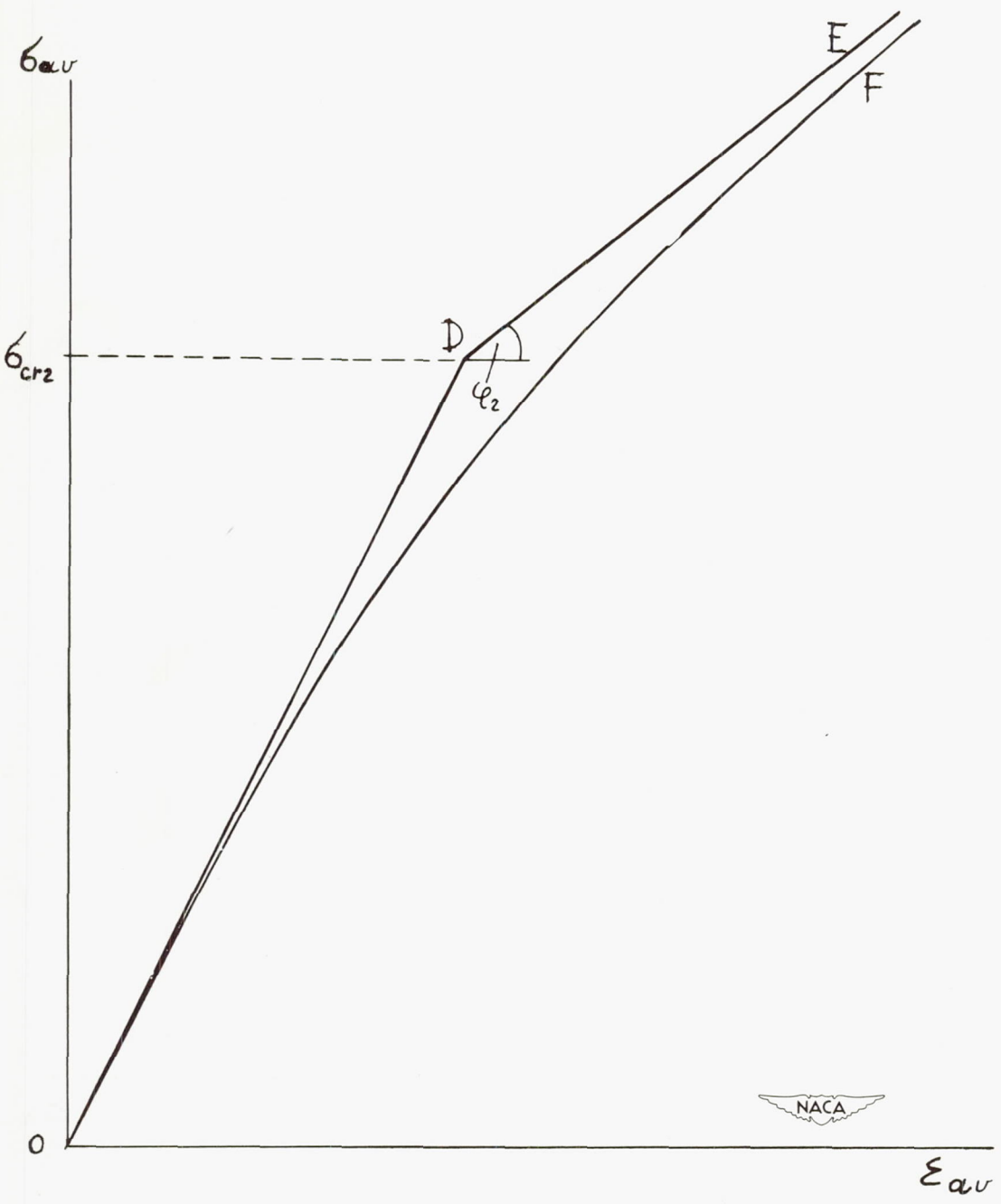

Figure 4.- Diagram of average stress σ_{av} plotted against unit shortening ϵ_{av} for a plate that is elastically restrained along the sides. Broken line ODE and curve OF apply in case of an initially flat plate and of a plate with initial deflection, respectively.

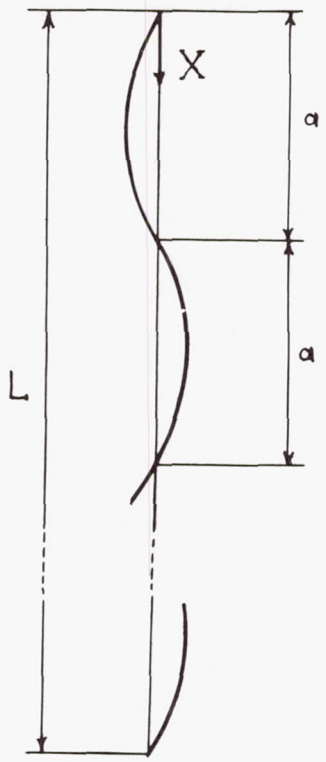

(a) Plate buckling with half wave length a in longitudinal direction.

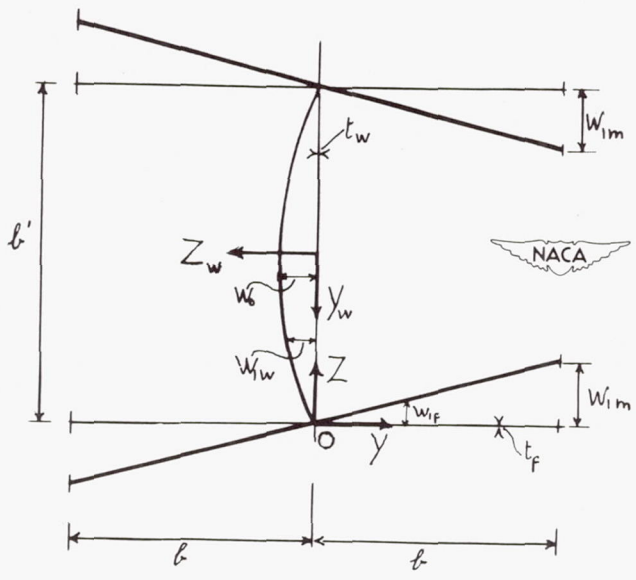

(b) Local deflections w_1 in postbuckling range of straight column.

Figure 5.- Distortions of and stresses in column with H-section before and after column buckling in postbuckling range of plates.

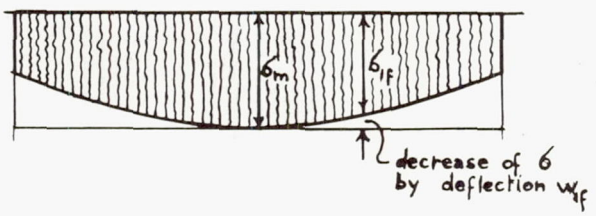

(c) Compressive stresses σ_1 in postbuckling range in flange of straight column.

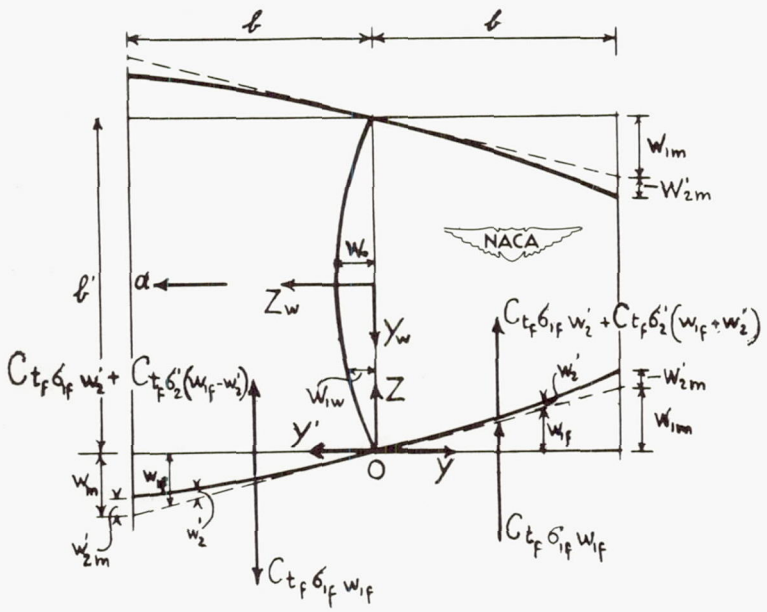

(d) Local deflections $w_1 + w_2'$ after incipient column buckling.

Figure 5.- Continued.

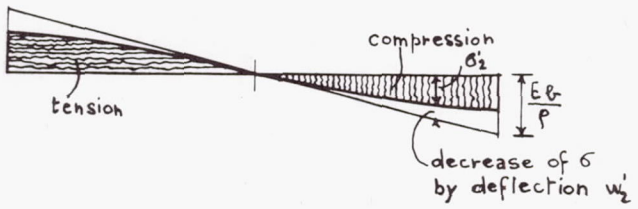

(e) Column bending stresses σ_2' caused by column buckling.

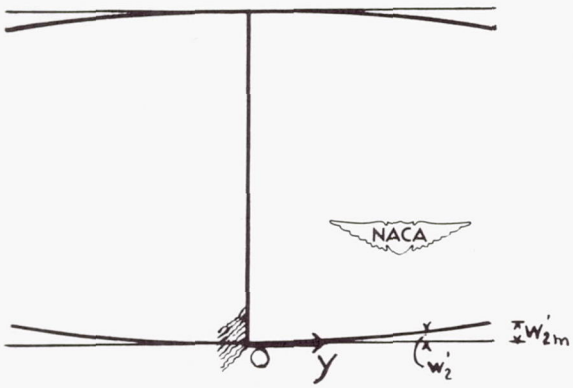

(f) Excess deflections w_2' occurring after incipient column buckling.

Figure 5.- Concluded.

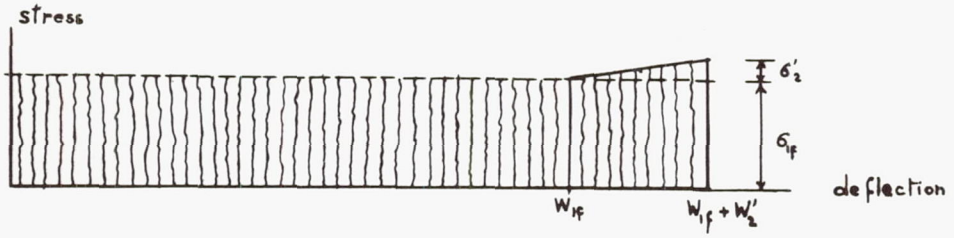

(a) Variation of σ_{1f} and σ_2' in right flange with local deflections w_{1f} and w_2'.

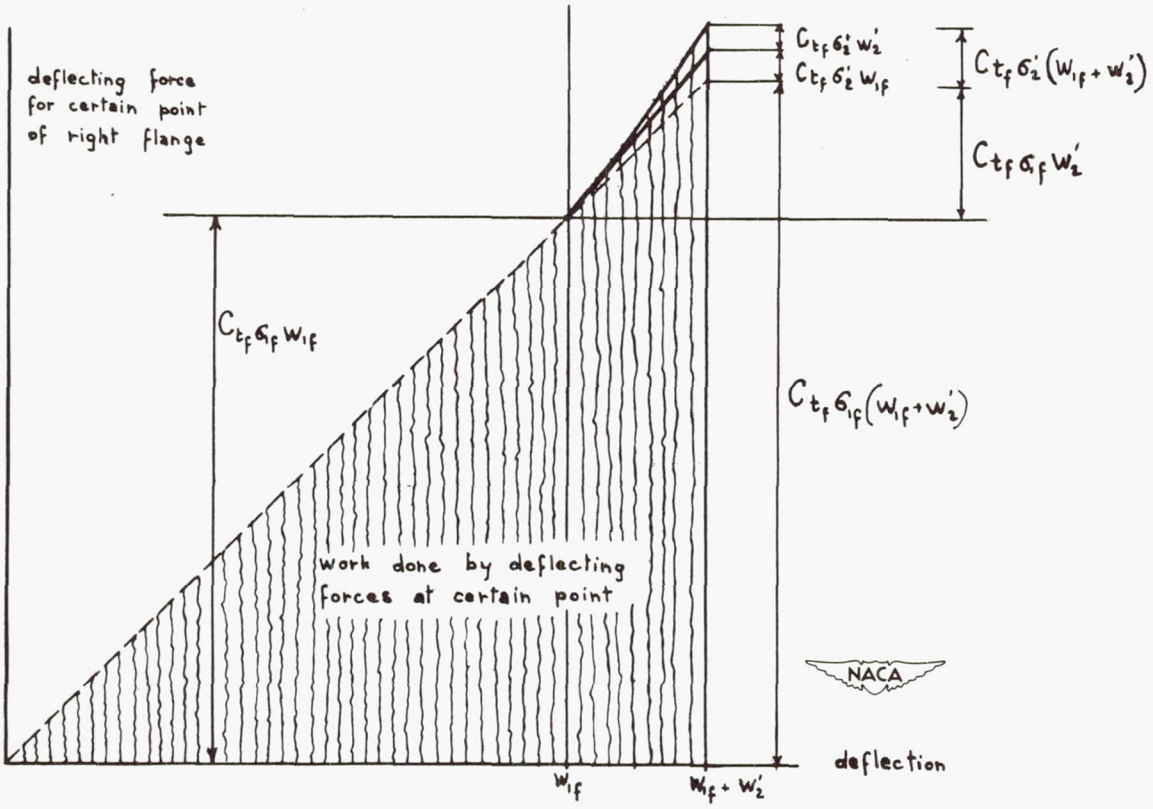

(b) Variation of the deflecting forces at a certain point of right flange with deflections w_{1f} and w_2'.

Figure 6.- Determination of the work done during local deflections of right and left flanges of H-section.

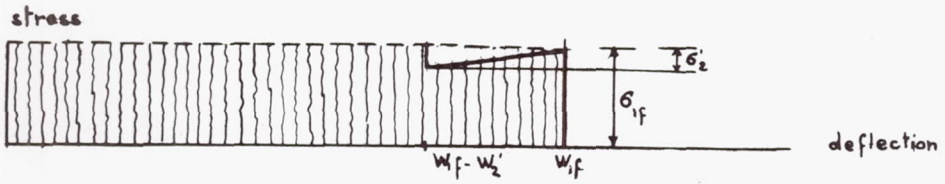

(c) Variation of σ_{1f} and σ_2' in left flange with local deflections w_{1f} and w_2'.

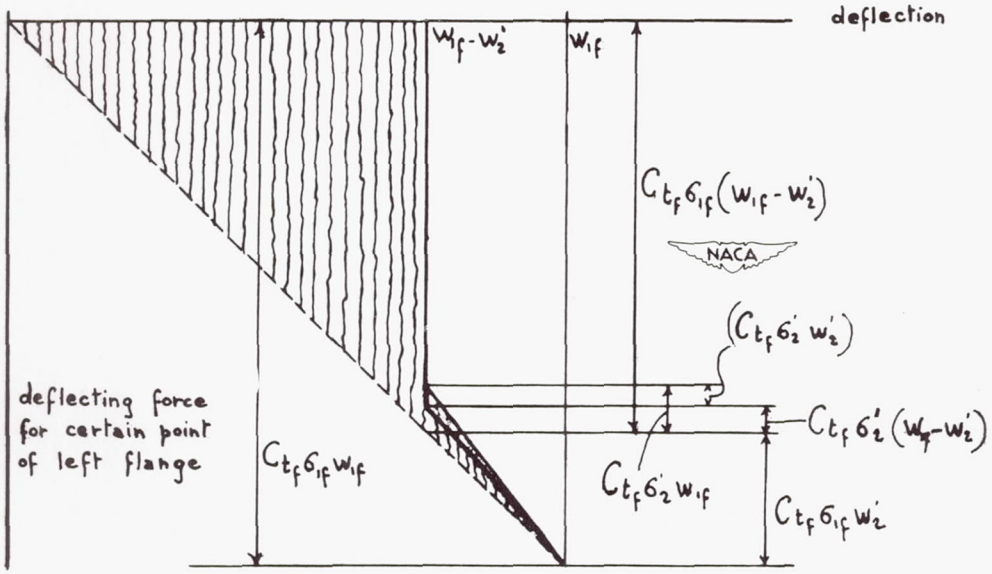

(d) Variation of deflecting forces at a certain point of left flange with deflections w_{1f} and w_2'.

Figure 6.- Concluded.

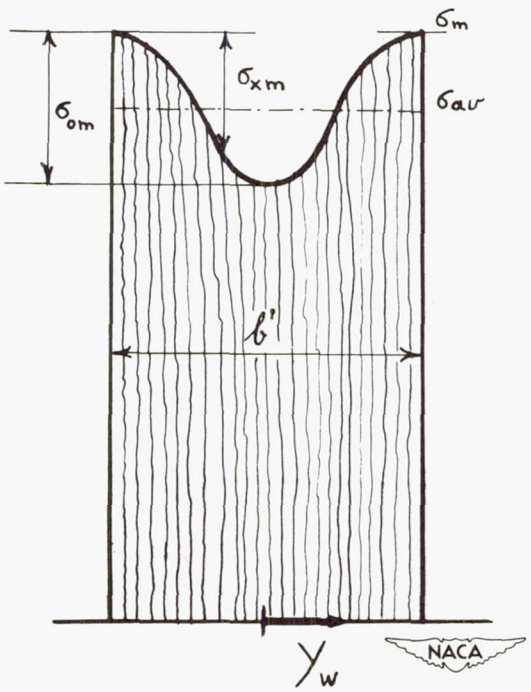

Figure 7.- Compressive stresses σ_{lw} in web of H-section.

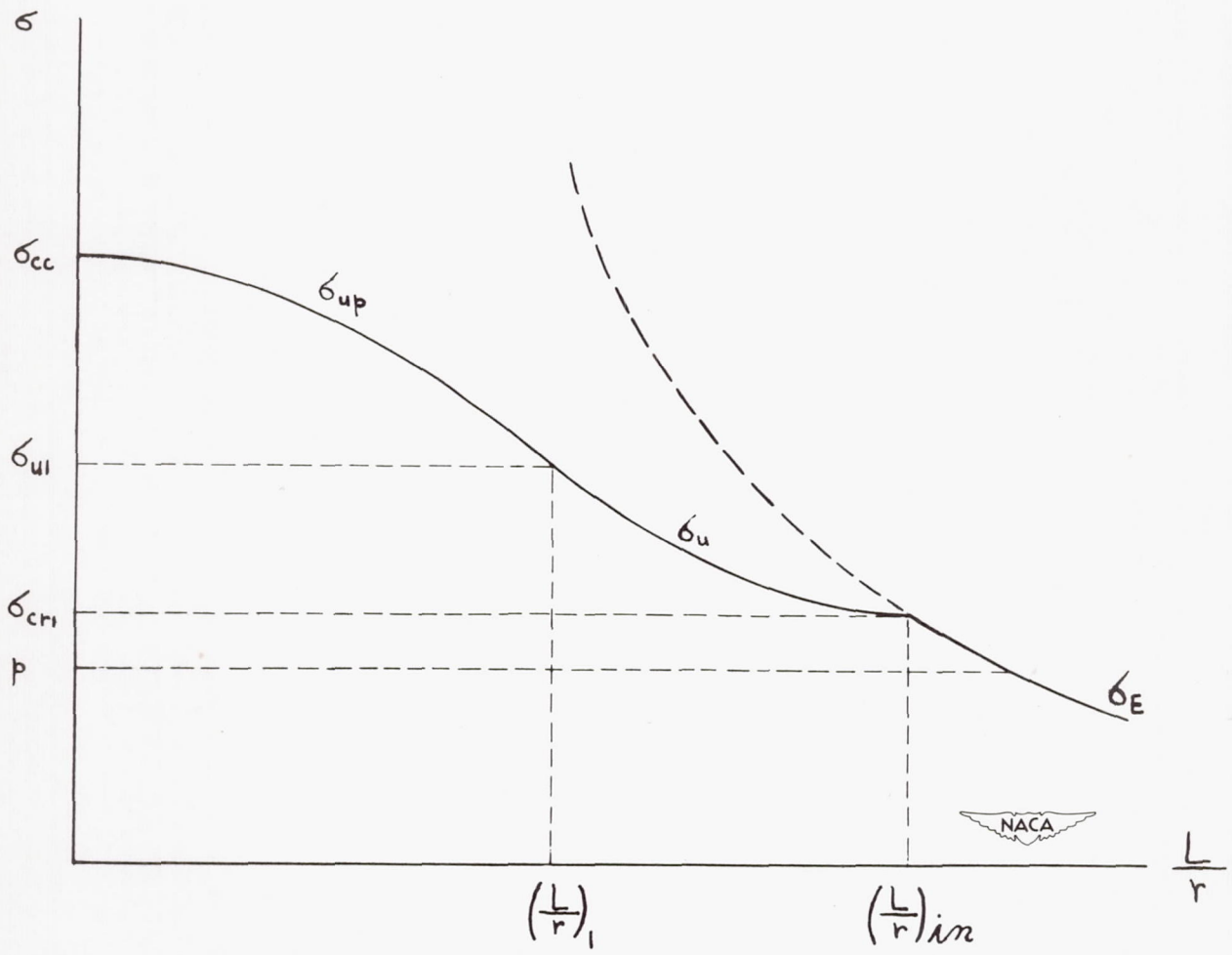

Figure 8.- Diagram of Euler stress σ_E and ultimate stress plotted against slenderness L/r. The branches σ_u and σ_{up} of the ultimate stress refer to the elastic and plastic range, respectively.

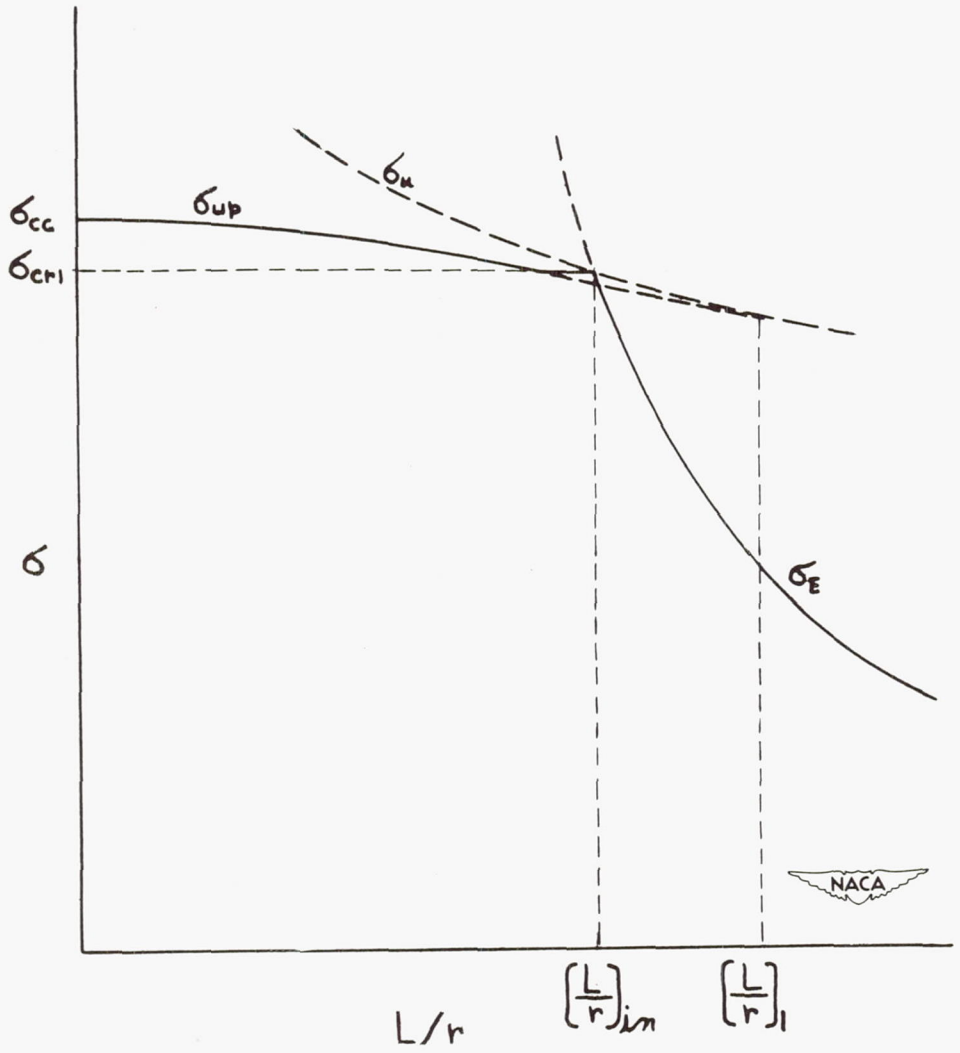

Figure 9.- Diagram of σ_E, σ_u, and σ_{up} plotted against slenderness L/r in case where, with column buckling in the postbuckling range, plastic deformations occur from the beginning.

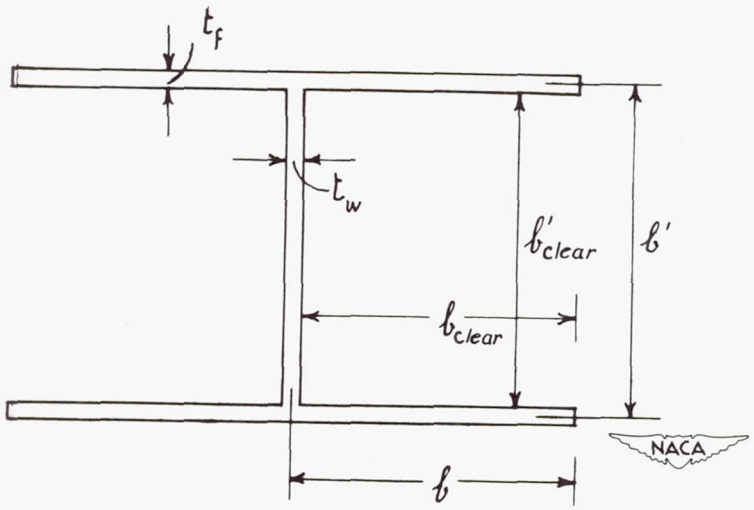

Figure 10.- Cross section of H-section, showing notations.

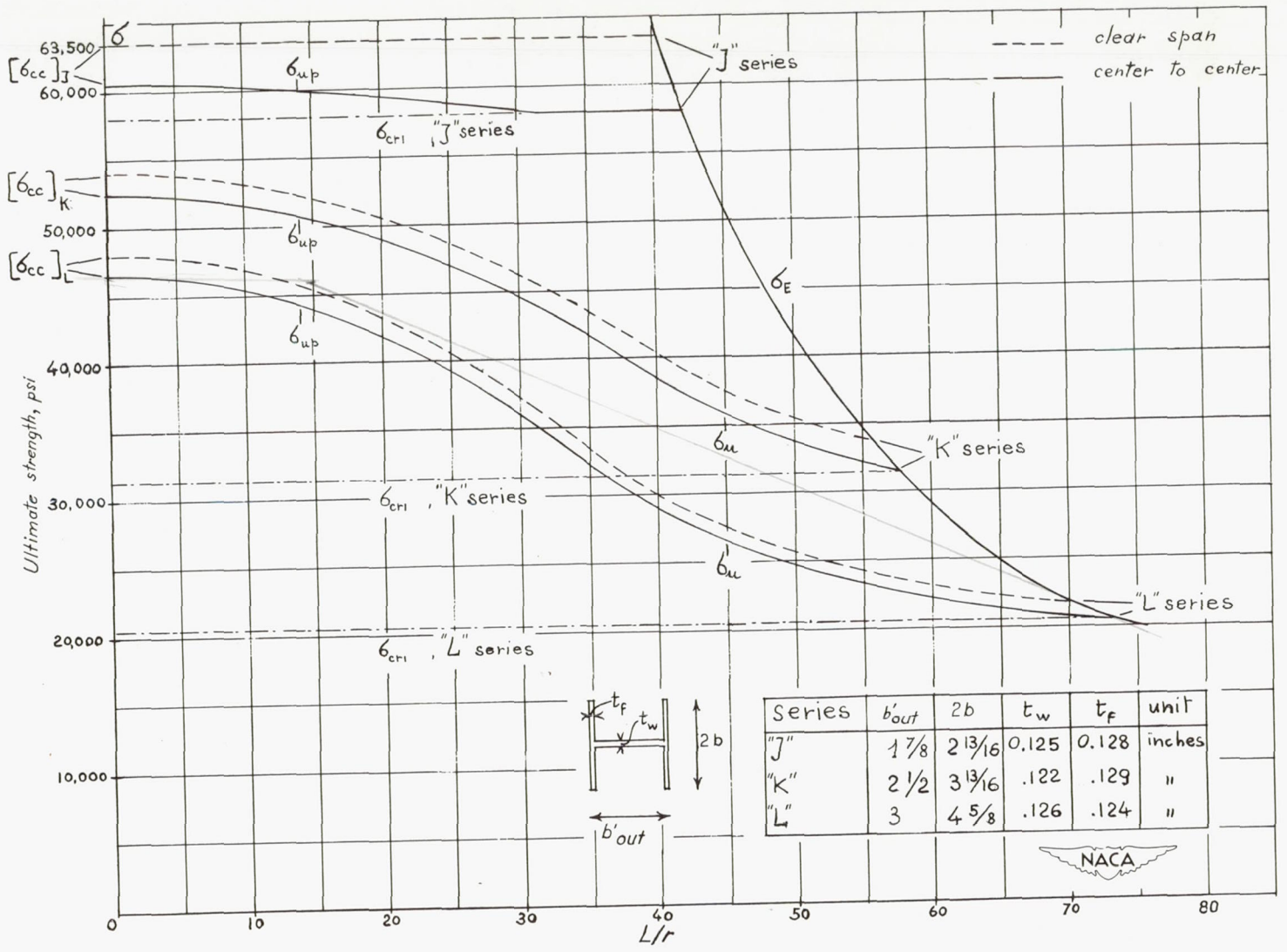

Series	b'_{out}	2b	t_w	t_f	unit
"J"	1 7/8	2 13/16	0.125	0.128	inches
"K"	2 1/2	3 13/16	.122	.129	"
"L"	3	4 5/8	.126	.124	"

Figure 11.- Graph of ultimate stresses plotted against slenderness ratios L/r for H-section columns.

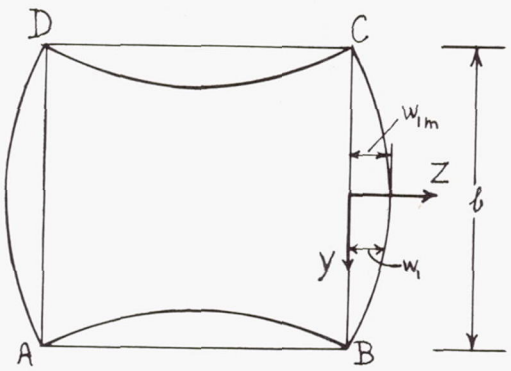

(a) Local deflections w_1 in postbuckling range of straight tube.

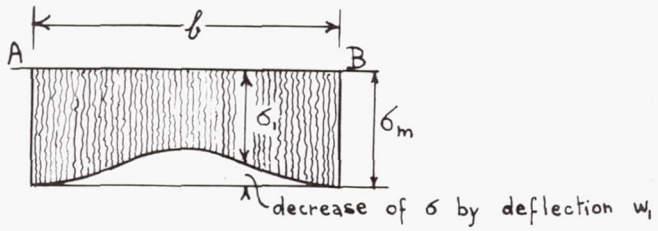

(b) Compressive stresses σ_1 in postbuckling range of straight tube.

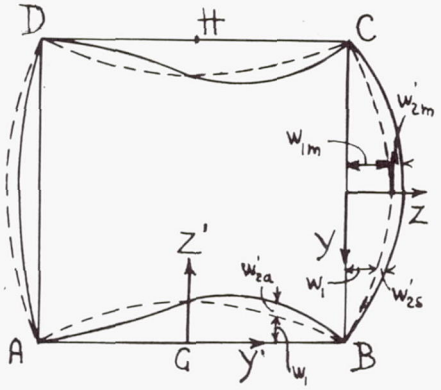

(c) Local deflections $w_1 + w_2'$ after incipient column buckling.

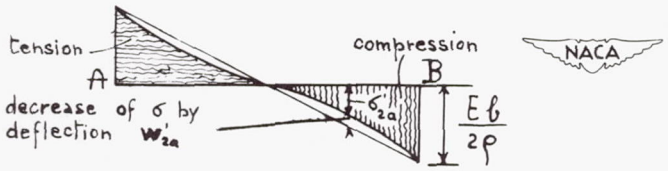

(d) Column bending stresses σ_{2a}' in plates AB and DC caused by column buckling.

Figure 12.- Distortions of cross section and stresses in tube with square cross section before and after column buckling in the postbuckling region of the plates.

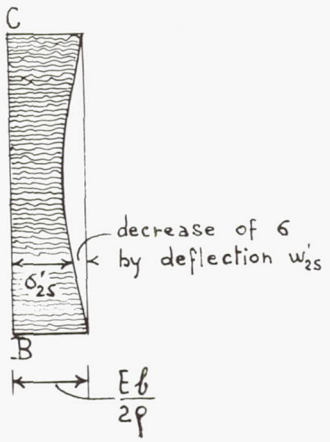

(e) Column bending stresses σ_{2s}' in plate BC caused by column buckling.

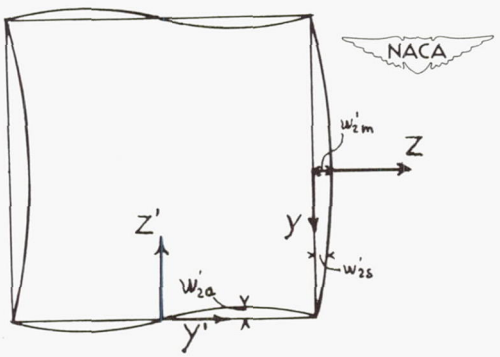

(f) Excess deflections w_2' occurring after incipient column buckling.

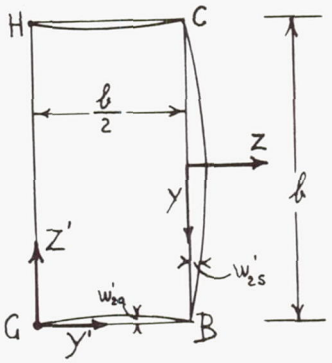

(g) Right half of figure 12(f).

Figure 12.- Concluded.

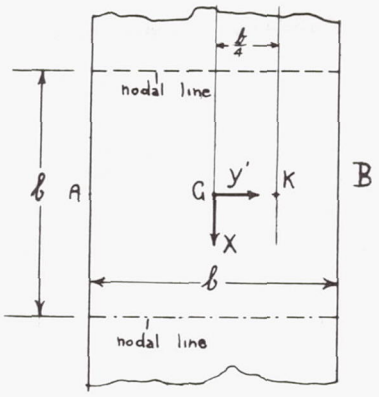

(a) Plan view of plate AB.

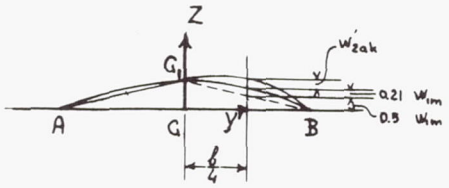

(b) Section of deflected plate AB at $x = 0$, showing deflections at point K.

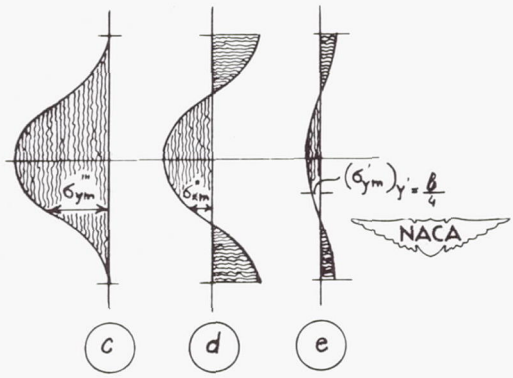

(c) Tensile membrane stresses σ_{ym}''' caused by excess deflections w_{2a}' for $y' > 0$ in case at $y' = 0$ and $y' = b/2$ no displacement in the Y'-direction occurs.

(d) Membrane stresses σ_{ym}'' caused by w_{2a}' for $y' > 0$ if lines $y' = 0$ and $y' = b/2$ are free to move in the Y'-direction, but are held straight.

(e) Actual membrane stresses σ_{ym}' at $y' = b/4$.

Figure 13.- Determination of the membrane stresses σ_{xm}' to which the membrane stresses σ_{ym}' are equivalent.

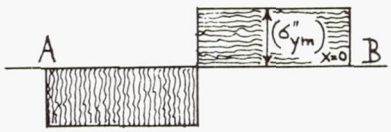

(f) Membrane stresses σ_{ym}'' at $x = 0$.

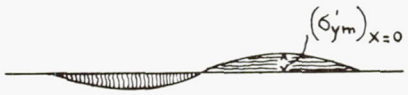

(g) Actual membrane stresses σ_{ym}' at $x = 0$.

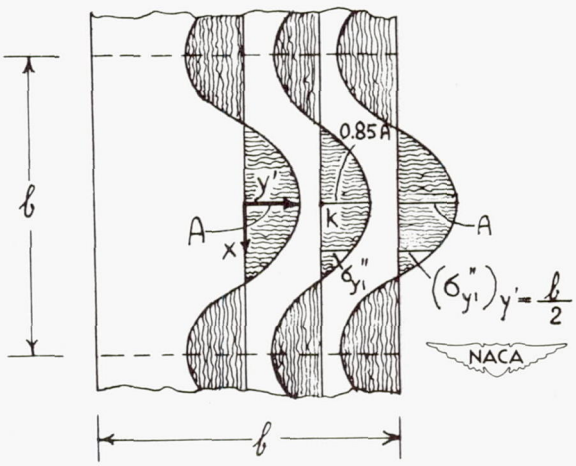

(h) Superimposed membrane stresses σ_{y1}'' in order to reduce membrane stresses σ_y'' to actual membrane stresses σ_y'.

Figure 13.- Concluded.

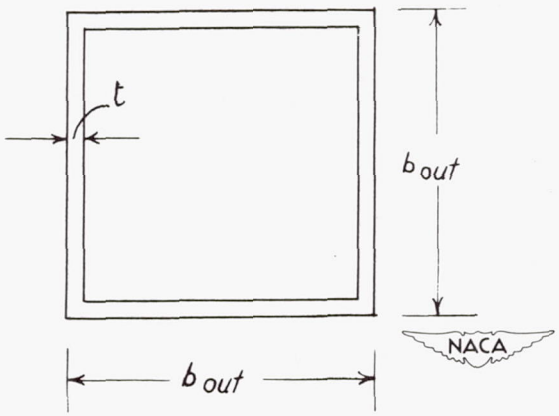

Figure 14.- Cross section of tube, showing notations.

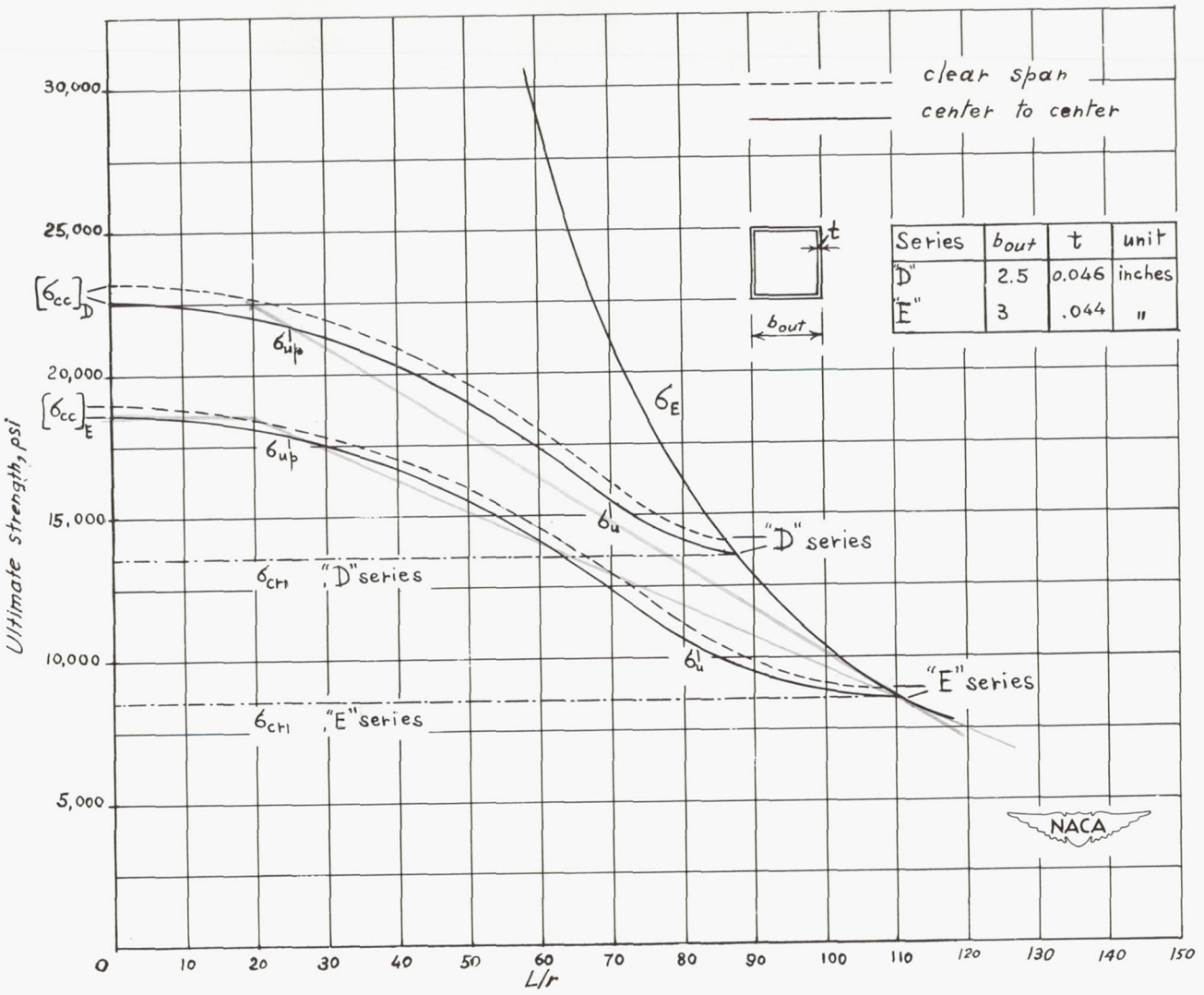

Figure 15.- Graph of ultimate stresses plotted against slenderness ratios L/r for tubes with square cross section.

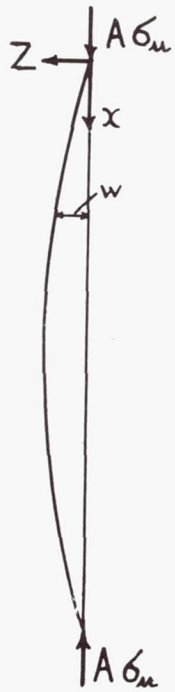

(a) Buckling of initially straight column.

(b) Deflection of column with initial eccentricity w_i.

Figure 16.- Determination of effect of crookedness of column.

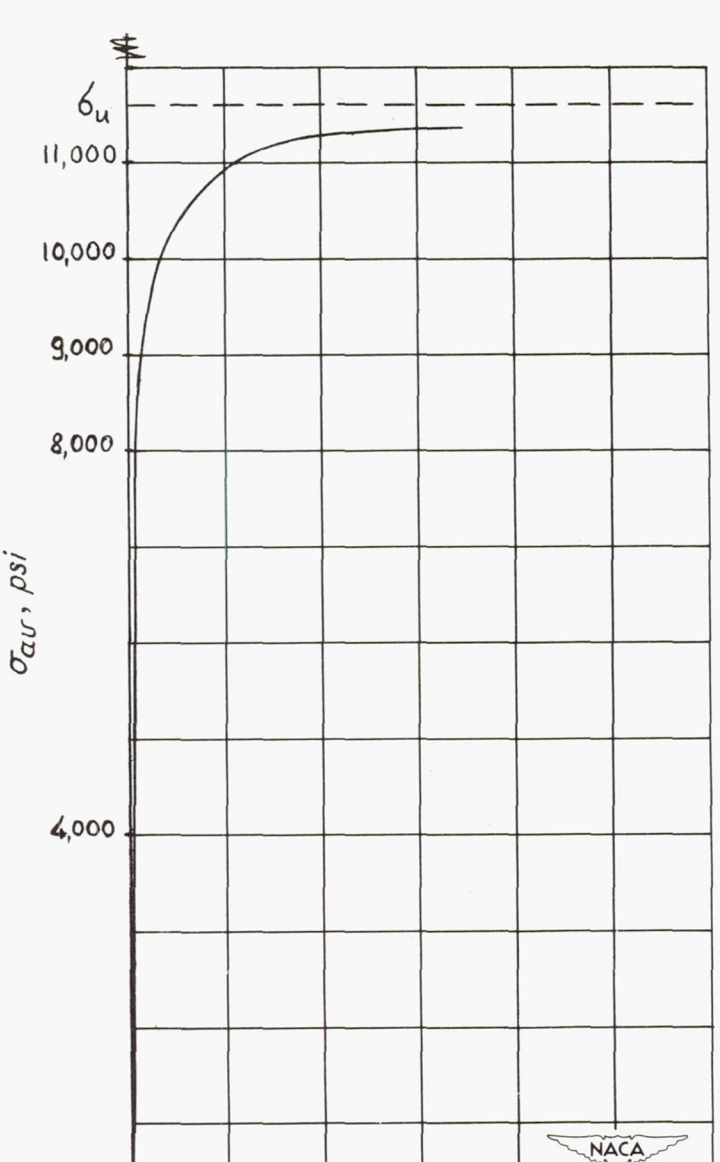

Figure 17.- Load-deflection diagram of square tube of "E" series with slenderness ratio $L/r = 75$ and initial eccentricity w_i.

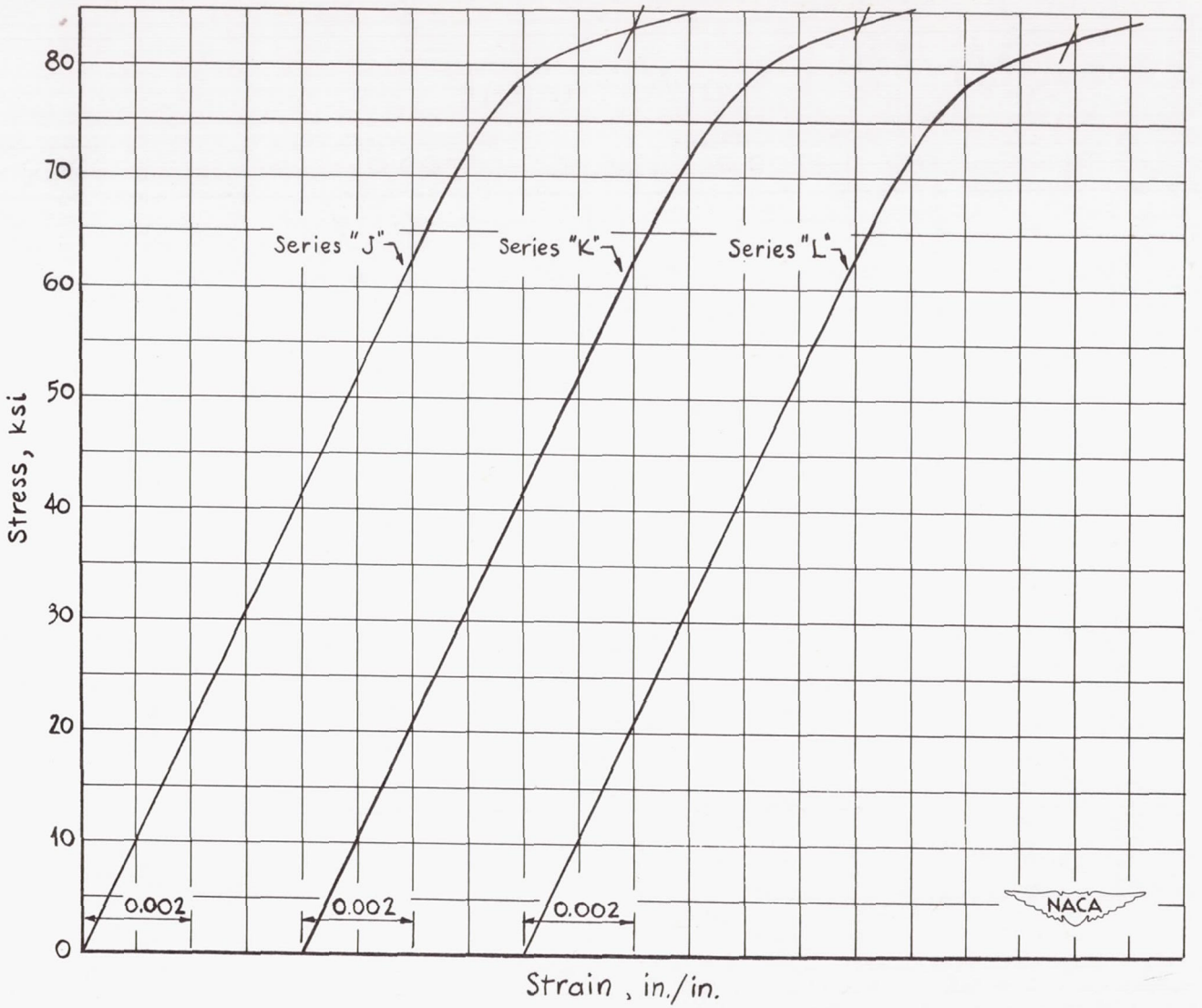

Figure 18.- Stress-strain curves for H-sections.

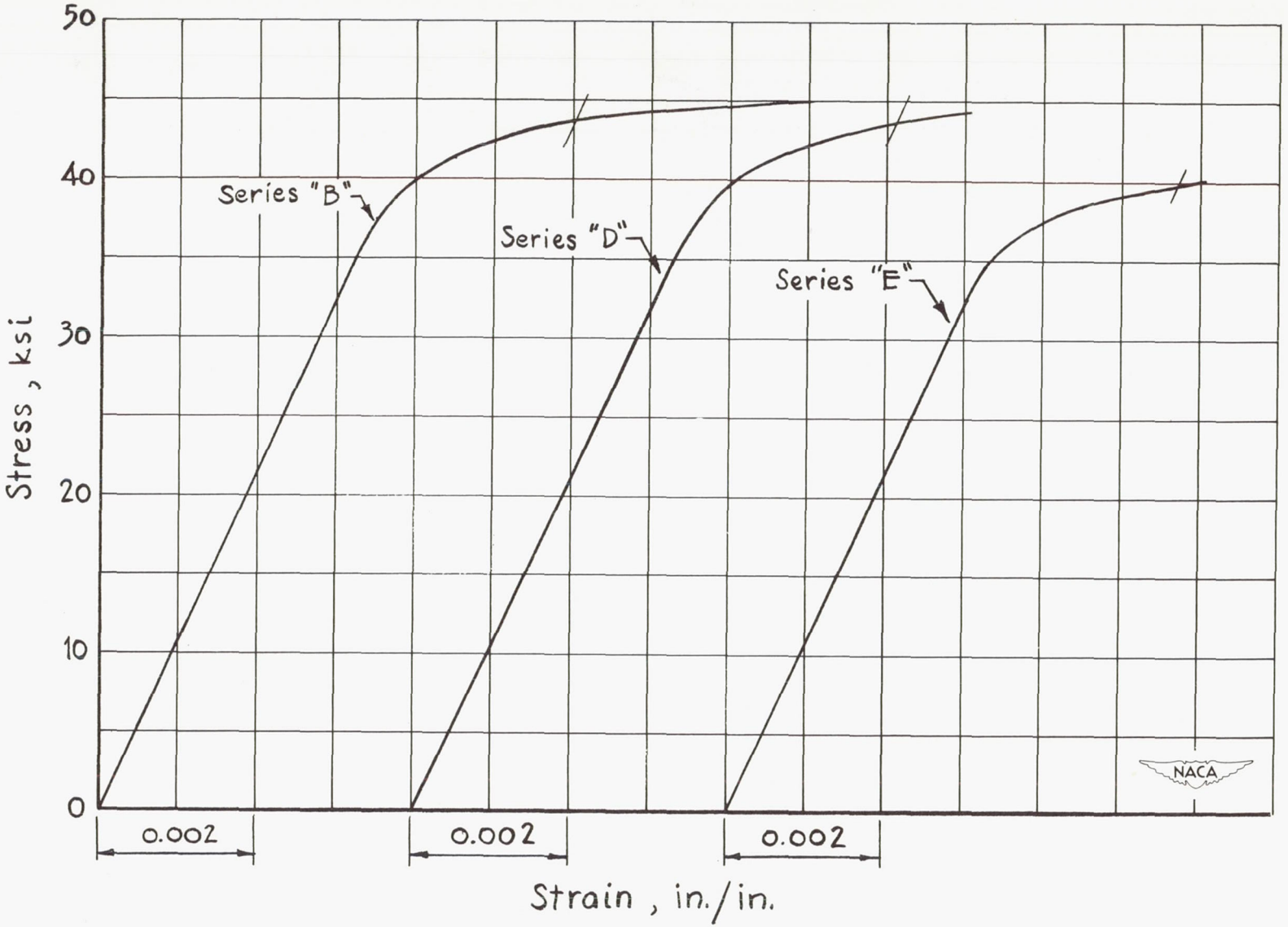

Figure 19.- Stress-strain curves for square tubes.

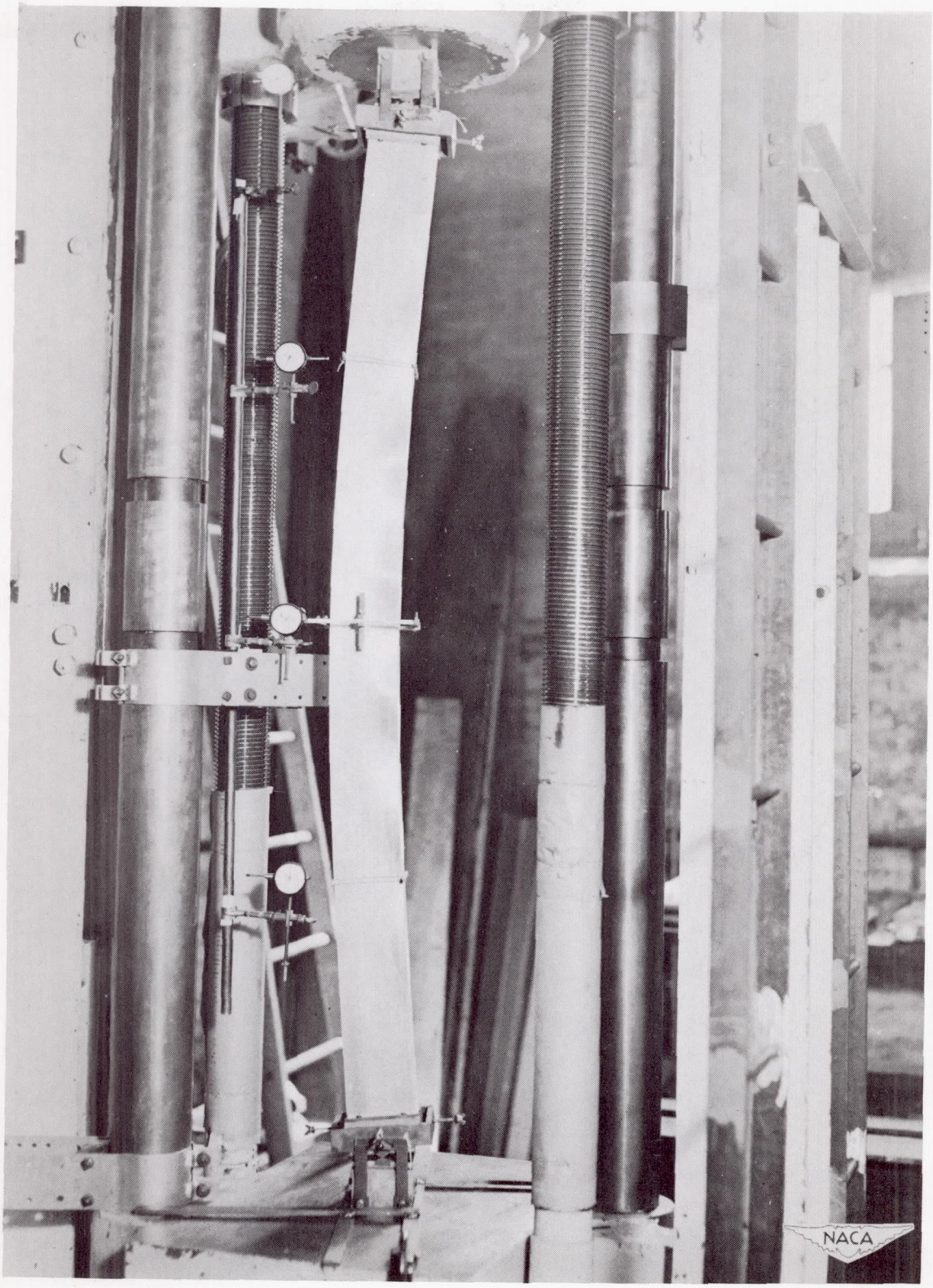

Figure 20.- View of test setup. Column shown is L3-ML2.

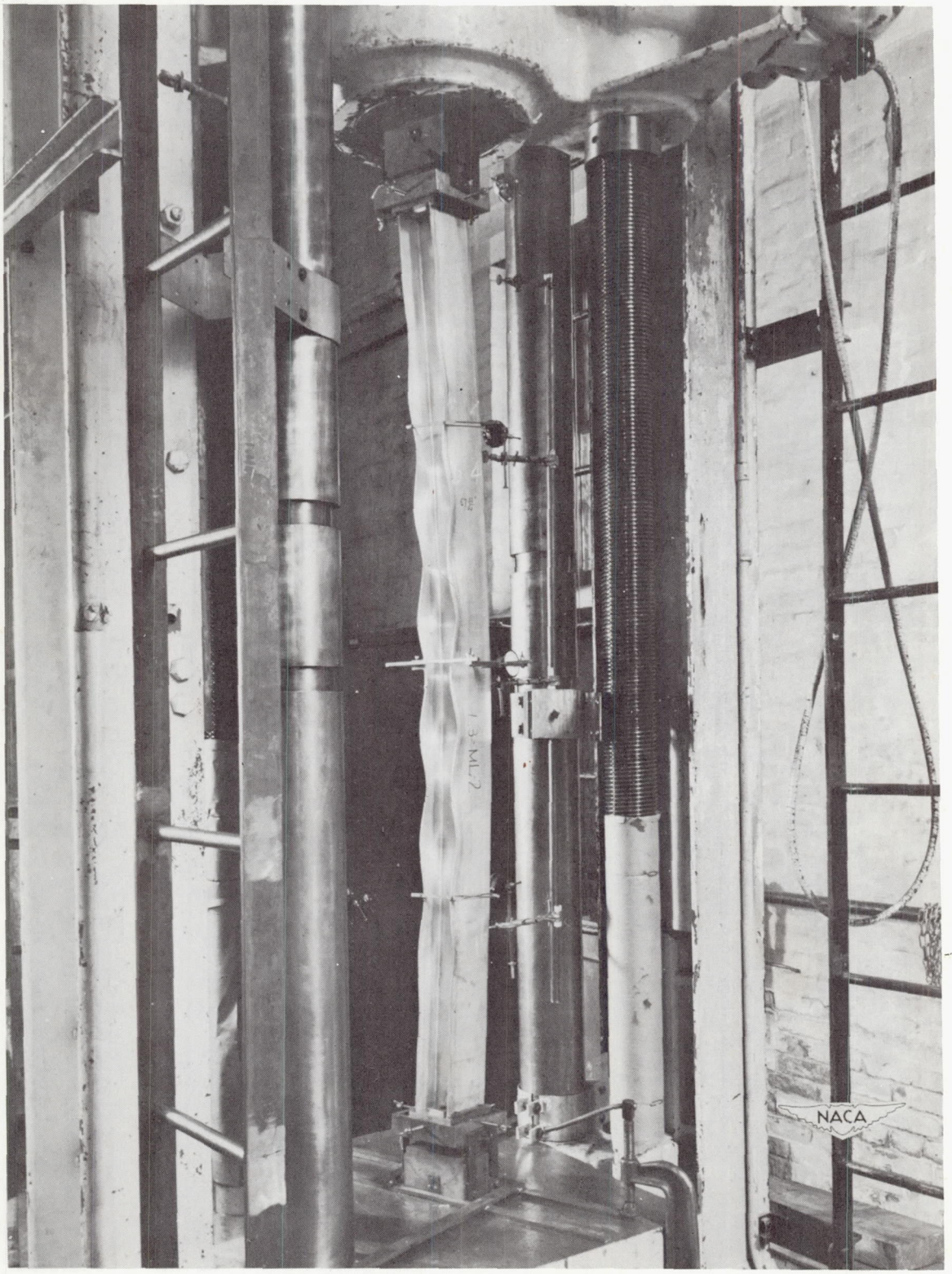

Figure 21.- Side view of test setup.

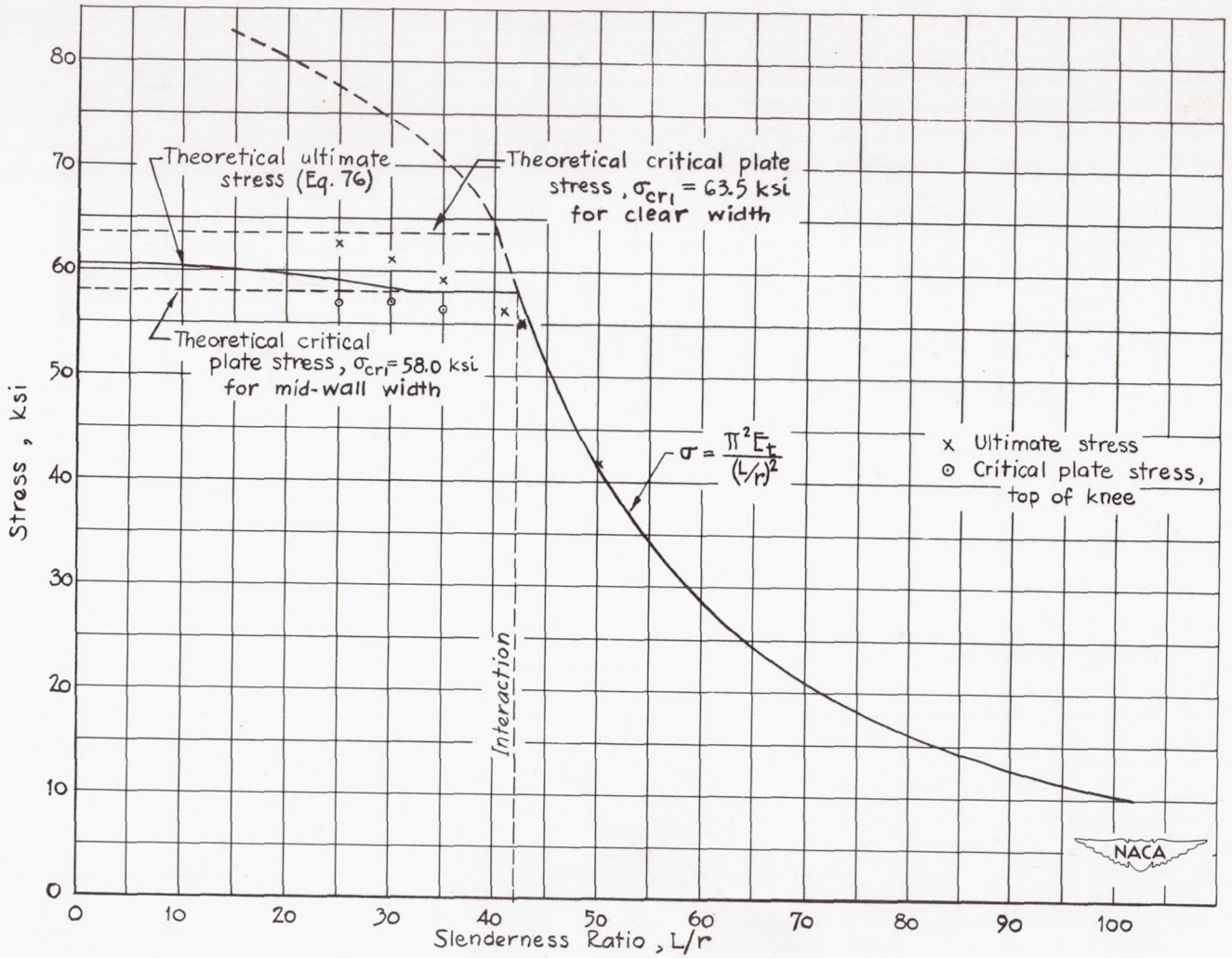

Figure 22.- Test results for "J" series H-sections. $\sigma_{cr1}/\sigma_{cy} = 0.70$; $\sigma_{cr1}/\sigma_{cc} = 0.96$.

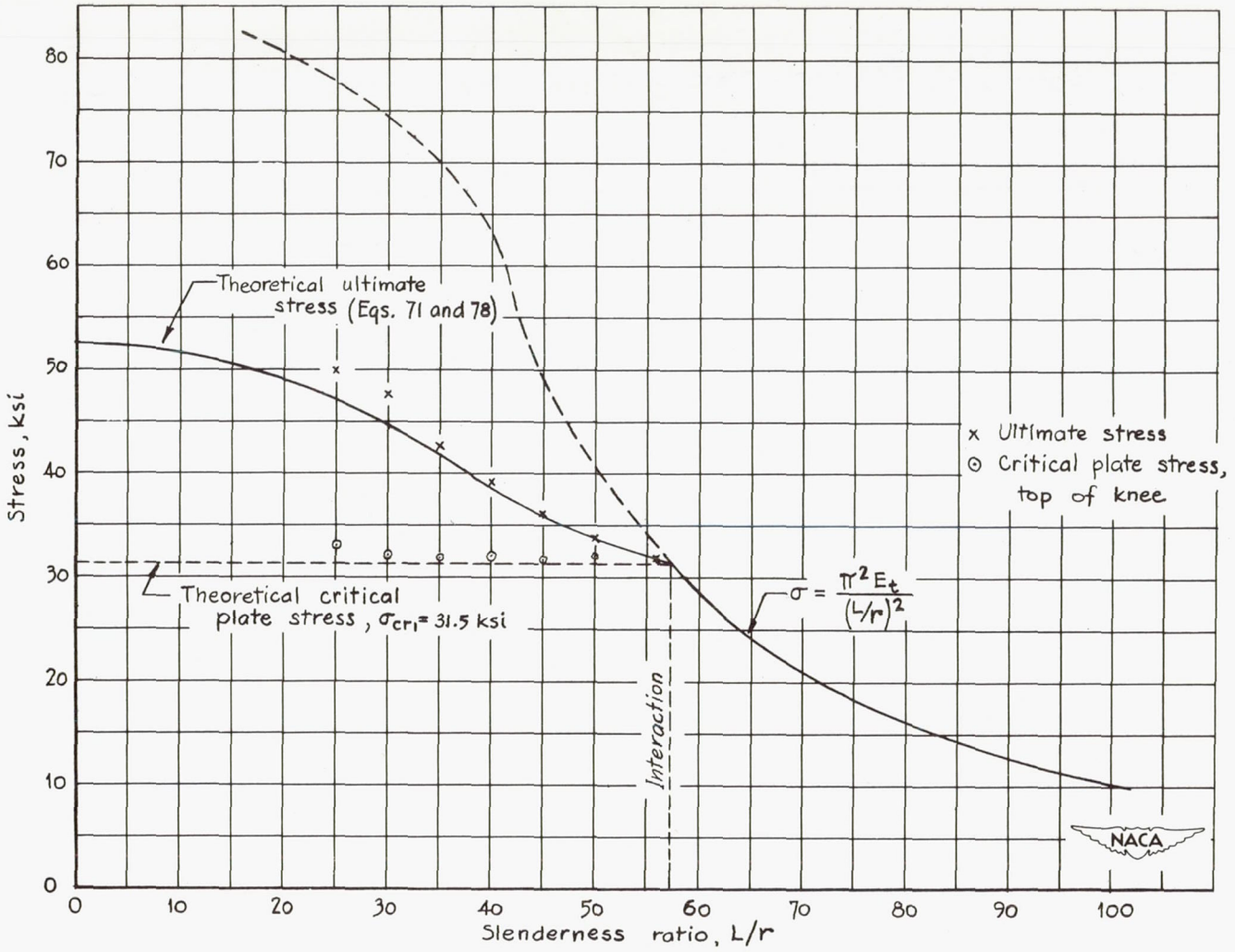

Figure 23.- Test results for "K" series H-sections. $\sigma_{cr1}/\sigma_{cy} = 0.375$; $\sigma_{cr1}/\sigma_{cc} = 0.60$.

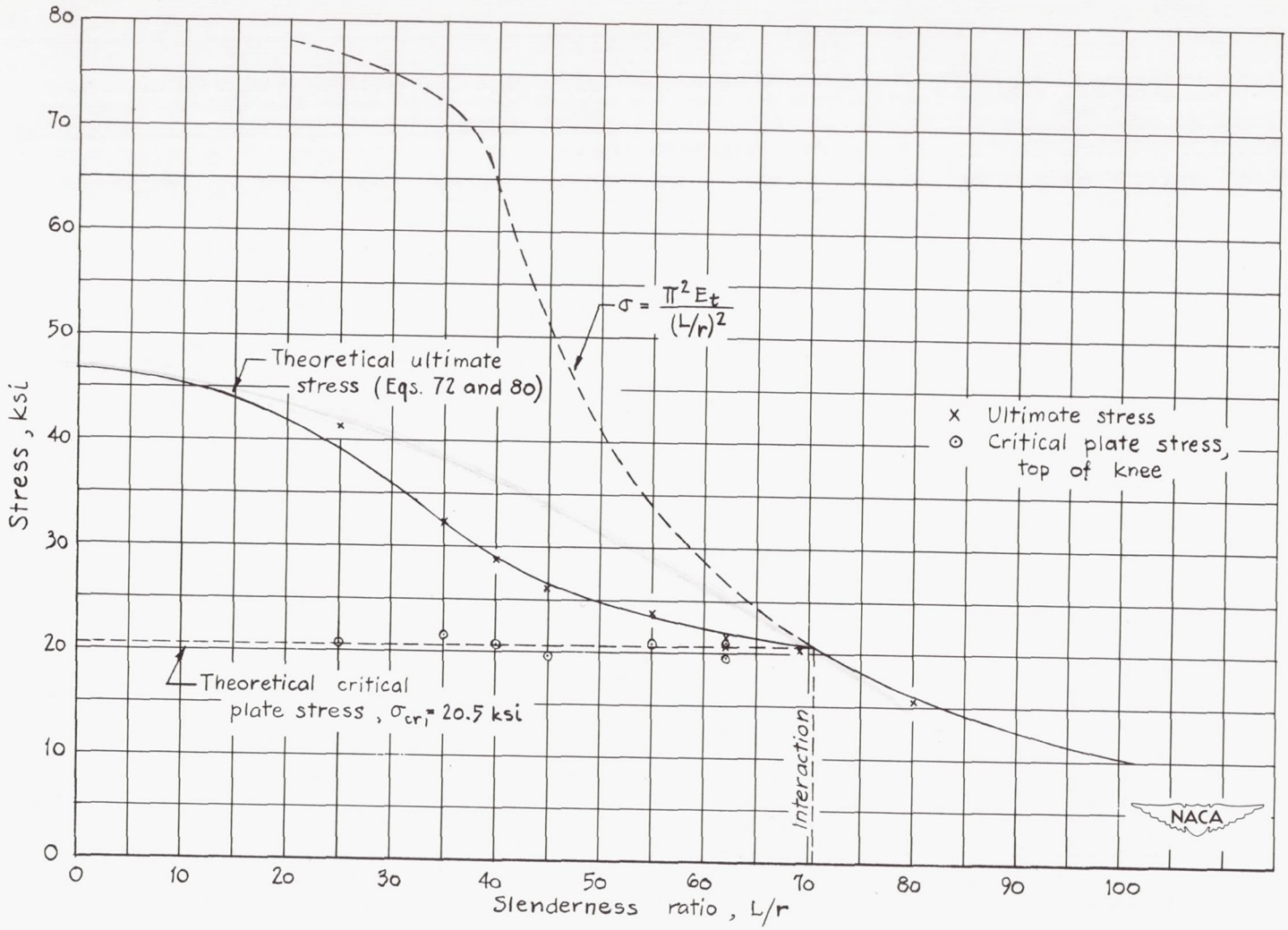

Figure 24.- Test results for "L" series H-sections. $\sigma_{cr1}/\sigma_{cy} = 0.25$; $\sigma_{cr1}/\sigma_{cc} = 0.44$.

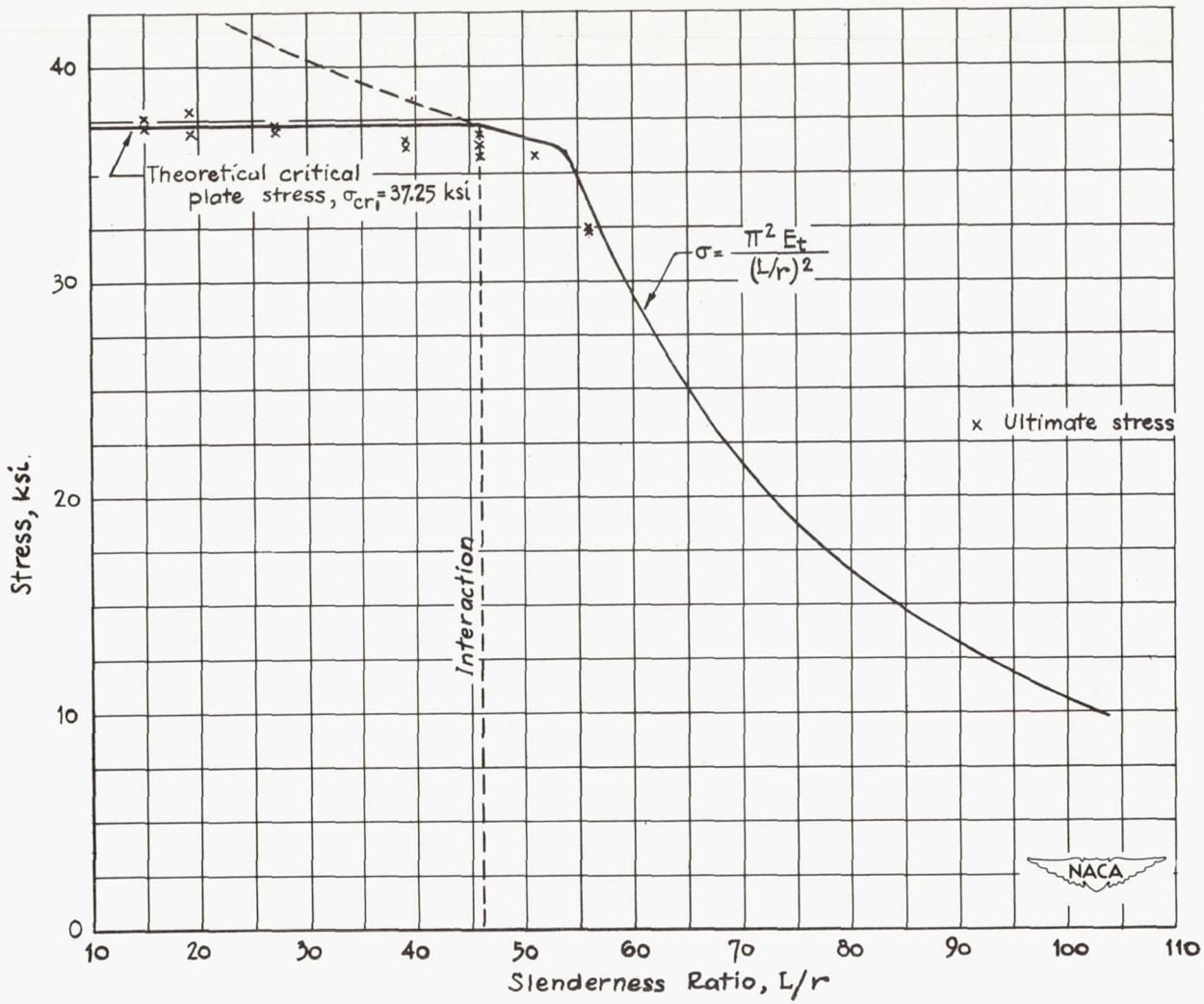

Figure 25.- Test results for "B" series square tubes. $\sigma_{cr1}/\sigma_{cy} = 0.85$; $\sigma_{cr1}/\sigma_{cc} = 1.00$.

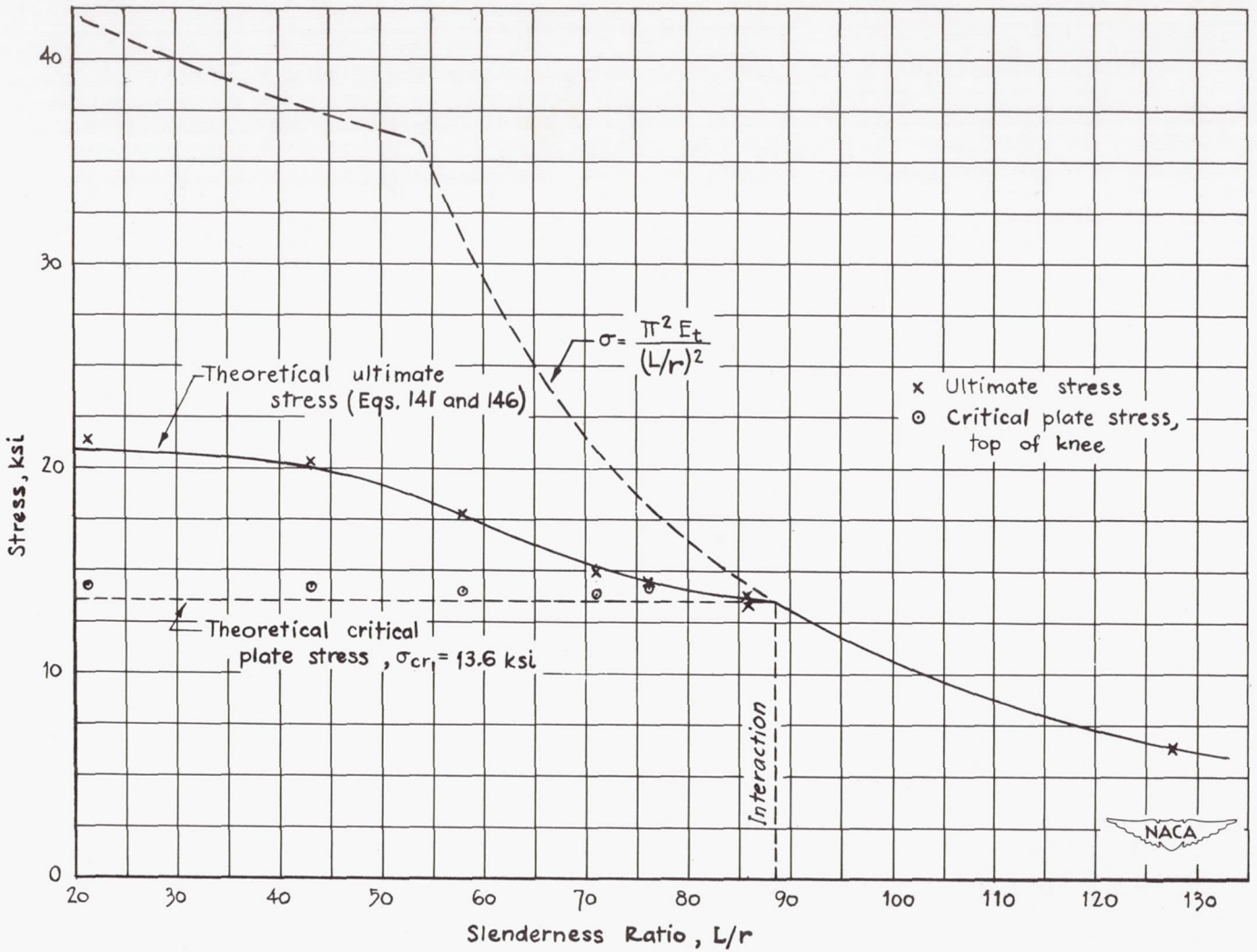

Figure 26.- Test results for "D" series square tubes. $\sigma_{cr1}/\sigma_{cy} = 0.31$; $\sigma_{cr1}/\sigma_{cc} = 0.60$.

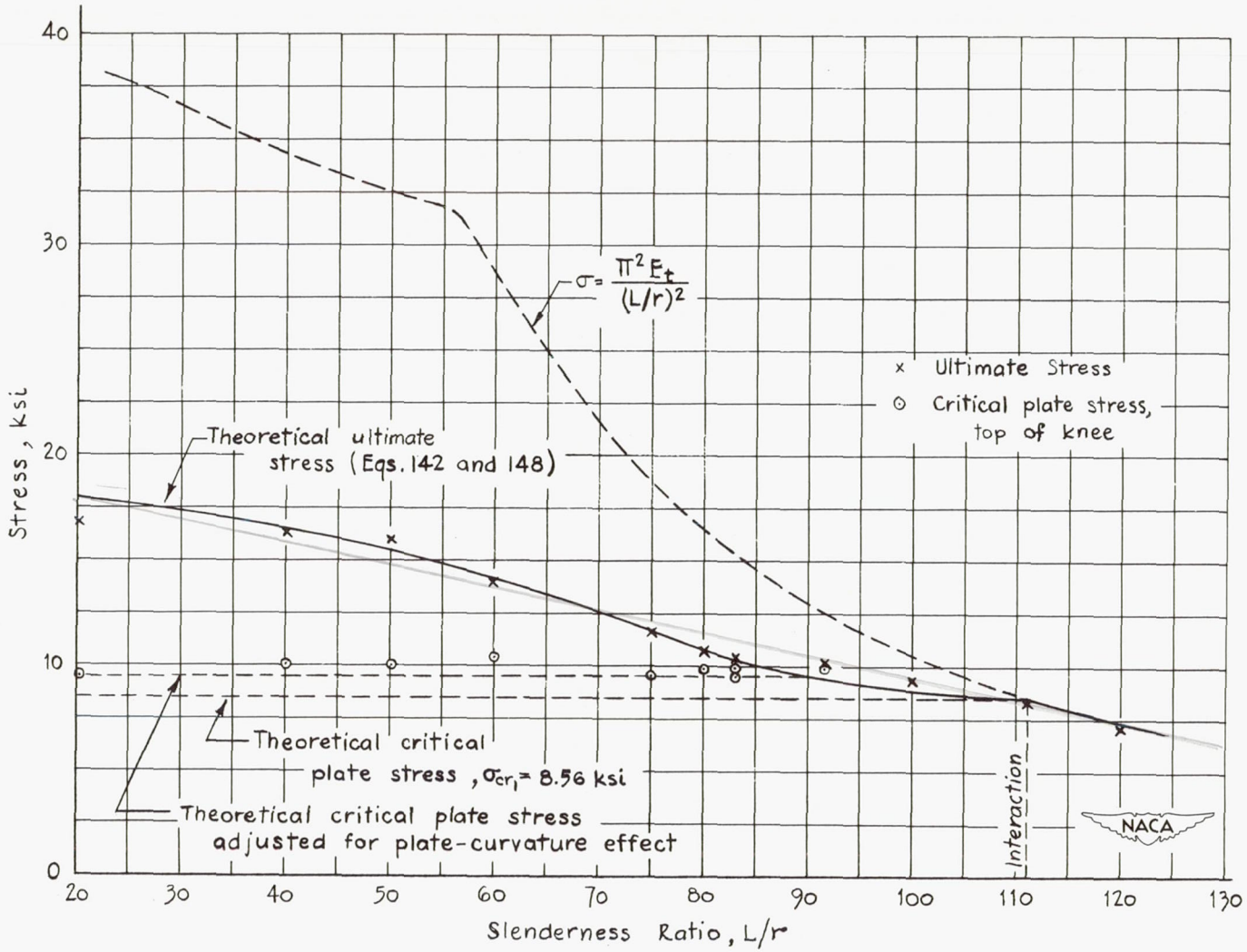

Figure 27.- Test results for "E" series square tubes. $\sigma_{cr1}/\sigma_{cy} = 0.21$; $\sigma_{cr1}/\sigma_{cc} = 0.46$.

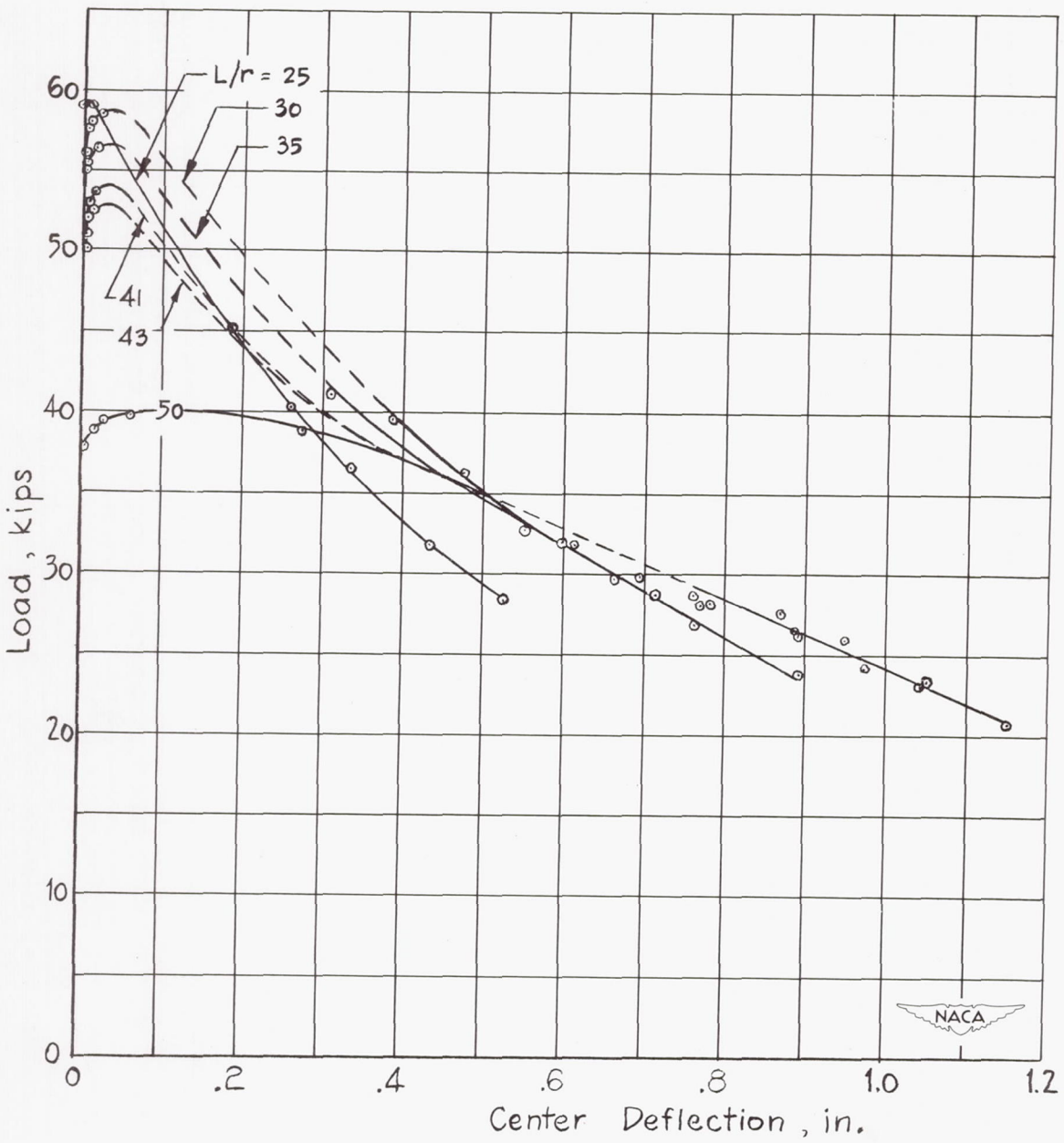

Figure 28.- Column-deflection curves for "J" series H-sections.

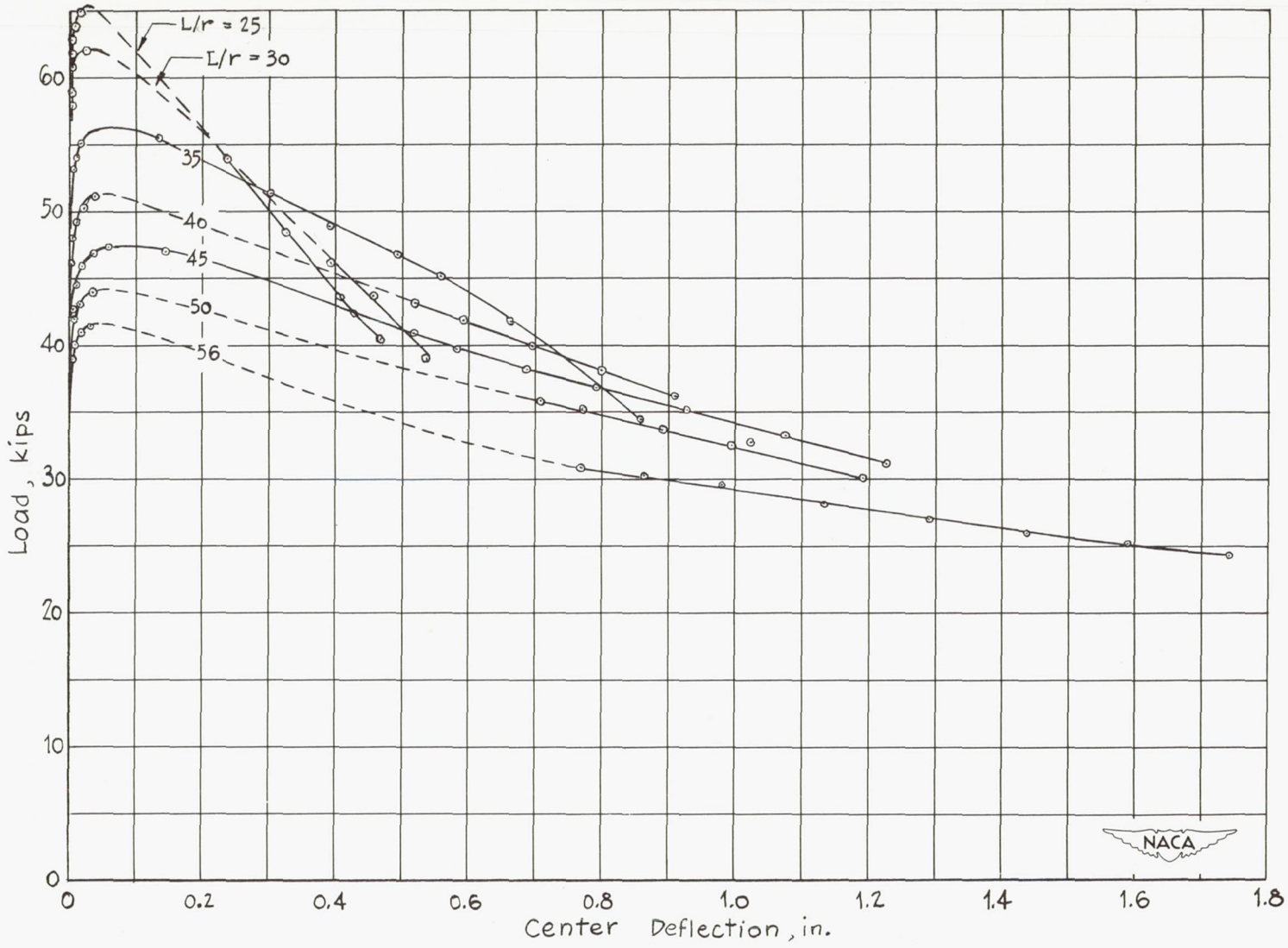

Figure 29.- Column-deflection curves for "K" series H-sections.

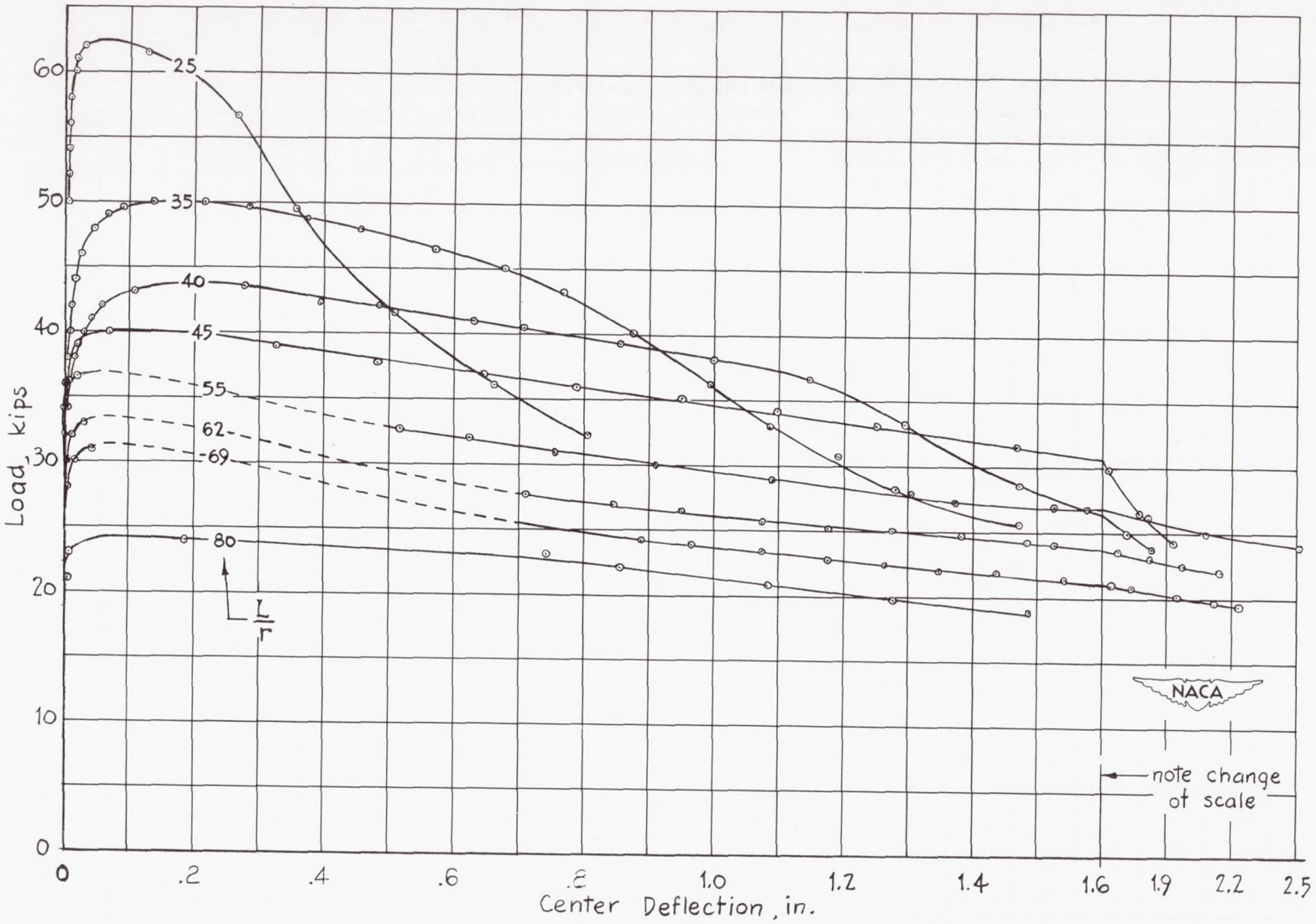

Figure 30.- Column-deflection curves for "L" series H-sections.

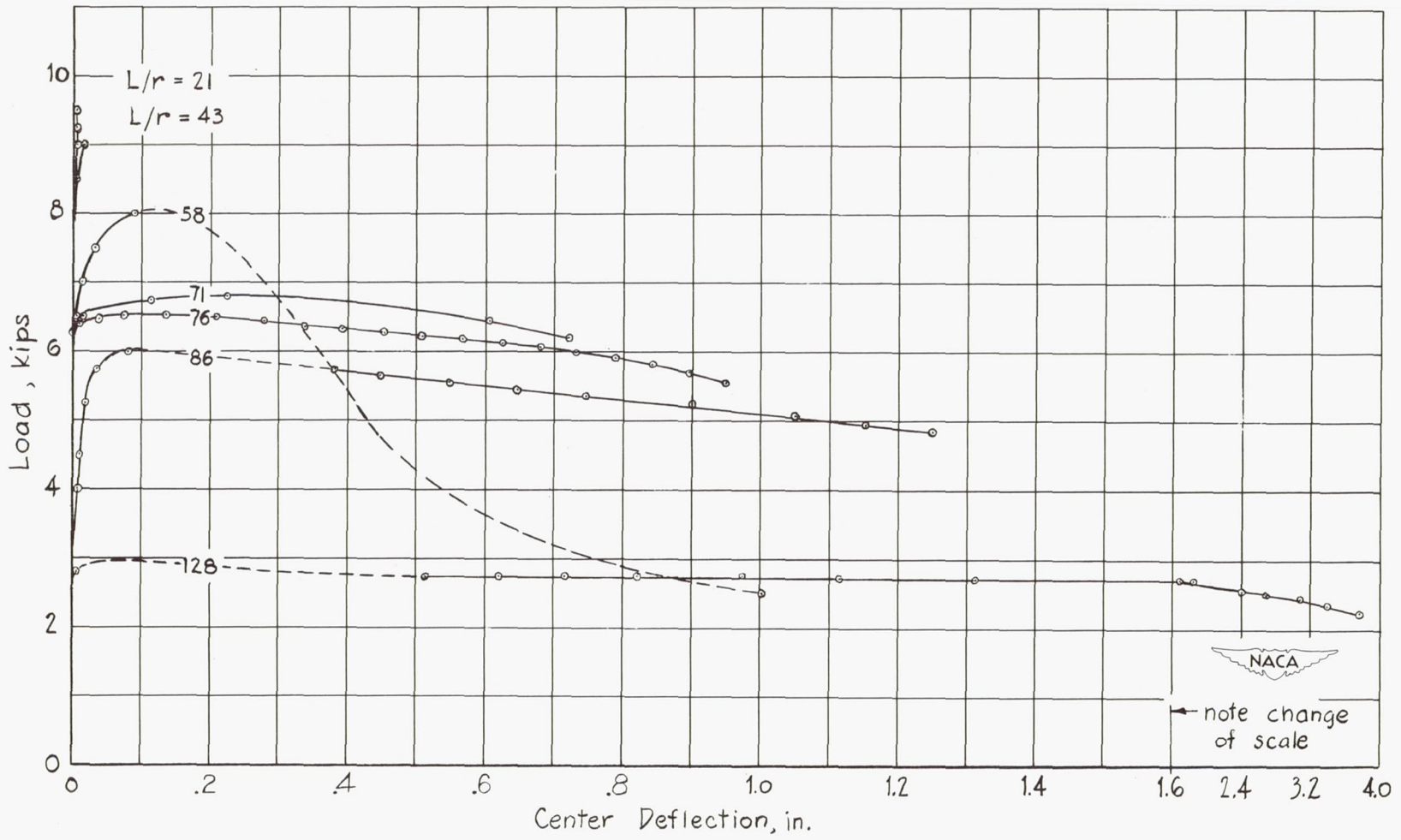

Figure 31.- Column-deflection curves for "D" series square tubes.

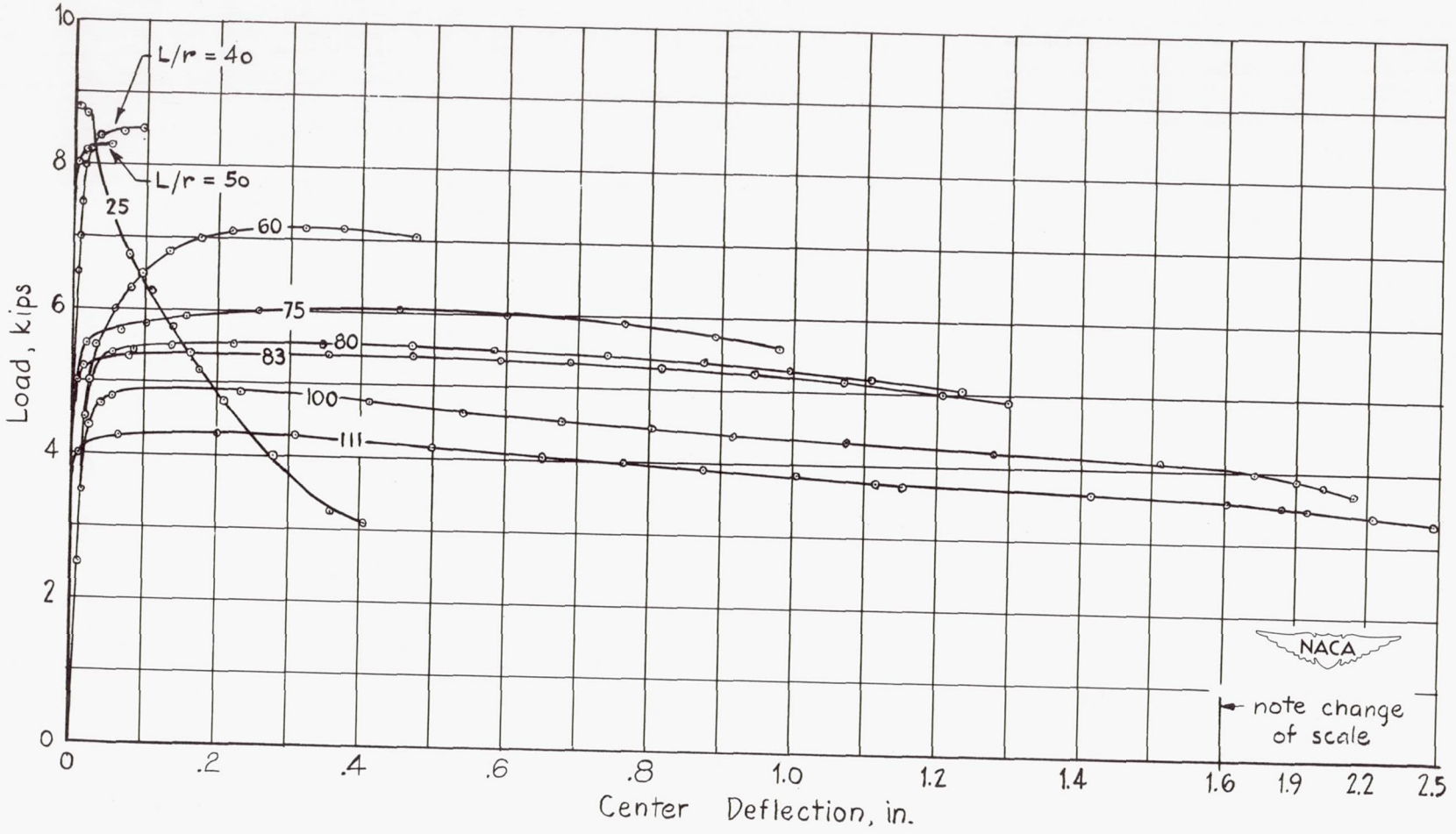

Figure 32.- Column-deflection curves for "E" series square tubes.

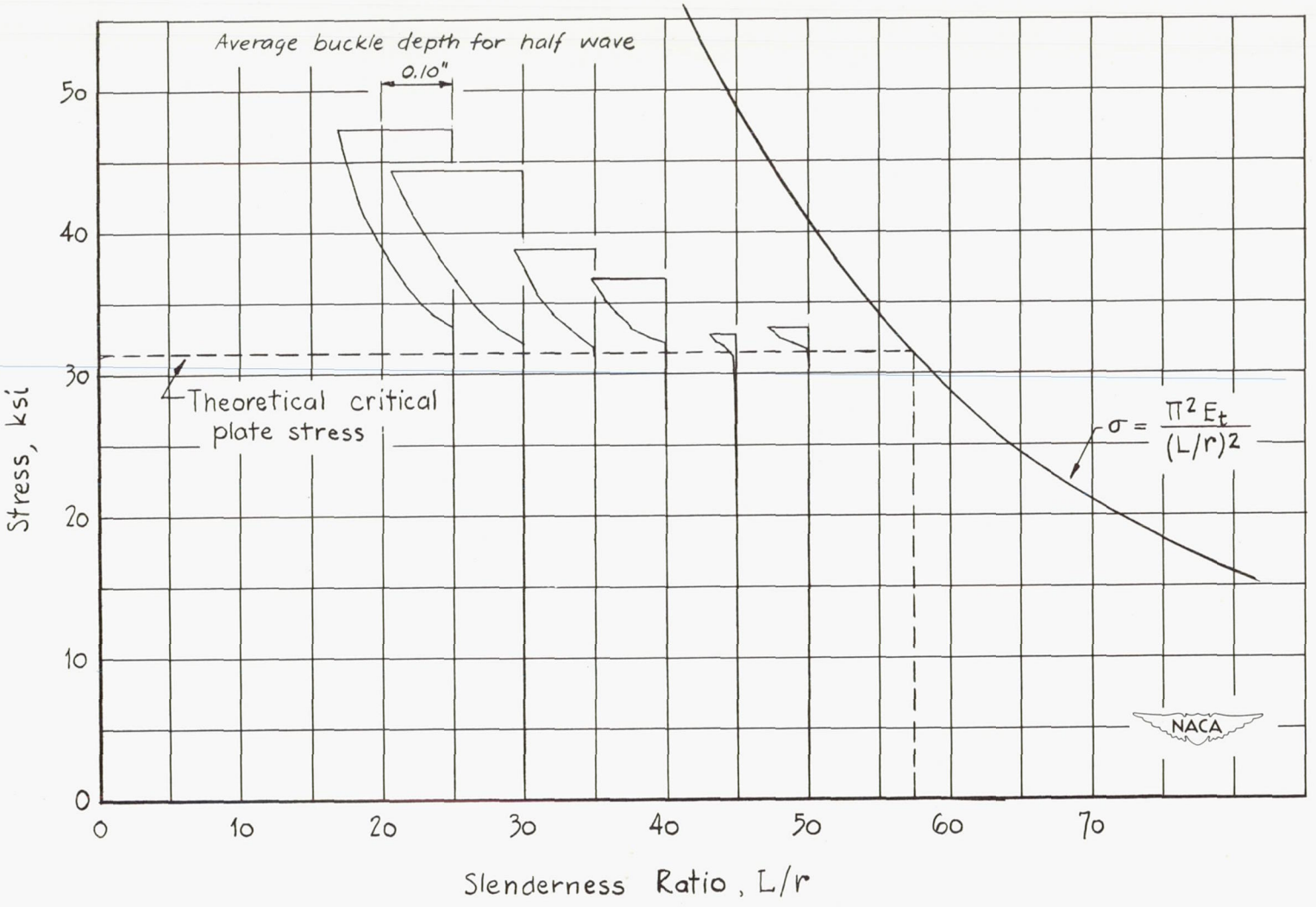

Figure 33.- Buckle-depth variation for "K" series H-sections. Average half wave length = 4.75 inches.

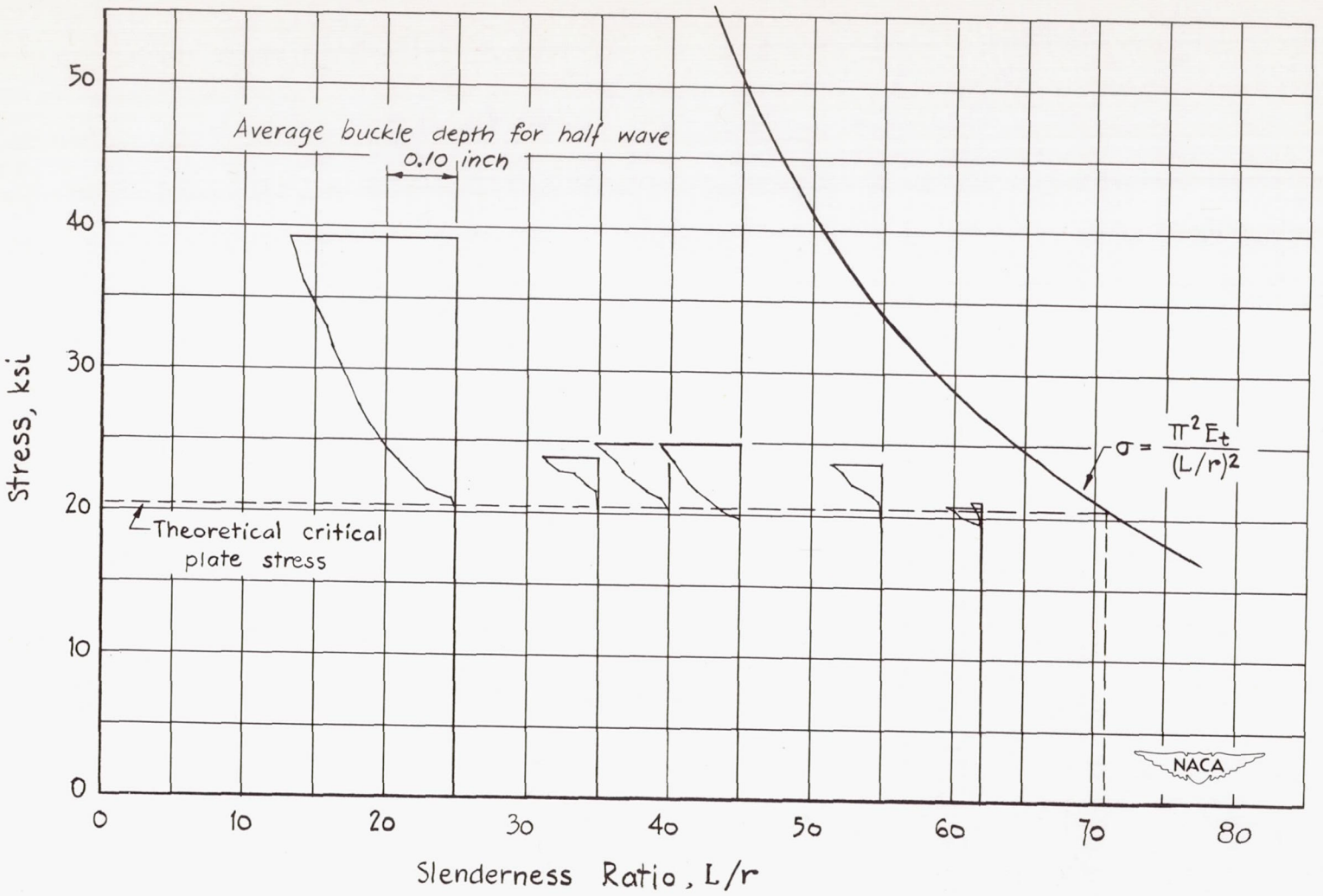

Figure 34.- Buckle-depth variation for "L" series H-sections. Average half wave length = 5.75 inches.

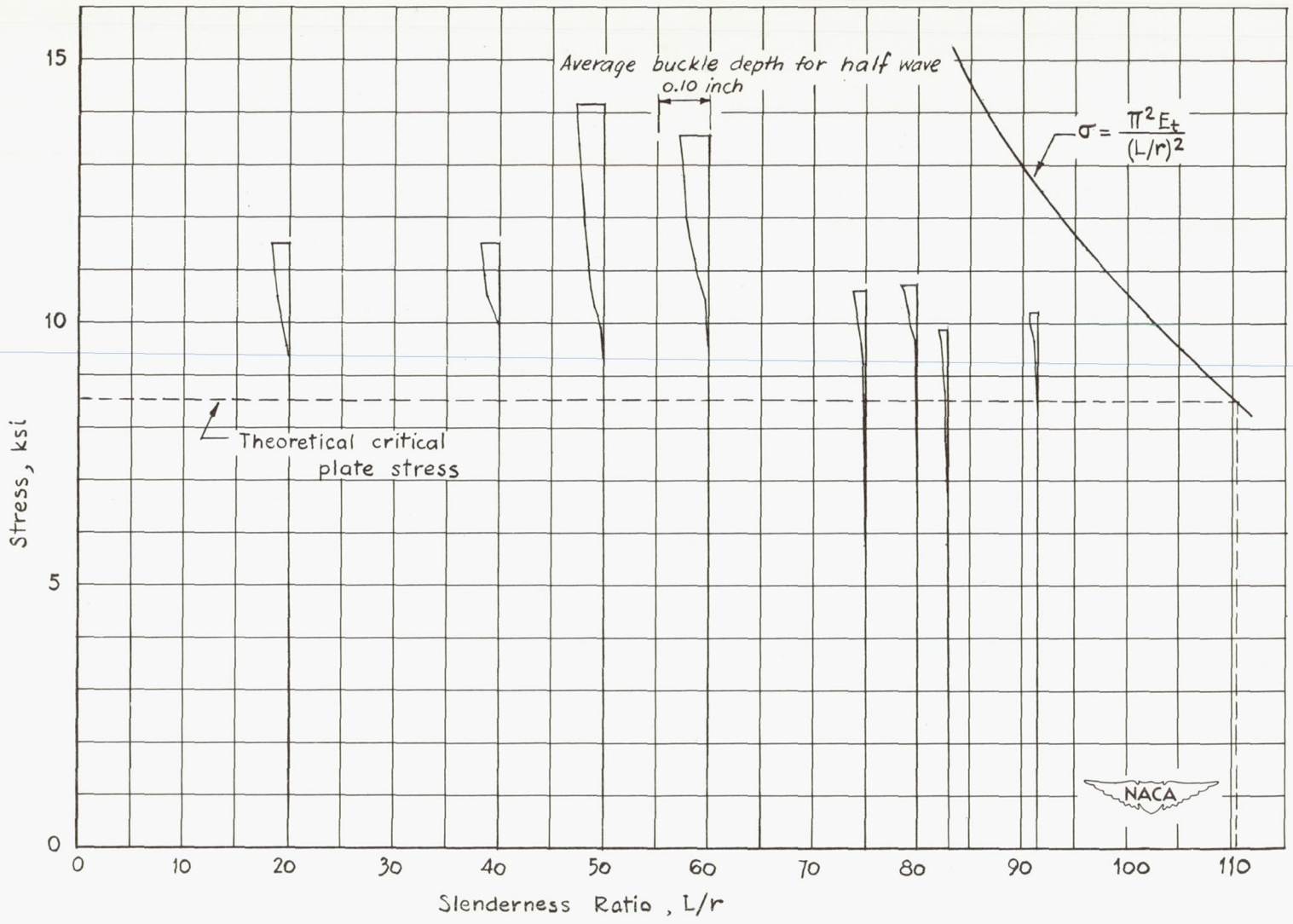

Figure 35.- Buckle-depth variation for "E" series square tubes. Average half wave length = 3.0 inches.

NACA-Langley - 8-28-53 - 1000